THE BRIGHTNESS DISTRIBUTION OF CORE-HALO RADIO SOURCES

Thesis by

Richard Sramek

In Partial Fulfillment of the Requirements

For the Degree of

Doctor of Philosophy

California Institute of Technology

Pasadena, California

1970

(Submitted May 4, 1970)

ACKNOWLEDGEMENTS

Many people have assisted me in the preparation of this thesis. I especially thank Dr. Ed Fomalont for the vast amount of time he spent explaining the theory and practice of radio interferometry and discussing with me his work on radio source structures. I would like to thank my thesis advisor, Dr. A. Moffet for suggesting the project, for his guidance in building the 610 MHz receiving system, and for his close reading and valuable criticism of the manuscript. Gordon Stanley, Director of the Owens Valley Radio Observatory, and the OVRO staff were extremely helpful throughout the project. Most of the computer programs used in this work were written by J. F. Bartlett, E. Fomalont, and D. Rogstad. I especially thank W. Wright for the many months he spent observing with me for no reward other than the pleasure of working in astronomy at OVRO. I also thank D. Rogstad, G. Seielstad, D. Keeley, K. Weiler, R. O'Connell, S. Shostak, and R. Read for those innumerable, endless conversations on all manners of astronomical topics which have contributed greatly to my education in astronomy. I thank my wife Priscilla for assistance with the drawings and for keeping the entire project in perspective.

During my stay at C.I.T. I have been the grateful recipient of a N.A.S.A. Traineeship and a C.I.T. Special Fellowship and assistantship. The research at the Owens Valley Radio Observatory has been supported by the U.S. Office of Naval Research under contract N0014-67-A-0094-0008.

THE BRIGHTNESS DISTRIBUTION OF CORE-HALO RADIO SOURCES.

ABSTRACT

The east-west visibility of 28 extragalactic radio sources with both large and very small components was obtained at 605 MHz using the radio interferometer at the Owens Valley Radio Observatory. A 2' HPBW fan beam was synthesized from observations made at twelve spacings between 62 and 977 wavelengths. The availability of such low spatial frequencies permitted the calculation of the brightness distribution of components as large as 56'. The brightness distributions of the following galaxies are plotted: (spiral galaxies) P0045-25, P1302-49 P1334-29, (elliptical galaxies) 3C40, 3C105, P0843-33, 3C236, 3C247, 3C264, P1216-10, 3C274, 3C287.1, 3C293, and P2247+11.

Fourteen of the observed sources had a core-halo or asymmetric double structure and had their large components well resolved at the 977λ spacing. The spectral indices of the large and small components of these sources were obtained by comparing the flux densities given here with those at other frequencies. The spectra of the large components are generally steeper than those of the small components with an average difference of spectral indices

of $\Delta\alpha = +0.3$.

Assuming equipartition of magnetic and particle energies the total energies of the large halos are $\sim 10^{60}$ ergs. This is sufficient energy to maintain the current radio luminosities for $\sim 10^{10}$ years.

Three of these fourteen sources have a core-halo structure and are associated with spiral galaxies; the remaining eleven are associated with elliptical galaxies. Two of the remaining sources are asymmetric doubles, and nine have a core-halo structure. Four of the core-halo sources have simple halos, two have double halos, and three have an undetermined halo structure. The ratio of observed double to simple halos can be explained by the projection of double halos randomly oriented in three dimensions provided the ratio of component separation to diameter, R, is less than two. Since doubles without a core have R between two and four, the mechanism of radio galaxy formation is likely to produce a core for low values of R. From the present investigation it is impossible to conclude whether there exists a class of core-halo radio galaxies with simple halos ($R \leq 1$) or whether the observed core-halo objects represent the low-R end of the ensemble of double radio sources.

TABLE OF CONTENTS

I. INTRODUCTION

The study of radio source structures has been an active area of radio astronomy for the last decade. To obtain the resolution needed, most of this work has been done with interferometers and synthetic apertures (Ryle and Hewish 1960). Early studies of a large number of sources were done by Moffet (1962) and Maltby (1962) at 960 MHz and by Lequeux (1962) at 1420 MHz. More recent work was done by Fomalont (EF II)* at 1425 MHz, by Bash (1968a) at 2695 MHz, and by Ekers (1969) at 468 and 1403 MHz. To resolve extremely small sources, very long baselines have been obtained both by conventional interferometry (Allen et al. 1962, Anderson and Donaldson 1967, Palmer et al. 1967, and Basart et al. 1968) and with independent local oscillators (Cohen 1969). The group at Cambridge has pioneered the synthesis of a two dimensional aperture utilizing the earth's rotation to obtain various baseline orientations (Ryle 1962, Rowson 1963, and Elsmore et al. 1966). Two dimensional structures derived in this way are given by Macdonald et al. (1968).

The observed radio structures are usually classified in a rather simple fashion, not because radio sources

---

*Extensive reference is made to the 1425 MHz survey of radio source structures by Fomalont. His results are presented in three papers which we shall call EF I (Fomalont 1967), EF II (Fomalont 1968), and EF III (Fomalont 1969).

are all simple, but rather because the resolution is so poor. A detailed classification like the de Vaucouleurs system for optical galaxies is not warranted by the data presently available. The following classes are generally sufficient (Maltby and Moffet 1962, Bash 1968b):

1) simple - a single emission region with no indication of subsidiary components. This assumes that the source is resolved so that additional components would be seen if present.

2) double - two separate components. The ratio of component separation to diameter may vary from one to over a hundred.

3) triple or complex - three or more components. This is a general class for sources with a wide range of structures. Increased resolution may reveal that many of the simpler sources are actually complex.

4) core-halo - a small central emission region embedded in a large diameter envelope. This class is characterized by a very large ratio of component diameters, a large difference in component brightness, and a small separation of component centers.

The simple, double, and triple or complex sources seem to be directly related. In a statistical analysis of a large number of resolved sources, Fomalont (EF III) shows that the relatively small number of simple sources observed can be explained as doubles seen end on. Triple or complex sources often show a basic double structure with additional components nearby. The double sources with optical identifications usually have the optical object (quasar or galaxy) between the two components and near the line joining them. It is generally believed that the relativistic electrons responsible for the radio emission have been ejected from this central object. The discrete components are formed either at the time of ejection or by the intergalactic medium. Some sources show evidence of multiple ejections. For example, Centaurus A consists of a very large double which straddles a galaxy plus a small double within the optical object.

The core-halo objects do not fit into this picture. Rather than lying between two discrete components, the galaxy is embedded in a large radio emission region. At the center of the region, coinciding with the galaxy, is an extremely bright, small radio source. Good examples of this class are 3C84 and 3C274.

Intermediate between the core-halo and double structure is a fifth class which Fomalont (EF III) calls "unequal doubles." These are asymmetric doubles in which

the ratio of the component diameters exceeds two. The position of the optical galaxy suggests that these are physically different from the normal doubles. In equal diameter doubles the optical galaxy is roughly midway between the two components. However, when the diameter ratio exceeds 1½ or 2 the galaxy is systematically closer to the smaller component, and sometimes coincident with it (e.g. 3C31, 3C83.1). Core-halo galaxies are like these asymmetric doubles except that the separation of the component centers is relatively small. Fomalont (EF III) points out that the core-halo objects are not simply the asymmetric doubles seen end on since there are far too many of them to be explained as a projection effect.

Any complete understanding of the origin and evolution of radio sources must account for the core-halo objects. These may be explained in two ways. The first is that a single process is involved in forming radio sources and that core-halo sources are the limiting case of normal doubles. The halo would be the expanded remnant of an old outburst, and the core would be a more recent event. However, Fomalont (EF III) notes that in this case halos without cores should be seen, but that the observed simple sources can be statistically explained as doubles seen end on. The second theory is that the cores and halos are formed from a single outburst, the difference in structure arising from different physical conditions during the

outburst and subsequent evolution. Perhaps both cases are found in nature. Certainly more data is needed on these objects. The existence of some halos is uncertain and many are based on only one or two interferometer spacings. The first possibility given above, that the halos are the greatly expanded remnants of old doubles, might be checked by low resolution observations of the halo. Moffet and Palmer (1965) suggest that the spectra of the halos are steeper than those of the cores. This could be easily checked by flux density measurements at two or more frequencies.

The observations presented here were undertaken to gather more information on the large diameter components of radio galaxies, in particular of core-halo objects. The two element interferometer at the Owens Valley Radio Observatory was used to synthesize a two arc-minute fan beam at a frequency of 605 MHz (50 cm wavelength). Twelve antenna spacings were used on an east-west track with separations ranging from 100 ft. to 1600 ft. (62 to 977 wavelengths). The one-dimensional brightness distribution of twenty-nine objects was obtained. In addition to transit observations, which were made of all the sources, certain high declination objects were observed off transit to obtain additional baseline orientations. The resulting one-dimensional brightness distributions at 605 MHz were compared with Fomalont's measurements at 1425 MHz to obtain separate

spectral indices for the large and small components. The basic observations are presented in Chapter II. The inversion method for the interferometric data and a table of results are given in Chapter III Chapter IV contains a description of the structures of individual sources. Chapter V contains a general discussion of core-halo galaxies.

II. OBSERVATIONS

a) The Radio Interferometer

The use of an interferometer to obtain radio source structures has been described in detail by previous authors (Bracewell 1958, Moffet 1962, EF I). The response of the interferometer is proportional to the Fourier transform of the brightness distribution of the source. For an east-west baseline it is given by

$$R = G(t)S'V(u,v)\cos\{\Phi(u,v) + 2\pi[-s_o\cos\delta_o\sin H_o + \psi_{BL} + \psi_I(t)]\}. \quad (1)$$

$V(u,v)$ and $\Phi(u,v)$ form the <u>complex visibility</u>,

$$\hat{V}(u,v) = V(u,v)e^{i\Phi(u,v)} = 1/S' \iint A(x,y)B(x,y)e^{i2\pi(ux+vy)}dxdy. \quad (2)$$

In these expressions $B(x,y)$ is the radio source brightness distribution, and x and y are Cartesian coordinates in a small region of sky centered on hour angle and declination H_o, δ_o and locally parallel to the equatorial coordinate system. The components of the projection of the baseline on the plane of the sky parallel to x and y in the vicinity of H_o, δ_o are designated by u and v;

$$u = s_o\cos H_o,$$

$$v = s_o\sin\delta_o\sin H_o.$$

The full length of the interferometer baseline, measured in wavelengths at the observing frequency is s_o, while S' is a normalization factor defined by

$$S' = \int\int A(x,y)B(x,y)\,dxdy.$$

The time varying system gain is represented by G(t) and ψ_{BL} and $\psi_I(t)$ are the phase corrections due to baseline errors and instrumental phase drifts. These will be discussed more fully in Section II-d.

The product of the voltage response patterns of the two antennas is represented by A(x,y). For identical antennas this is equal to the power pattern of one antenna. Thus the complex visibility $\hat{V}(u,v)$ is the Fourier transform of the radio source brightness distribution B(x,y) modified by the effective beam pattern, A(x,y). The intensity normalization factor S' is the apparent flux density of the source as seen with this beam pattern.

The major time dependence in (1) is in the term $s_o \cos\delta_o \sin H_o$, where H_o increases at the siderial rate, giving rise to the oscillatory interferometer output often referred to as "fringes." A measure of the amplitude and phase of these fringes gives the value of the complex visibility at a point in the u,v plane.

The source brightness distribution is obtained by inverting Eq. (2),

$$B'(x,y) = A(x,y)B(x,y) = S' \int\int \hat{V}(u,v) e^{-i2\pi(ux+vy)} dudv. \qquad (3)$$

Finding values for $\hat{V}(u,v)$ in two dimensions is very time consuming and was not attempted in this work. Instead the brightness distribution projected into one dimension was obtained.

Let x',y' be a Cartesian coordinate system rotated with respect to x,y, and let u',v' be the components of the baseline projected onto the axis of this rotated coordinate system.

$$du'dv' = dudv$$

$$u'x' + v'y' = ux+vy$$

The one-dimensional brightness distribution projected onto the x' axis is then

$$B'(x') = \int B'(x',y')dy' = S' \int \hat{V}(u',0) e^{-i2\pi u'x'} du'. \qquad (4)$$

Samples of $\hat{V}(u',0)$ are obtained by observing a source at constant hour angle, H_o, with baselines of the same orientation but various lengths $<s_o$. The position angle of the u' axis, and thus the position angle of the one dimensional brightness distribution, is given by

$$P = \pi/2 - \arctan(v/u) = \pi/2 - \arctan(\sin\delta_o \tan H_o). \qquad (5a)$$

The length of the projected baseline is

$$u' = \sqrt{(u^2+v^2)} = s_o(\cos^2 H_o + \sin^2\delta_o \sin^2 H_o)^{\frac{1}{2}}. \qquad (5b)$$

For sources observed at transit, $H_o = 0$, there is no rotation or shortening of the baseline, $P = \pi/2$ and $u' = s_o$.

b) Selection of Sources

The sources observed in this program were selected from the resolved sources of Fomalont (EF II) and Ekers (1969). Several criteria were used in this selection:

1) the source must have a known or suspected large component in addition to small structure. This is indicated by a rise in the visibility at small spacings.
2) the source must be extragalactic.
3) the halo must have a half power width greater than 2'. This guarantees that the halo will be resolved (visibility <0.3) at the maximum spacing.
4) the halo must have a flux density four times greater than the confusion flux at 605 MHz. For the Owens Valley antennas, the expectation value of confusion is 0.6 f.u.* This sets a lower limit of 2.4 f.u. at 605 MHz for the

---

*The unit of flux density is the "flux unit," abbreviated "f.u." 1 f.u. = $10^{-26} Wm^{-2} Hz^{-1}$.

halos. In general, only the flux density at 1425 MHz was known. Assuming a spectral index -0.8 for the halos, a lower limit of 1.2 f.u. at 1425 MHz is required.

Confusion flux is the name for the flux contribution from unknown sources in the beam. For a given antenna, the confusion level increases with wavelength since the beamwidth is wider and the radio sources are generally stronger. The experimental determination of confusion level at 605 MHz is described in Appendix A.

Criteria 3) and 4) were sometimes relaxed for marginal cases. Twenty-eight sources were chosen in this way. Twenty of these are listed by Fomalont as either core-halo or unequal double. Sagittarius A was also observed. Since this is not an extragalactic radio source it is treated separately and a discussion of it and its brightness distribution are given in Appendix B.

c) Observing Procedure and Equipment

All observations were made at the Owens Valley Radio Observatory using the two 90' antennas as an east-west interferometer. The dates at various spacings, the

antenna separations in wavelengths, and the local oscillator frequencies are given in Table 1. The observing frequency was shifted occasionally to avoid interference. Observations at 100 ft. were made only at night due to strong solar interference. At larger spacings the sun was sufficiently resolved to allow daytime operations

An attempt was made to observe each source three times at each spacing. Each observation lasted eight to ten minutes All sources were observed at zero hour angle to get the east-west brightness distribution. In addition, where scheduling permitted, high declination objects were observed off transit to obtain other baseline orientations. As can be seen from Eq. 5a), baseline rotations greater than 30° can be had for objects with $|\delta_o|>20°$ while staying within the $|H_o|\leq 4^h$ tracking limits of the antennas.

The receiving system used is similar to that described by Read (1963). A corner reflector feed was used for the 1967 observations and a diagonal horn (Love 1962) for the rest. In both cases the feed was linearly polarized with the E vector at position angle zero. The receiver was a crystal mixer with no r.f. amplification. Both sidebands were accepted. The I.F. bandpass had a center frequency of 10 MHz and a width of 5 MHz. The total system temperature was about 300°K. The phase of one local oscillator signal was continually shifted to produce fringes with a constant period of one minute in all parts of the

TABLE I

OBSERVING SCHEDULE

Dates		S_o	S_o	ν
Start	End	(ft.)	(λ)	(MHz)
1967 Dec 18	1967 Dec 22	1600	978	601.12
1967 Dec 22	1967 Dec 27	800	489	601.12
1967 Dec 27	1968 Jan 1	400	244	601.12
1968 Jan 2	1968 Jan 5	100	61	601.12
1968 Jan 5	1968 Jan 8	200	122	601.75
1968 July 10	1968 July 12	100	63	615.00
1968 July 12	1968 July 16	1200	733	601.00
1968 Nov 25	1968 Nov 27	100	62	607.28
1968 Nov 27	1968 Dec 2	300	185	607.28
1968 Dec 17	1968 Dec 20	600	370	607.00
1968 Dec 20	1968 Dec 23	1400	864	607.00
1968 Dec 23	1968 Dec 27	1000	617	607.00
1968 Dec 27	1968 Dec 31	700	432	607.00
1968 Dec 31	1969 Jan 3	1100	679	607.00

sky. Delay cable was added in one I.F. line to keep the source centered in the delay pattern (Swenson 1969). The output of the correlator was passed through a 1/60 Hz bandpass filter, and the fringes were then sampled each 5 seconds. These samples were recorded in digital form on magnetic tape along with the time and the amount of phase shift introduced in the local oscillator signal. The tapes were later reduced on an IBM 7094 computer. The program for calculating the visibility amplitude and phase is described by Fomalont et al. (1967).

The noise level at the output of each I.F. channel was kept at a constant level by an automatic gain control (A.G.C.). As long as the system noise, primarily generated in the mixer and the first stage of the I.F. amplifier, is constant, the A.G.C. stabilizes the I.F. gain However, when the observed source is strong enough to appreciably increase the system noise, the gain is decreased for that observation. The gain change is determined by removing the A.G.C. and measuring the increase in I.F. noise power when the antenna is pointed at the source. If the fractional change in noise power for the two antennas is ΔP_1 and ΔP_2, the correction applied to the measured visibility amplitude is $C = \sqrt{\Delta P_1 \Delta P_2}$. This is called the A.G.C. correction. This correction was only significant for 3C274 and SGR A.

d) Calibration

Three calibration parameters must be inserted in Eq. (1) to obtain the visibility; these are the instrumental gain, G(t), the instrumental phase, $\psi_I(t)$, and the phase error due to error in the baseline, ψ_{BL}. These parameters are determined by observations of standard sources, i.e. sources with small diameters and accurately known positions and flux densities, which therefore have zero visibility phase and constant apparent flux density at all spacings. The standard sources used in this work are given in Table 2. The first part of the table contains the sources used for the hourly gain and phase calibration while the latter part contains additional sources used in the baseline calibration.

Most of the 605 MHz flux densities were taken from Adgie and Gent (1966) and Conway *et al.* (1965). When there was a difference between the flux values in the two papers, the mean value was used. The flux scale thus established was later found to be on the average 2.3% higher than the values obtained by interpolating between the fluxes at 178 and 750 MHz given by Kellermann *et al.* (1969). The flux scale used in this work does not include this 2.3% correction.

TABLE 2

PHASE AND FLUX CALIBRATORS

SOURCE	R.A. (1950.0)	DEC. (1950.0)	FLUX (f.u.)
	h m s	° ' "	
3C2	00 03 48.70	-00 21 06.6	6.3
3C48	01 34 49.82	+32 54 20.2	28.9
3C71	02 40 07.10	-00 13 31.5	8.6
CTA21	03 16 09.1	+16 17 40.	9.4
3C91	03 34 03.80	+50 36 03.0	6.2
3C133	04 59 54.3	+25 12 12.	10.8
3C147	05 38 43.53	+49 49 43.1	36.8
3C161	06 24 43.01	-05 51 15.	30.7
3C181	07 25 20.36	+14 43 47.2	4.4
3C196	08 09 59.39	+48 22 08.0	27.5
3C216	09 06 17.26	+43 05 59.0	8.1
3C237	10 05 22.07	+07 44 59.	11.6
3C254	11 11 53.35	+40 53 42.0	6.9
P1151-34	11 51 49.8	-34 48 40.	7.5
3C273	12 26 32.9	+02 19 38.	50.0
3C287	13 28 16.12	+25 24 37.1	10.5
3C298	14 16 38.82	+06 42 21.6	14.4
3C317	15 14 17.00	+07 12 16.7	15.5
3C336	16 22 32.6	+23 52 07.	5.0
3C351	17 04 04.8	+60 48 50.	4.7
3C380	18 28 13.38	+48 42 39.3	25.9
3C401	19 39 38.82	+60 34 31.5	9.9
3C424	20 45 44.40	+06 50 10.2	5.3
3C438	21 53 45.5	+37 46 14.	15.7
3C459	23 14 02.30	+03 48 56.0	9.2

TABLE 2 CONT.

ADDITIONAL BASELINE CALIBRATORS

SOURCE	R.A. (1950.0)	DEC. (1950.0)
	h m s	° ' "
3C43	01 27 15.18	+23 22 52.0
3C93	03 40 51.47	+04 48 21.6
3C119	04 29 07.84	+41 32 08.7
3C123	04 33 55.30	+29 34 13.4
PO438-43	04 38 43.8	-43 38 51.
3C138	05 18 16.51	+16 35 26.2
PO521-36	05 21 13.2	-36 30 17.
3C171	06 51 11.00	+54 12 48.0
PO704-23	07 04 27.3	-23 06 54.
PO736+01	07 36 42.4	+01 44 00.
PO825-20	08 25 03.4	-20 16 30.
3C207	08 38 01.73	+13 23 05.4
3C212	08 55 55.62	+14 21 24.2
3C241	10 19 09.49	+22 14 20.0
3C245	10 40 06.11	+12 19 15.1
P1116+12	11 16 20.79	+12 51 06.3
P1215-45	12 15 28.3	-45 43 36.
3C270.1	12 18 04.00	+33 59 50.0
3C345	16 41 17.70	+39 54 11.1
3C360	17 30 13.55	-13 02 50.
P1827-36	18 27 37.0	-36 04 48.
P1938-15	19 38 24.3	-15 31 34.
3C418	20 37 07.4	+51 08 35.
P2115-30	21 15 11.0	-30 31 53.
3C446	22 23 11.05	-05 12 17.0
3C454.3	22 51 29.61	+15 52 53.6
P2322-12	23 22 43.72	-12 23 56.4

The positions given in Table 2 were taken primarily from Fomalont (EF II), Fomalont *et al.* (1967), Wyndham (1966), Griffin (1963), Sandage *et al.* (1965), and Veron (1966).

The calibration procedure is the same as that used by Fomalont (EF I). Calibrators were observed at least once an hour. On an average day the system gain might vary by 15% and the phase by 0.080 lobes in ten hours. Both gain and phase variations were greatest during the day.

A special set of observations was made at each spacing to determine the baseline parameters. The baseline is defined as the line between the intersection of the polar and declination axes on the two antennas. The interferometer pole is the point where the extension of this line intersects the celestial sphere. The baseline is described by three parameters, the baseline length (s), measured in wavelengths at the observing frequency and the hour angle (h) and declination (d) of the interferometer pole. For an east-west interferometer:

$$h = +\pi/2 + h'$$
$$d = 0 + d'$$
$$s = s_o + s',$$

where h', d', and s' are errors in the assumed baseline parameters. These baseline errors introduce errors in the visibility phase given by:

$$\psi_{BL} = -s' \cos\delta_o \sin H_o - s_o d' \sin\delta_o + s_o h' \cos\delta_o \cos H_o .$$

To make the baseline calibration, twelve to sixteen calibrators were observed at night, when the instrumental phase variation is small. Observation of such a large number of sources gives a large amount of redundancy in determining s', d', and h'. Typical values obtained for the corrections were $s' \simeq 0.01 \pm 0.01$ wavelengths, $h' \simeq 3^s \pm 0^s.3$, and $d' \simeq 40'' \pm 3''$.

e) Errors in the Complex Visibility

There are two main sources of error in the visibility amplitude; these are i) the internal error in measuring the fringe amplitude at the output of the interferometer, and ii) the error in calibrating this fringe amplitude in terms of flux density. Let σ_i and σ_c be the r.m.s. errors in V due to these two effects.

An estimate of σ_i is obtained from the variance in the measured flux density of sources which were observed several times on successive days at the same spacing. Since the same calibrators were used each day, this standard deviation does not reflect the calibration error. Using S' to normalize the variance, an empirical estimate of σ_i for a single observation is obtained;

$$\sigma_i' = 0.04/S' + \gamma V$$

where γ is an error factor which is roughly 0.01. The first

term is the error in the fringe amplitude due to system noise. This agrees with the r.m.s. flux error expected from an interferometer with a system temperature of 300°K, a bandwidth of 5 MHz, and an eight minute integration time. The second term probably arises from small changes in the system gain during the eight minute observing period. For sources with a flux density greater than 20 or 30 f.u., the error factor γ falls to 0.005. Most sources were observed several times; since the internal errors are independent from day to day, the resulting internal visibility amplitude error is $\sigma_i = \sigma_i' / \sqrt{N}$, where N is the number of observations of a source at a given spacing. σ_i is usually one or two percent.

The main source of error is in the calibration. The error in the absolute flux density of the flux standards is about 5%. An additional error is introduced by confusing sources in the beam during the observations of these calibrators. Since at each spacing the phase of the confusion may have an arbitrary value the confusion flux combines with the calibrator flux like a random error. The average calibrator flux density is about 15 f.u. and the expectation value of the confusion is 0.6 f.u. This leads to an average r.m.s. confusion error of 4% which agrees well with the observed variations of the calibrator visibility amplitudes with spacing. Combining the error in the absolute flux

density and the confusion error quadratically, the variance of a single calibrator flux density is 6.4%. In general several flux calibrators were used to determine the instrumental gain at the time of each source observation. Since the errors of each of these calibrators are independent, the final calibration error is reduced by the square root of the number of standards used, generally about four. Thus, the r.m.s. error due to calibration of a single observation is $\sigma_c \simeq 6.4\% / \sqrt{4} = 3.2\%$. Since the same standards were used to calibrate a given source on successive days, the calibration errors are strongly correlated and repeated observations will not reduce σ_c.

The standard deviation of the visibility amplitude is given by $\sigma_A = \sqrt{(\sigma_i^2 + \sigma_c^2)}$, which generally equals about 4%.

The error in the visibility phase is derived in a similar way. There is an internal error in measuring the fringe phase, σ_i, and a calibration error σ_c. An estimate of the internal phase error is obtained by noting the spread of observed phases for sources which were observed several times at a single spacing. This error is about 0.007 lobes which is far larger than that expected from system noise. It probably arises from phase instability in the interferometer during the eight minute observing period. Error in the final baseline parameters contributes another 0.005 lobe error to σ_i. Since the sources were generally

observed at the same hour angle each day, the baseline contribution is non-random and is not reduced by repeated observations.

$$\sigma_i = \sqrt{[(0.007)^2/N + (0.005)^2]} \approx 0.006$$

for N, the number of observations, equal to two or three.

Four factors contribute to the error in the phase of a calibrator. The average error in the adopted positions of the calibrators is about 2" which produces a phase error of about 0.005 lobes at a spacing of 800 feet. Although this phase error is spacing dependent the value of 0.005 lobes will be used in the error analysis. The 4% confusion level introduces an additional error of 0.007 lobes. The 0.007 lobe error due to phase instability and the 0.005 lobe error due to baseline error are also present. If M calibrators are used to determine the instrumental phase at the time of a source observation, the final calibration error is

$$\sigma_c = \sqrt{\{[(0.005)^2 + (0.007)^2 + (0.007)^2/N + (0.005)^2]\ 1/M\}}.$$

Since the calibrator phase error due to instrumental instability is uncorrelated on successive days it is divided by N, the number of observations of the source. For M equal to four and N equal to three $\sigma_c \sim 0.006$ lobes. The total phase standard deviation is $\sigma_p = \sqrt{(\sigma_i^2 + \sigma_c^2)} \simeq 0.009$ lobes. At the larger spacings and for off transit sources the baseline and calibrator position errors are more

important and σ_p may be about 50% larger.

Confusion in the source observations is less of a problem since the synthesized beam has about 1/20 of the area of the primary beam. Therefore the probability that a background source lies within a synthesized beamwidth of some part of the main source is reduced considerably. Background sources are more likely to stand out as separate objects on the synthesized maps. Even with the increased resolution, the best criterion for distinguishing confusing objects from physically related parts of the main source is that the further apart they are, the more likely they are to be unrelated.

f) Visibilities

The measured source visibilities are given in Table 3. Under source parameters are listed the source name, an alternate name if one exists, the right ascension and declination used in the reduction (1950.0 coordinates), and a flux density. If additional observations were made off transit, the visibility values are listed after the on transit values and the position angle (in degrees) of the projected baseline is given. For the on transit observations the position angle is 90°. Under source observations are listed the projected antenna spacing (in wavelengths),

the visibility amplitude and phase with errors enclosed in parenthesis, and the number of observations at each spacing. These errors do not include the calibration error.

The visibility amplitudes are normalized to the flux value listed This flux usually includes any confusing sources which may be in the beam and is not necessarily the flux of the main source alone. The phases are relative to the positions given. A few notes on individual sources are at the end of the table.

SOURCE VISIBILITY FUNCTIONS

TABLE 3

SOURCE VISIBILITY FUNCTIONS

SOURCE PARAMETERS	SPACING	VIS AMP	VIS PHASE	NO
3C20				
RA 0 40 19.70	62.	1.01 (0.02)	-0.010 (.003)	5
DEC 51 46 53.0	122.	1.05 (0.02)	-0.013 (.005)	1
FLUX 18.7	185.	1.02 (0.02)	-0.001 (.003)	3
	244.	1.06 (0.01)	-0.003 (.006)	3
	370.	1.03 (0.01)	0.007 (.002)	2
	431.	1.06 (0.01)	0.005 (.003)	3
	489.	1.02 (0.01)	-0.010 (.009)	2
	615.	1.03 (0.05)	-0.001 (.004)	2
	677.	1.01 (0.01)	-0.006 (.003)	3
	732.	0.94 (0.03)	0.003 (.007)	2
	863.	1.03 (0.01)	-0.002 (.003)	3
	978.	0.95 (0.01)	0.002 (.011)	2
P0045-25 NGC 253				
RA 0 45 6.00	62.	0.99 (0.02)	-0.005 (.015)	6
DEC -25 33 52.0	122.	0.92 (0.02)	0.025 (.005)	1
FLUX 9.4	185.	0.82 (0.01)	0.017 (.003)	3
	245.	0.62 (0.01)	-0.019 (.005)	3
	370.	0.53 (0.01)	0.002 (.002)	2
	432.	0.47 (0.01)	-0.036 (.005)	3
	489.	0.49 (0.01)	-0.000 (.007)	3
	617.	0.41 (0.01)	-0.021 (.005)	2
	679.	0.37 (0.01)	0.001 (.005)	3
	733.	0.33 (0.01)	-0.060 (.006)	3
	864.	0.34 (0.01)	-0.038 (.005)	3
	975.	0.13 (0.02)	-0.044 (.017)	2
P0045-25				
	91.	0.81 (0.02)	-0.008 (.003)	2
P.A. = 65.2	138.	0.75 (0.01)	0.019 (.003)	3
	184.	0.70 (0.01)	-0.018 (.004)	4
	281.	0.51 (0.01)	0.008 (.003)	2
	322.	0.49 (0.01)	-0.109 (.003)	3
	367.	0.42 (0.02)	0.050 (.016)	2
	466.	0.41 (0.01)	0.008 (.005)	3
	509.	0.41 (0.01)	-0.018 (.004)	3
	557.	0.32 (0.01)	0.010 (.006)	3
	651.	0.36 (0.01)	-0.024 (.006)	2
	738.	0.35 (0.03)	-0.175 (.017)	1

SOURCE VISIBILITY FUNCTIONS

SOURCE PARAMETERS	SPACING	VIS AMP	VIS PHASE	NO
P0045-25				
	90.	0.98 (0.02)	0.028 (.003)	2
P.A. = 116.2	137.	0.98 (0.02)	-0.004 (.003)	3
	177.	0.96 (0.01)	-0.010 (.006)	3
	277.	0.79 (0.01)	0.014 (.002)	2
	316.	0.75 (0.02)	-0.032 (.003)	3
	353.	0.75 (0.02)	0.024 (.005)	4
	448.	0.57 (0.02)	-0.018 (.006)	2
	502.	0.69 (0.01)	-0.018 (.004)	3
	538.	0.60 (0.01)	-0.041 (.006)	3
	630.	0.54 (0.01)	-0.035 (.006)	2
	745.	0.44 (0.02)	0.026 (.011)	2
3C31 NGC 383				
RA 1 4 41.90	62.	0.90 (0.02)	-0.015 (.004)	5
DEC 32 8 45.0	122.	0.97 (0.02)	0.018 (.006)	2
FLUX 9.4	185.	0.97 (0.02)	-0.013 (.009)	2
	244.	0.80 (0.01)	-0.031 (.004)	3
	370.	0.77 (0.01)	-0.023 (.002)	2
	431.	0.62 (0.04)	0.031 (.003)	3
	489.	0.66 (0.02)	0.004 (.007)	2
	616.	0.65 (0.04)	0.004 (.004)	2
	678.	0.61 (0.03)	-0.028 (.009)	3
	733.	0.46 (0.01)	-0.017 (.006)	3
	863.	0.48 (0.01)	-0.032 (.008)	3
	978.	0.31 (0.02)	-0.004 (.012)	2
3C31				
	95.	0.81 (0.02)	-0.003 (.003)	2
P.A. = 120.0	144.	0.77 (0.01)	0.018 (.003)	3
	192.	0.58 (0.01)	-0.019 (.004)	3
	291.	0.38 (0.01)	0.053 (.003)	2
	337.	0.50 (0.01)	-0.092 (.003)	3
	381.	0.19 (0.01)	0.017 (.012)	3
	485.	0.28 (0.01)	0.046 (.005)	3
	531.	0.18 (0.01)	0.005 (.014)	2
	579.	0.13 (0.01)	0.243 (.010)	2
	677.	0.12 (0.01)	-0.336 (.014)	2
	765.	0.17 (0.02)	-0.388 (.036)	3

SOURCE VISIBILITY FUNCTIONS

TABLE 3 CONT.

SOURCE VISIBILITY FUNCTIONS

SOURCE PARAMETERS		SOURCE OBSERVATIONS			
		SPACING	VIS AMP	VIS PHASE	NO
3C40	P0123-01				
RA	1 23 26.30	62.	0.98 (0.02)	-0.001 (.002)	3
DEC	-1 37 9.0	185.	0.73 (0.01)	-0.005 (.005)	3
FLUX	13.6	370.	0.37 (0.01)	0.034 (.002)	2
		432.	0.31 (0.01)	0.101 (.005)	3
		616.	0.34 (0.01)	0.208 (.009)	2
		678.	0.34 (0.01)	0.227 (.005)	3
		733.	0.33 (0.01)	0.251 (.006)	3
		864.	0.32 (0.01)	0.280 (.004)	3
3C66					
RA	2 19 57.60	62.	0.93 (0.02)	0.003 (.003)	2
DEC	42 45 47.0	122.	0.76 (0.01)	-0.007 (.002)	4
FLUX	18.9	185.	0.47 (0.01)	-0.017 (.003)	3
		244.	0.31 (0.01)	0.039 (.004)	3
		370.	0.42 (0.01)	0.275 (.002)	2
		432.	0.50 (0.01)	0.301 (.003)	3
		489.	0.44 (0.01)	0.263 (.006)	3
		617.	0.21 (0.02)	0.202 (.011)	2
		679.	0.08 (0.00)	0.099 (.008)	3
		733.	0.14 (0.00)	-0.207 (.006)	3
		864.	0.33 (0.01)	-0.313 (.005)	3
		978.	0.25 (0.01)	-0.407 (.016)	3
3C78	P0305+03				
RA	3 5 48.70	62.	0.95 (0.02)	0.006 (.003)	2
DEC	3 55 13.0	122.	1.02 (0.02)	0.008 (.005)	3
FLUX	12.5	185.	0.96 (0.02)	-0.004 (.003)	3
		244.	1.00 (0.01)	0.002 (.004)	3
		370.	0.95 (0.01)	0.011 (.003)	1
		432.	0.91 (0.01)	0.015 (.003)	3
		489.	0.90 (0.01)	0.006 (.005)	3
		617.	0.86 (0.01)	0.006 (.004)	2
		679.	0.77 (0.01)	0.005 (.004)	3
		732.	0.75 (0.02)	0.020 (.006)	3
		864.	0.70 (0.01)	0.017 (.004)	3
		978.	0.58 (0.01)	0.036 (.014)	4

SOURCE PARAMETERS		SOURCE OBSERVATIONS			
		SPACING	VIS AMP	VIS PHASE	NO
3C105	P0404+03				
RA	4 4 44.88	62.	1.00 (0.02)	-0.004 (.003)	3
DEC	3 33 18.0	122.	1.00 (0.05)	0.018 (.003)	2
FLUX	9.5	185.	0.90 (0.02)	-0.022 (.003)	3
		244.	0.84 (0.01)	-0.008 (.004)	3
		370.	0.65 (0.01)	0.011 (.004)	2
		431.	0.65 (0.01)	0.048 (.003)	3
		486.	0.60 (0.01)	0.037 (.006)	3
		615.	0.50 (0.01)	0.104 (.004)	2
		678.	0.54 (0.01)	0.142 (.005)	3
		732.	0.63 (0.01)	0.180 (.006)	3
		862.	0.69 (0.01)	0.190 (.005)	2
		978.	0.66 (0.01)	0.196 (.008)	4
3C120	P0430+05				
RA	4 30 29.40	62.	0.88 (0.02)	0.002 (.003)	3
DEC	5 14 40.0	122.	0.99 (0.02)	0.041 (.003)	3
FLUX	5.9	185.	0.87 (0.02)	0.016 (.003)	3
		244.	0.96 (0.02)	0.032 (.004)	3
		370.	0.83 (0.01)	0.093 (.002)	2
		432.	0.93 (0.01)	0.070 (.003)	3
		489.	0.74 (0.02)	0.083 (.017)	3
		616.	0.77 (0.02)	0.106 (.004)	2
		679.	0.87 (0.01)	0.120 (.004)	3
		733.	0.68 (0.02)	0.134 (.006)	3
		864.	0.78 (0.02)	0.130 (.005)	3
		978.	0.69 (0.03)	0.158 (.009)	3
3C130					
RA	4 48 54.30	62.	0.84 (0.02)	0.017 (.003)	3
DEC	51 59 45.0	122.	0.93 (0.02)	-0.009 (.003)	3
FLUX	7.0	185.	0.94 (0.02)	0.009 (.003)	3
		244.	0.74 (0.02)	-0.013 (.004)	3
		370.	0.67 (0.01)	-0.021 (.003)	2
		432.	0.53 (0.01)	-0.006 (.003)	3
		489.	0.41 (0.02)	0.006 (.008)	3
		617.	0.23 (0.02)	-0.035 (.013)	2
		679.	0.26 (0.01)	0.010 (.006)	3
		733.	0.16 (0.01)	0.030 (.009)	3
		864.	0.06 (0.01)	0.254 (.031)	4
		978.	0.04 (0.02)	0.242 (.071)	3

TABLE 3 CONT.

SOURCE VISIBILITY FUNCTIONS

SOURCE PARAMETERS	SOURCE OBSERVATIONS			
	SPACING	VIS AMP	VIS PHASE	NO
3C130				
P.A. = 41.6	106.	0.64 (0.02)	-0.004 (.003)	3
	159.	0.65 (0.01)	0.008 (.003)	3
	212.	0.58 (0.02)	-0.007 (.009)	3
	321.	0.44 (0.01)	0.038 (.006)	2
	372.	0.26 (0.01)	0.009 (.006)	2
	422.	0.26 (0.02)	-0.061 (.015)	3
	532.	0.10 (0.02)	-0.079 (.019)	2
	587.	0.04 (0.01)	0.042 (.038)	2
	635.	0.10 (0.01)	0.469 (.012)	3
	742.	0.04 (0.02)	-0.453 (.050)	2
	844.	0.16 (0.02)	-0.487 (.015)	3
+ +	+	+ +	+ +	
3C130				
P.A. = 127.7	56.	0.86 (0.04)	0.011 (.004)	2
	110.	0.69 (0.02)	-0.019 (.007)	2
	167.	0.78 (0.02)	0.007 (.003)	3
	220.	0.81 (0.02)	0.032 (.004)	3
	335.	0.81 (0.01)	-0.029 (.004)	2
	392.	0.87 (0.01)	-0.056 (.004)	2
	440.	0.80 (0.02)	0.028 (.011)	3
	557.	0.81 (0.02)	0.040 (.005)	1
	614.	0.89 (0.01)	0.017 (.007)	2
	665.	0.84 (0.02)	0.020 (.005)	4
	784.	0.70 (0.04)	0.012 (.005)	2
	877.	0.79 (0.03)	0.021 (.012)	2
P0625-35 M06-3/8				
RA 6 25 20.80	62.	1.00 (0.04)	-0.035 (.003)	3
DEC -35 27 12.0	122.	1.00 (0.05)	0.023 (.003)	3
FLUX 7.2	185.	0.98 (0.02)	-0.004 (.003)	3
	244.	0.97 (0.02)	-0.004 (.004)	3
	370.	0.95 (0.01)	0.006 (.002)	2
	432.	0.85 (0.01)	-0.035 (.003)	3
	489.	0.85 (0.02)	0.017 (.007)	2
	617.	0.74 (0.02)	0.009 (.004)	2
	678.	0.68 (0.01)	-0.001 (.005)	2
	733.	0.65 (0.02)	-0.016 (.011)	3
	864.	0.57 (0.02)	-0.016 (.005)	2
	978.	0.45 (0.02)	0.021 (.015)	3

SOURCE VISIBILITY FUNCTIONS

SOURCE PARAMETERS	SOURCE OBSERVATIONS			
	SPACING	VIS AMP	VIS PHASE	NO
P0715-36 M07-3/5				
RA 7 15 19.20	62.	0.94 (0.02)	-0.061 (.006)	3
DEC -36 15 48.0	122.	0.76 (0.02)	-0.014 (.003)	3
FLUX 5.5	185.	0.56 (0.02)	-0.033 (.004)	3
	244.	0.58 (0.04)	-0.044 (.007)	3
	370.	0.65 (0.05)	0.036 (.009)	2
	432.	0.59 (0.01)	0.003 (.004)	3
	489.	0.65 (0.03)	0.080 (.010)	3
	616.	0.50 (0.03)	0.017 (.021)	2
	679.	0.27 (0.03)	-0.053 (.008)	2
	733.	0.18 (0.03)	-0.037 (.015)	2
	863.	0.29 (0.02)	0.235 (.010)	2
	977.	0.45 (0.03)	0.197 (.013)	2
P0843-33 NGC 2663				
RA 8 43 8.70	62.	0.87 (0.03)	-0.002 (.004)	3
DEC -33 37 6.0	122.	1.01 (0.04)	0.006 (.003)	3
FLUX 3.4	185.	0.94 (0.03)	0.020 (.004)	3
	245.	0.94 (0.05)	-0.001 (.005)	2
	370.	0.81 (0.02)	0.018 (.011)	2
	432.	0.61 (0.02)	-0.042 (.006)	2
	489.	0.73 (0.04)	0.026 (.009)	3
	617.	0.72 (0.03)	-0.018 (.007)	3
	679.	0.62 (0.02)	-0.014 (.010)	2
	733.	0.54 (0.02)	-0.050 (.016)	2
	863.	0.49 (0.04)	-0.022 (.010)	2
	977.	0.56 (0.05)	-0.017 (.013)	3
3C218 HYA A				
RA 9 15 41.30	62.	0.98 (0.02)	-0.008 (.002)	3
DEC -11 53 4.0	122.	0.94 (0.01)	0.019 (.003)	2
FLUX 92.3	185.	0.90 (0.02)	0.006 (.002)	3
	244.	0.92 (0.00)	-0.005 (.004)	4
	370.	0.88 (0.01)	0.006 (.002)	2
	431.	0.92 (0.01)	-0.000 (.003)	3
	489.	0.88 (0.01)	0.004 (.005)	3
	615.	0.82 (0.01)	0.019 (.007)	2
	679.	0.86 (0.01)	-0.008 (.003)	3
	733.	0.84 (0.02)	-0.004 (.006)	3
	862.	0.80 (0.01)	0.006 (.004)	2
	976.	0.78 (0.02)	0.002 (.009)	3

TABLE 3 CONT.

SOURCE VISIBILITY FUNCTIONS

SOURCE PARAMETERS	SOURCE OBSERVATIONS			
	SPACING	VIS AMP	VIS PHASE	NO
P0935-28 M09-2/7				
RA 9 35 49.10	62.	0.98 (0.02)	-0.022 (.003)	3
DEC -28 59 6.0	122.	0.96 (0.04)	0.004 (.003)	2
FLUX 4.4	164.	0.80 (0.02)	0.009 (.003)	5
	245.	0.83 (0.03)	0.012 (.004)	3
	370.	0.86 (0.02)	0.006 (.005)	3
	432.	0.61 (0.01)	-0.016 (.004)	3
	489.	0.55 (0.04)	-0.004 (.012)	2
	617.	0.59 (0.03)	0.019 (.010)	2
	679.	0.45 (0.01)	-0.004 (.006)	3
	733.	0.35 (0.02)	-0.073 (.020)	3
	863.	0.12 (0.03)	-0.108 (.028)	2
	977.	0.17 (0.04)	-0.039 (.022)	3
3C231				
RA 9 51 43.75	62.	1.01 (0.02)	-0.015 (.003)	3
DEC 69 54 56.0	122.	0.97 (0.02)	-0.016 (.003)	2
FLUX 11.2	185.	0.99 (0.02)	-0.017 (.003)	3
	245.	0.98 (0.01)	0.004 (.004)	3
	370.	0.83 (0.01)	-0.009 (.002)	2
	432.	1.00 (0.02)	-0.019 (.003)	3
	489.	0.92 (0.03)	0.013 (.007)	2
	617.	0.87 (0.01)	-0.007 (.004)	2
	679.	0.91 (0.01)	-0.014 (.003)	3
	733.	0.86 (0.02)	-0.002 (.006)	3
	864.	0.83 (0.03)	-0.012 (.004)	2
	978.	0.79 (0.02)	-0.005 (.010)	3
+ + + + + + +				
3C231				
	60.	1.00 (0.02)	-0.017 (.003)	2
P.A. = 47.3	119.	0.95 (0.02)	-0.013 (.003)	2
	180.	0.87 (0.02)	-0.003 (.003)	3
	238.	1.00 (0.01)	0.010 (.005)	2
	359.	0.92 (0.02)	0.002 (.002)	2
	419.	0.84 (0.01)	-0.018 (.003)	3
	475.	0.89 (0.02)	0.024 (.007)	2
	599.	0.90 (0.01)	-0.004 (.004)	2
	659.	0.88 (0.01)	0.028 (.003)	3
	712.	0.78 (0.02)	0.009 (.006)	3
	838.	0.81 (0.02)	0.017 (.004)	3
	950.	0.87 (0.02)	0.014 (.009)	3
+ + + + + + +				

SOURCE VISIBILITY FUNCTIONS

SOURCE PARAMETERS	SOURCE OBSERVATIONS			
	SPACING	VIS AMP	VIS PHASE	NO
3C231				
	60.	1.01 (0.02)	-0.011 (.003)	2
P.A. = 134.0	118.	0.95 (0.02)	-0.027 (.005)	1
	180.	0.99 (0.03)	-0.000 (.003)	3
	237.	0.94 (0.02)	-0.009 (.004)	4
	359.	0.96 (0.01)	-0.014 (.003)	1
	418.	0.96 (0.01)	-0.050 (.004)	2
	475.	0.84 (0.02)	0.029 (.011)	2
	598.	0.94 (0.01)	-0.017 (.004)	2
	657.	0.87 (0.02)	-0.010 (.006)	1
	711.	0.94 (0.04)	-0.015 (.007)	2
	837.	0.82 (0.02)	-0.021 (.006)	1
	949.	0.92 (0.02)	-0.002 (.011)	2
3C236				
RA 10 3 5.50	62.	0.78 (0.02)	-0.007 (.003)	3
DEC 35 8 49.0	122.	0.61 (0.02)	-0.058 (.003)	2
FLUX 7.8	185.	0.64 (0.01)	-0.013 (.006)	3
	244.	0.64 (0.02)	0.047 (.004)	3
	370.	0.67 (0.01)	-0.007 (.002)	2
	432.	0.59 (0.01)	0.020 (.003)	3
	489.	0.58 (0.02)	-0.014 (.008)	2
	616.	0.64 (0.02)	0.014 (.006)	2
	679.	0.57 (0.01)	-0.003 (.004)	3
	733.	0.59 (0.02)	0.028 (.006)	3
	864.	0.65 (0.02)	0.012 (.005)	2
	976.	0.53 (0.02)	-0.018 (.017)	3
3C247				
RA 10 56 9.40	62.	0.87 (0.02)	-0.036 (.003)	3
DEC 43 17 35.0	122.	0.68 (0.02)	-0.035 (.002)	4
FLUX 6.8	185.	0.54 (0.01)	-0.012 (.004)	3
	245.	0.77 (0.02)	0.023 (.004)	3
	370.	0.88 (0.02)	-0.051 (.006)	2
	432.	0.72 (0.01)	-0.048 (.004)	3
	489.	0.68 (0.02)	-0.059 (.012)	3
	617.	0.78 (0.02)	-0.031 (.004)	2
	679.	0.86 (0.01)	-0.057 (.004)	3
	733.	0.84 (0.02)	-0.056 (.007)	2
	864.	0.72 (0.01)	-0.019 (.004)	3
	978.	0.86 (0.02)	-0.070 (.023)	3
+ + + + + + +				

TABLE 3 CONT.

SOURCE VISIBILITY FUNCTIONS

SOURCE PARAMETERS	SOURCE OBSERVATIONS			
	SPACING	VIS AMP	VIS PHASE	NO
3C247				
P.A. = 44.8	97.	0.77 (0.02)	-0.038 (.003)	3
	148.	0.71 (0.03)	-0.012 (.005)	3
	198.	0.80 (0.02)	-0.011 (.005)	2
	294.	0.62 (0.01)	-0.028 (.003)	2
	345.	0.66 (0.01)	-0.015 (.003)	3
	389.	0.80 (0.02)	0.004 (.008)	2
	493.	0.66 (0.02)	-0.026 (.004)	2
	544.	0.80 (0.01)	0.011 (.004)	3
	584.	0.84 (0.02)	-0.027 (.006)	3
	689.	0.83 (0.01)	-0.060 (.004)	3
	782.	0.77 (0.02)	-0.082 (.009)	3
+ +	+ +	+ +	+	
3C247				
P.A. = 124.2	104.	0.85 (0.02)	-0.030 (.003)	3
	161.	0.70 (0.02)	-0.023 (.003)	3
	209.	0.79 (0.02)	-0.008 (.009)	3
	317.	0.79 (0.01)	-0.030 (.004)	2
	370.	0.80 (0.02)	-0.068 (.003)	3
	420.	0.73 (0.02)	-0.019 (.009)	3
	531.	0.71 (0.02)	-0.000 (.005)	1
	583.	0.78 (0.01)	-0.007 (.008)	2
	627.	0.81 (0.02)	0.000 (.007)	3
	747.	0.73 (0.02)	-0.072 (.010)	2
	838.	0.66 (0.02)	-0.010 (.010)	3
3C264 P1142+19				
RA 11 42 32.20	61.	0.98 (0.02)	0.001 (.003)	2
DEC 19 53 3.0	122.	1.00 (0.01)	0.020 (.003)	3
FLUX 10.8	185.	0.88 (0.01)	0.005 (.002)	4
	244.	0.88 (0.01)	0.010 (.004)	3
	370.	0.74 (0.01)	-0.023 (.002)	2
	432.	0.74 (0.01)	-0.006 (.003)	3
	488.	0.67 (0.02)	-0.023 (.007)	2
	617.	0.59 (0.01)	-0.039 (.004)	2
	679.	0.60 (0.01)	-0.064 (.004)	3
	733.	0.57 (0.01)	-0.061 (.006)	3
	864.	0.57 (0.01)	-0.064 (.004)	3
	978.	0.53 (0.02)	-0.107 (.008)	4

SOURCE VISIBILITY FUNCTIONS

SOURCE PARAMETERS	SOURCE OBSERVATIONS			
	SPACING	VIS AMP	VIS PHASE	NO
P1216-10 M12-0/9				
RA 12 16 1.70	60.	0.97 (0.03)	-0.024 (.004)	2
DEC -10 2 0.0	122.	0.96 (0.03)	-0.010 (.003)	2
FLUX 5.4	185.	0.83 (0.02)	-0.003 (.003)	3
	244.	1.00 (0.02)	-0.012 (.004)	3
	370.	0.72 (0.01)	-0.003 (.003)	2
	432.	0.80 (0.01)	-0.019 (.003)	3
	488.	0.96 (0.03)	0.006 (.006)	3
	617.	0.83 (0.02)	-0.016 (.004)	2
	679.	0.81 (0.01)	-0.064 (.004)	3
	732.	0.87 (0.03)	-0.051 (.006)	3
	864.	0.66 (0.02)	-0.071 (.005)	3
	976.	0.68 (0.03)	-0.042 (.008)	4
3C274 VIR A				
RA 12 28 18.10	62.	0.97 (0.02)	-0.009 (.002)	3
DEC 12 39 43.0	122.	0.86 (0.01)	-0.009 (.003)	2
FLUX 405.0	185.	0.81 (0.02)	-0.018 (.003)	2
	245.	0.76 (0.00)	-0.002 (.005)	2
	370.	0.53 (0.00)	-0.021 (.002)	2
	432.	0.49 (0.01)	-0.016 (.003)	2
	489.	0.48 (0.01)	-0.028 (.006)	2
	617.	0.44 (0.00)	-0.030 (.004)	2
	679.	0.44 (0.00)	-0.041 (.003)	3
	733.	0.43 (0.01)	-0.044 (.006)	3
	864.	0.45 (0.00)	-0.023 (.004)	3
	978.	0.48 (0.00)	-0.018 (.009)	3
P1302-49 NGC 4945				
RA 13 2 33.10	61.	0.96 (0.07)	-0.037 (.012)	1
DEC -49 12 6.0	122.	0.84 (0.06)	0.016 (.005)	3
FLUX 9.4	185.	0.77 (0.02)	0.013 (.004)	2
	244.	0.77 (0.02)	-0.008 (.005)	2
	370.	0.59 (0.01)	0.013 (.004)	2
	432.	0.61 (0.01)	-0.069 (.003)	3
	489.	0.57 (0.02)	0.068 (.007)	3
	617.	0.56 (0.01)	-0.015 (.004)	2
	679.	0.49 (0.01)	0.013 (.005)	3
	733.	0.58 (0.04)	-0.041 (.011)	3
	864.	0.54 (0.01)	-0.007 (.012)	3
	978.	0.57 (0.02)	0.027 (.009)	3

TABLE 3 CONT.

SOURCE VISIBILITY FUNCTIONS

SOURCE PARAMETERS	SOURCE OBSERVATIONS			
	SPACING	VIS AMP	VIS PHASE	NO
3C287.1 P1330+02				
RA 13 30 21.00	62.	0.96 (0.05)	0.006 (.011)	2
DEC 2 16 18.0	122.	0.86 (0.02)	-0.006 (.003)	3
FLUX 5.5	185.	0.83 (0.02)	0.008 (.004)	2
	244.	0.83 (0.02)	0.004 (.004)	3
	369.	0.63 (0.01)	0.027 (.003)	2
	432.	0.55 (0.01)	0.004 (.004)	3
	489.	0.57 (0.03)	-0.008 (.010)	2
	617.	0.52 (0.02)	0.069 (.004)	2
	678.	0.50 (0.01)	0.051 (.005)	3
	733.	0.44 (0.01)	0.035 (.006)	3
	863.	0.46 (0.02)	0.080 (.007)	3
	977.	0.47 (0.03)	0.104 (.012)	2
P1334-29 NGC 5436				
RA 13 34 10.90	122.	0.71 (0.03)	0.021 (.003)	3
DEC -29 36 18.0	185.	0.80 (0.03)	0.000 (.005)	2
FLUX 4.2	244.	0.77 (0.03)	-0.007 (.004)	3
	370.	0.25 (0.01)	-0.023 (.008)	2
	432.	0.32 (0.01)	-0.175 (.006)	3
	489.	0.34 (0.05)	0.004 (.025)	1
	617.	0.08 (0.03)	-0.389 (.022)	2
	679.	0.07 (0.02)	-0.061 (.036)	3
	732.	0.22 (0.03)	-0.040 (.010)	3
	864.	0.09 (0.04)	-0.229 (.070)	2
	978.	0.22 (0.05)	0.031 (.024)	2
3C293				
RA 13 50 2.90	63.	0.84 (0.03)	-0.008 (.003)	2
DEC 31 41 32.0	122.	0.86 (0.02)	-0.028 (.003)	3
FLUX 8.4	185.	0.94 (0.05)	0.002 (.008)	2
	244.	0.85 (0.02)	0.012 (.004)	3
	369.	0.84 (0.01)	0.018 (.005)	2
	431.	0.75 (0.01)	0.001 (.003)	3
	488.	0.84 (0.02)	-0.008 (.007)	2
	616.	0.82 (0.02)	0.011 (.005)	1
	678.	0.81 (0.01)	-0.013 (.004)	3
	733.	0.79 (0.04)	-0.005 (.006)	3
	862.	0.82 (0.01)	-0.001 (.006)	3
	976.	0.67 (0.02)	-0.026 (.011)	2

SOURCE VISIBILITY FUNCTIONS

SOURCE PARAMETERS	SOURCE OBSERVATIONS			
	SPACING	VIS AMP	VIS PHASE	NO
3C293				
P.A. = 64.0	101.	0.95 (0.03)	-0.014 (.005)	1
	152.	0.92 (0.01)	0.040 (.002)	4
	203.	0.76 (0.02)	-0.021 (.007)	3
	305.	0.77 (0.03)	0.029 (.002)	2
	350.	0.84 (0.01)	0.000 (.003)	3
	397.	0.90 (0.02)	0.035 (.006)	3
	505.	0.88 (0.02)	0.010 (.005)	1
	551.	0.77 (0.01)	0.010 (.004)	3
	594.	0.86 (0.02)	-0.011 (.006)	3
	705.	0.78 (0.01)	0.011 (.005)	2
	777.	0.74 (0.02)	0.044 (.011)	2
3C293				
P.A. = 118.8	94.	0.99 (0.02)	-0.002 (.003)	2
	147.	0.91 (0.02)	0.016 (.003)	3
	190.	0.96 (0.02)	0.019 (.006)	3
	293.	0.80 (0.01)	0.007 (.004)	2
	341.	0.79 (0.02)	-0.027 (.004)	3
	388.	0.78 (0.02)	0.016 (.007)	2
	492.	0.78 (0.01)	-0.012 (.004)	2
	533.	0.79 (0.01)	-0.008 (.004)	3
	581.	0.71 (0.02)	-0.011 (.011)	3
	686.	0.80 (0.02)	-0.022 (.013)	3
	776.	0.79 (0.02)	0.071 (.012)	3
SGRA				
RA 17 42 34.00	62.	2.17 (0.04)	0.034 (.003)	4
DEC -28 58 0.0	122.	0.96 (0.01)	0.034 (.005)	1
FLUX 170.0	185.	0.91 (0.01)	0.011 (.002)	3
	244.	0.84 (0.00)	-0.063 (.004)	3
	370.	0.51 (0.01)	-0.020 (.003)	1
	432.	0.42 (0.01)	-0.067 (.003)	4
	489.	0.46 (0.01)	-0.037 (.009)	1
	617.	0.27 (0.00)	-0.010 (.004)	2
	679.	0.22 (0.00)	-0.029 (.004)	2
	732.	0.18 (0.00)	-0.046 (.006)	3
	864.	0.12 (0.00)	0.019 (.004)	2
	977.	0.08 (0.00)	0.049 (.011)	2

TABLE 3 CONT.

SOURCE VISIBILITY FUNCTIONS

SOURCE PARAMETERS	SPACING	VIS AMP	VIS PHASE	NO
P2058-28 M20-2/15				
RA 20 58 40.40	62.	0.87 (0.02)	-0.016 (.012)	4
DEC -28 13 30.0	122.	0.99 (0.04)	0.012 (.003)	2
FLUX 10.0	185.	0.96 (0.02)	0.003 (.007)	3
	245.	1.01 (0.01)	-0.057 (.004)	4
	370.	0.97 (0.01)	-0.022 (.002)	2
	432.	0.67 (0.01)	-0.017 (.003)	3
	489.	0.75 (0.03)	-0.021 (.007)	2
	617.	0.53 (0.01)	-0.027 (.003)	3
	679.	0.75 (0.01)	0.032 (.004)	3
	733.	0.51 (0.01)	-0.014 (.006)	3
	864.	0.40 (0.01)	0.026 (.004)	3
	978.	0.26 (0.02)	0.092 (.023)	2
3C435 P2126+07				
RA 21 26 37.55	62.	0.81 (0.04)	-0.021 (.004)	5
DEC 7 20 0.0	122.	0.69 (0.03)	0.030 (.007)	2
FLUX 5.1	185.	1.01 (0.02)	0.001 (.004)	4
	244.	0.87 (0.02)	-0.034 (.004)	4
	370.	0.78 (0.01)	0.008 (.004)	2
	432.	0.93 (0.01)	0.016 (.004)	3
	489.	0.94 (0.03)	-0.036 (.014)	3
	617.	0.94 (0.02)	0.043 (.003)	3
	678.	0.87 (0.02)	-0.011 (.004)	3
	733.	0.78 (0.02)	0.010 (.006)	3
	864.	0.86 (0.02)	-0.002 (.004)	3
	977.	0.81 (0.04)	0.034 (.037)	2
P2247+11 NGC 7385				
RA 22 47 21.10	62.	0.87 (0.04)	-0.002 (.004)	6
DEC 11 19 12.0	122.	0.64 (0.03)	0.045 (.005)	2
FLUX 5.7	185.	0.35 (0.01)	-0.015 (.006)	3
	245.	0.31 (0.02)	-0.110 (.006)	4
	370.	0.48 (0.01)	-0.035 (.004)	2
	432.	0.46 (0.01)	0.034 (.004)	3
	489.	0.51 (0.02)	0.116 (.008)	3
	617.	0.32 (0.02)	0.198 (.004)	3
	679.	0.10 (0.01)	0.161 (.016)	3
	733.	0.20 (0.01)	0.166 (.009)	3
	864.	0.32 (0.02)	0.129 (.008)	3
	978.	0.35 (0.03)	0.242 (.017)	2

SOURCE VISIBILITY FUNCTIONS

SOURCE PARAMETERS	SPACING	VIS AMP	VIS PHASE	NO
P2331-41 M23-4/4				
RA 23 31 45.40	62.	0.82 (0.02)	-0.008 (.021)	5
DEC -41 42 48.0	122.	1.04 (0.02)	0.026 (.005)	1
FLUX 10.2	185.	0.84 (0.02)	0.015 (.003)	3
	244.	0.86 (0.02)	-0.032 (.006)	3
	370.	0.88 (0.01)	0.011 (.002)	2
	432.	1.06 (0.01)	-0.037 (.003)	3
	489.	0.83 (0.01)	0.055 (.015)	3
	617.	0.88 (0.02)	-0.003 (.003)	3
	679.	1.00 (0.01)	-0.007 (.003)	3
	733.	1.04 (0.02)	-0.004 (.006)	3
	863.	0.94 (0.02)	0.010 (.006)	1
	978.	0.83 (0.02)	-0.003 (.015)	3

Notes to Table 3

3C120 -- Since this source is variable in intensity, the observed amplitudes have been changed to their values for December 1968. See Section IV-e.

P1216-10 -- This source is listed under the alternate name M12-0/9 in EF 1 and II.

3C274 -- The observed amplitudes have been raised 12% to correct for the effect of the receiver A.G.C. See Section II-c.

P1302-49 -- An extinction correction of 7% has been made to all the visibility amplitudes because of the large zenith angle at which this source was necessarily observed.

SGR A -- The A.G.C. correction is unknown and may be as high as 30%. The flux given was determined by extrapolating to zero spacing the uncorrected visibility of the 3' diameter component. This flux does not include the contribution from the extended emission region at the galactic center.

III. INVERSIONS

a) The Inversion Methods

Two methods, model fitting and Fourier inversion, were used to obtain the source brightness distribution from the interferometer data. Both methods are described by Maltby and Moffet (1962) and by Fomalont (EF II).

Model fitting was primarily used for partially resolved sources where the structural information was not sufficient to warrant a Fourier inversion. Most of the sources were inverted by summing a Fourier series. Equation 4) may be rewritten:

$$B'(x) = S'\left\{V(0) + \sum_{n=1}^{\infty} V(nu_o)\left[e^{-i[2\pi x n u_o - \Phi(nu_o)]} + e^{+i[2\pi x n u_o - \Phi(nu_o)]}\right]\right\} u_o$$

$$= S'\left\{1 + 2\sum_{n=1}^{\infty} V(nu_o)\cos[2\pi x n u_o - \Phi(nu_o)]\right\} u_o \qquad (6)$$

In the present observations $u_o = 62\lambda$, and thus the recovered brightness distribution $B'(x)$ is periodic with a period of $56'$. The $56'$ periodicity corresponds to the sidelobe response of the synthesized grating array. For most sources, the visibility was measured for n = 1, 2, 3, 4, 6, 7, 8, 10, 11, 12, 14, and 16. When spacings were missing the visibility was quadratically interpolated in both its real and imaginary parts. Since the series was truncated at n = 16, the principal solution of Eq. 4) is

obtained (Bracewell and Roberts 1954). The untapered synthesized beam has a half power width of 2.'1 and a 22% first sidelobe 2.'4 from the main beam. In most cases the visibility was tapered, resulting in a beam width between 2.'5 and 2.'9 with sidelobes less than 5%.

For most of the sources, no correction was needed for primary beam attenuation; exceptions are indicated in the notes to Table 4. For the 90' antennas at 605 MHz, the half power beam width is 78'. The power response is down only 5% when off the beam axis by ± 12'. At the position of the first grating lobe (± 56') the response is down 80%. The antennas were pointed to the positions listed in Table 3 (precessed to the observing epoch).

Most of the observed sources are dominated by a bright, small-diameter component. To study the weaker extended components the contribution from this bright object was subtracted from the complex visibility, thereby removing both the unresolved source and its sidelobes. This procedure is made possible by the linearity of the Fourier transform.

The total flux density in the beam, S', which appears in Eq. 6) was either taken from published values (Kellermann et al. 1969, C.S.I.R.O. Radiophysics Division 1969) or from the zero spacing intercept of the visibility.

b) Errors in the Inversion

The errors in the brightness distribution were estimated by measuring the r.m.s. deviation from zero in a region free of known or suspected sources. There will be deviations with positive and negative peaks due to errors in the visibility, faulty interpolation, and sidelobes. In most of the observations the latter two sources of error are not very important. The interpolation never extends over more than one spacing and is only used for n = 5, 9, 13, and 15. Most of the halos are well resolved by the largest spacing, effectively smoothing out the sidelobes.

The propagation of errors from the visibility to the brightness distribution may be estimated analytically. Introducing an error term into Eq. 4)

$$B'(x) + E(x) = S' \int_{-\infty}^{+\infty} \left\{ \hat{V}(u) + \hat{e}(u) \right\} e^{-i 2\pi x u} du$$

$$E(x) = S' u_o \left\{ e(0) + 2 \sum_{n=1}^{N} e(nu_o) \cos[2\pi x n u_o - \Phi_e(nu_o)] \right\}.$$

$$\langle E^2(x) \rangle \simeq S'^2 u_o^2 \left\{ 2^2 \sum_{n=1}^{N} \langle e^2(nu_o) \cos^2[2\pi x n u_o - \Phi_e(nu_o)] \rangle \right\}$$

If the phase of $\hat{e}(u)$ is completely random

$$\langle E^2(x) \rangle \simeq S'^2 u_o^2 \left\{ 2^2 \sum_{n=1}^{N} \langle e^2(nu_o) \rangle^{\frac{1}{2}} \right\} .$$

Let $\sigma_V = \sqrt{\langle e^2(u) \rangle}$ and $\sigma_B = \sqrt{\langle E^2(x) \rangle}$. If σ_V is the same for all spacings,

$$\sigma_B = S' u_o \sqrt{(2N)}\ \sigma_V\ 1/3438 \quad \text{f.u./arcmin}$$

where N is the total number of spacings. The brightness error may be represented as the result of a one-dimensional random walk along the real visibility axis with step size $\sqrt{2}\ \sigma_V$ and N steps. For $u_o = 62\lambda$, n = 16, and $\sigma_V \sim 0.05$

$$\sigma_B \simeq 0.005\ S' \quad \text{f.u./arcmin.}$$

This agrees very well with the noise actually measured from the inversions.

c) Results of the Inversions

The results of the east-west inversions are summarized in Table 4. A discussion of the individual objects and the one-dimensional brightness distributions are given in the next chapter. The table contains:

Column 1 - the source name

2 - a component designation

3 - the component flux at 605 MHz (in f.u.)

4 - the component flux at 1425 MHz from EF II

5 - the spectral index between these two frequencies given by $S \propto \nu^{\alpha}$

6 - the east-west diameter (minutes of arc)

7 - the east-west displacement from the centroid (minutes of arc) with plus to the east.

8 - the right ascention (1950.0) of the centroid, usually from EF II since the positions measured at 1425 MHz are more accurate. If there is a significant difference between the 605 MHz and 1425 MHz centroids the 605 MHz is given and a comment made in the notes.

9 - the nominal declination (1950.0)

10 - the degree of resolution of the large component at 605 MHz

SR: slightly resolved, visibility not out to the first minimum

PR: partially resolved, visibility beyond the first minimum

WR: well resolved, only the core left

An asterisk is used to indicate values obtained from the visibility function at 1425 MHz (EF I) or from the combined 605 MHz and 1425 MHz visibilities. Most information on the small diameter components (unresolved at 1000λ) is obtained in this way.

The 605 MHz fluxes were generally measured directly from the brightness distributions; individual component errors are about 0.2 f.u. or 5% for strong sources. The

errors of positions based solely on the 605 MHz visibility are roughly ± 0.'3.

A list of notes pertaining to the observations or data reduction follows the table.

TABLE 4

SUMMARY OF SOURCE BRIGHTNESS DISTRIBUTIONS

Name	Comp	Flux 605	Flux* 1425	α_{610}^{1425*}	Dia.	Disp.	R.A.	Dec.	Res.
(1)	(2)	(3)	(4)	(5)	(6)	(7)	(8)	(9)	(10)
							h m s	° '	
3C20		19.6	11.2	-0.66	0.'70*		00 40 19.7*	51 47	SR
P0045-25		9.7					00 45 06.5*	-25 34	WR
	A	3.2	2.5	-0.29	<0.3*	-0.15*			
	B	6.5	3.4	-0.80	3.3	0.0			
	C				14.1	+1.2			
3C31		8.7					01 04 41.9*	32 09	PR
	A	≤3.5	2.0	≥-0.66	0.6*	-0.5*			
	B	≥5.2	2.9	≤-0.70	2.1*	0.4*			
3C40		13.5					01 23 25	-01 37	WR
	A	8.2	4.4	-0.73	1.6*	1.4			
	B	5.3	1.2	-1.80	3.1	-2.1			
3C66		19.1					02 19 57.6*	42 46	WR
	A	4.8	2.0	-1.04	<0.4*	-4.8			
	B		2.9						
	C	14.3	1.8	-0.88	2.5	1.4			
	exten.		2.0						
3C78		12.5	7.2	-0.66			03 05 47.8*	03 55	SR
	A		5.4		1.5*	-0.1*			
	B		1.8		<0.5*	0.18*			

TABLE 4 CONT.

Name	Comp.	Flux 605	Flux 1425	α_{610}^{1425}*	Dia.	Disp.	R.A.	Dec.	Res.
(1)	(2)	(3)	(4)	(5)	(6)	(7)	(8)	(9)	(10)
							h m s	° '	
3C105		9.6					04 04 44.8*	03 33	PR
	A	4.8	2.9	-0.59	<0.3*	+0.8*			
	B	2.6	1.4	-0.73	3.0*	0.3			
	C	2.2	1.1	-0.81	2.0*	-2.4			
3C120		5.4					04 30 31.8	05 15	WR
	A	4.3	3.3	-0.32	<0.3'*	0.0'			
	B	1.1	0.5	-0.94	2.7	0.0			
3C130		7.0					04 48 54.3*	52 00	PR
	A }	6.0	1.0		<0.4*	+ .99*			
	B }		1.7		3.4	-0.3			
	C	1			8.7	+21.			
P0625-35		7.2	4.6	-0.56			06 25 20.8*	-35 27	SR
	A		3.2		1.9*	0.0*			
	B		1.3		<0.4*	0.0			
P0715-36		5.0					07 15 19.2*	-36 16	PR
	A }	4.3	1.3 }	-0.90	2.2*	-0.5*			
	B }		0.7 }		<0.5*	0.96*			
	C	0.7	~0.4	-0.66		-6.2			

TABLE 4 CONT.

Name	Comp	Flux 605	Flux* 1425	α_{610}^{1425*}	Dia.	Disp.	R.A.	Dec.	Res.
(1)	(2)	(3)	(4)	(5)	(6)	(7)	(8)	(9)	(10)
							h m s	° '	
P0843-33		3.3					08 43 08.7*	-33 37	WR
	A	2.2	1.9	-0.18	0.8*	-0.01			
	B	1.1	0.9	-0.20	4.3	+0.6			
3C218		92					09 15 41.3*	-11 53	WR
	A	80	41.4	-0.78	0.5*	0.0			
	B	12	2.5	-1.80	6.0	0.0			
P0935-28		4.6					09 35 49.1*	-28 59	PR
	A	1.3	0.8	-0.56	0.9*	-0.97*			
	B	3.0	1.1	-1.18	2.2	0.5			
	C	0.3				-10.2			
3C231		10.6	8.11	-0.30	0.7	0.0	09 51 43.75*	69 55	PR
3C236		7.4					10 02 58	35 09	WR
	A	4.7	3.2	-0.41	<0.25*	+1.5			
	B	0.9			5.2	3.0			
	C	1.5	1.0	-1.18	5.2	-6.9			
	Bridge	0.3							
NRAO 346		1.1	0.8	-0.37	4.5		10 04 30	34 57	

TABLE 4 CONT.

Name	Comp	Flux 605	Flux 1425	α_{610}^{1425}*	Dia.	Disp.	R.A.	Dec.	Res.
(1)	(2)	(3)	(4)	(5)	(6)	(7)	(8)	(9)	(10)
							h m s	° '	
3C247		6.7						43 18	PR
	A	5.3	2.7	-0.80	<0.3	0.0	10 56 08.3*		
	B	0.6			~2.0	-0.3	10 55 08.8		
	C	0.8			~2.0	+0.3			
3C264		10.8					11 42 32.2*	19 53	WR
	A	6.3	4.3	-0.46	0.6*	-0.6*			
	B	4.5	1.8	-1.08	4.0	+0.4			
P1216-10		5.7					12 16 01.7*	-10 02	WR
	A	3.6	1.7	-0.88	<0.3*	-0.36*			
	B	1.4	0.9	-0.56	≤2.0	+0.6			
	C	0.3			~2.0	-5.4			
	D	0.4			~2.0	-12.4			
3C274		409					12 18 17.6*	12 40	WR
	A	178	133	-0.35	0.7*	0.0			
	B	231	80	-1.25	6.0	0.0			
P1302-49		8.9					13 02 33.1*	-49 12	WR
	A	5.3	4.6	-0.18	<0.3*	0.0			
	B	3.6	2.5	-0.44	7.8	0.0			

TABLE 4 CONT.

Name	Comp	Flux 605	Flux 1425	α_{610}^{1425}*	Dia.	Disp.	R.A.	Dec.	Res.
(1)	(2)	(3)	(4)	(5)	(6)	(7)	(8)	(9)	(10)
							h m s	° '	
3C287.1		5.3					13 30 21.0*	02 16	WR
	A	2.5	1.4	-0.70	<0.3'*	+0.6'*			
	B	2.8	1.5	-0.71	3.8	-0.4			
P1334-29		4.3					13 34 10.9*	-29 36	WR
	A	0.4	0.3	-0.34	<0.4*	0.02*			
	B	3.9	2.4	-0.57	4.7	0.0			
3C293		8.2					13 50 02.9*	31 42	WR
	A	6.6	3.7	-0.66	<0.3*	+0.05*			
	B	1.6	1.1	-0.44	7	-3			
SGR A	See Appendix B								
P2058-28		10.2	5.7	-0.70	2.2		20 58 40.4*	-28 14	SR
3C435		4.2	2.12	-0.80	0.5*		21 26 37.6*	07 20	PR
P2247+11		4.3					22 47 17	11 19	WR
	A	2.2	1.5	-0.44	1.2	1.6			
	B	2.1	0.7	-1.30	5.0	-1.7			
P2331-41		8.7	4.5	-0.79	<0.3*		23 31 45.4*	-41 43	PR

Notes to Table 4

3C20 -- simple structure, no indication of a halo.

P0045-25 -- visibility also obtained at P A. = 65° and 116°. Roughly 60% of the disk flux comes from component B and 40% from component C.

3C31 -- visibility also obtained for P.A. = 120°.

3C40 -- R.A. of the centroid is from 50 cm data.

3C78 -- Less than 50% of the flux comes from the core.

3C120 -- R.A. of the centroid is from 50 cm data. The flux of the small variable component is for epoch 1968.95.

3C130 -- visibility also obtained for P.A. = 42° and 128°.

P0625-35 -- Less than 30% of the flux comes from the core.

P0715-36 -- possible additional source at -10'.8 with $\sim$ 0.5 f.u.

3C218 -- The model at 1425 MHz used here differs slightly from that given in EF II.

3C231 -- visibility also obtained at P.A. = 47° and 134°.

Notes to Table 4 Cont.

3C236 -- R.A. of centroids are from 50 cm data. The 21 cm fluxes for components B, C, and the bridge were obtained by subtracting the point source flux (EF II) from the total flux given by Kellermann et al. (1969). The 50 cm flux for NRAO 346 was corrected for beam attenuation.

3C247 -- visibility also obtained at P.A. = 45° and 124°. Several confusing sources are nearby, but no halo is seen.

P1216-10 -- The flux for component A is calculated assuming that only this component is unresolved at 1000λ, which is true at 21 cm.

P1302-49 -- Extinction corrections were made to both the 605 and 1425 MHz fluxes. See Section IV-b.

3C293 -- visibility also obtained at P.A. = 64° and 119°. The halo may consist of two components with about equal flux density.

Notes to Table 4 Cont.

P2058-28 -- There is insufficient resolution to resolve the central double. About 1 f.u. of confusion is in the beam, but no definite halo is seen.

3C435 -- Confusing sources are at -16' and +35' from the point source with a total flux of 1 f.u. There is no definite indication of large scale structure.

P2247+11 -- R.A. of centroid is from 50 cm data.

P2331-41 -- Confusing sources are at +8', -17' and -35' from the point source with a total flux of 1.5 f.u., but no halo is seen.

IV. SOURCE STRUCTURES

a) Types of Halos

The observed source structures are discussed in this chapter. These usually consist of a bright core superimposed on an extended background emission region. The sources are grouped according to the structure of this background. Core-halo and asymmetric double structures are not separated. Three groups are used:

Type I - simple halo: a single component usually many times larger than the core with no discernable structure. Spiral and elliptical galaxies of this type will be treated separately. P0045-25 (spiral) and 3C274 (elliptical) are good examples of this type.

Type II - double halo: a large faint halo with two components. Centaurus A is an excellent prototype.

Type III- a bright object with several weak discrete sources in the background. These can usually be explained as instances of confusion. A good example is 3C247. These are probably in no way related to the core-halo or asymmetric double

objects.

In most cases only the one-dimensional structure is known, and this may not accurately reflect the true source distribution in space. For instance, a spherical halo and an elongated jet will have the same appearance in one dimension.

Also, the projection onto one axis makes it difficult to distinguish a double halo from a simple halo, especially when the ratio of true separation to component diameter is small to start with. If this ratio is 1.5 and the components are assumed to be spherical, for 66% of the doubles the ratio projected to one-dimension will be less than one, and the structure will be difficult to distinguish from that of a simple source. This matter will be treated more thoroughly in Section V-d.

The brightness distribution plots given in this chapter are usually presented with the core removed in order to better reveal the features of the halos (as an example see Figure 2). The core is indicated by a vertical arrow at the proper position with its brightness written next to it. The horizontal scale is in minutes of arc with east to the left and is centered on the right ascension given in Table 4. The brightness distribution is generally indicated by a solid line. Where the brightness is close to the noise level some of the features on the inversion

may be questionable and an alternative interpretation is indicated by a dashed line. The r.m.s. noise of the inversion is given by a vertical error bar at the left side of the plot. The half power beam width of the synthesized beam is given at the right of the plot. Unless otherwise noted, the one-dimensional distributions are for P.A. = 90°. If the radio source is associated with an optical galaxy, the distance of this galaxy is used to establish a spatial distance scale which is given above the brightness distribution. When the distance of the galaxy is calculated from its redshift, a Hubble constant of 100 km sec^{-1} Mpc^{-1} is used.

b) Simple Halo-Spiral Galaxies

Three core-halo objects of this type were observed, the three bright southern galaxies NGC 253 (P0045-25), NGC 4945 (P1302-49), and NGC 5236 (P1334-29). These were first observed by Mills (1955) at 85 MHz with a 49' pencil beam. Mathewson and Rome (1963) observed the same galaxies with the Parkes 210-foot telescope at 1425 MHz with a half power beamwidth of 14'. They failed to detect any structure as large as the optical disks of the galaxies. Large structure was first seen by Mills and Glanfield (1965) using the east-west arm of the Molonglo

Cross at 408 MHz where the half power beamwidth is 1.'5 in right ascension and 4° in declination. They showed that the radiation from these galaxies extends at least as far as the optical object. The inability of Mathewson and Rome to detect the halos is probably due to their low resolution and the steep spectra of the halos.

P0045-25 (NGC 253)

NGC 253 is a bright, nearby spiral galaxy classified as Sc in the Hubble Atlas of Galaxies (Sandage 1961). With a visual magnitude of seven (Allen 1955) it is one of the brightest galaxies in the sky. I observed it at three different position angles and the resulting one-dimensional inversions are shown in Figure 1. The sampling in the u-v plane was not sufficiently dense to synthesize a satisfactory beam shape in two dimensions. However, a rough picture of the two-dimensional brightness was obtained by inspection of the three scans and by model fitting. The resulting brightness contours are shown superimposed on an optical photograph of the galaxy. The small core shown here was also seen by Mills and Glanfield (1965), Ekers (1969), and EF II. The brightness of the core at 605 MHz is greater than 3.2×10^{-18} W $Hz^{-1} m^{-2} ster^{-1}$ using the flux density presented here (3.2 f.u.) and the upper limit to the diameter established by Fomalont (EF II) of 0.'3. The core is centered on the nucleus of the galaxy. Optically

Figure 1 - The brightness distribution of P0045-25 at 605 MHz. The two dimensional distribution is constructed from three one-dimensional scans and shown superimposed on a photograph of NGC 253 (Hale Observatories photograph).

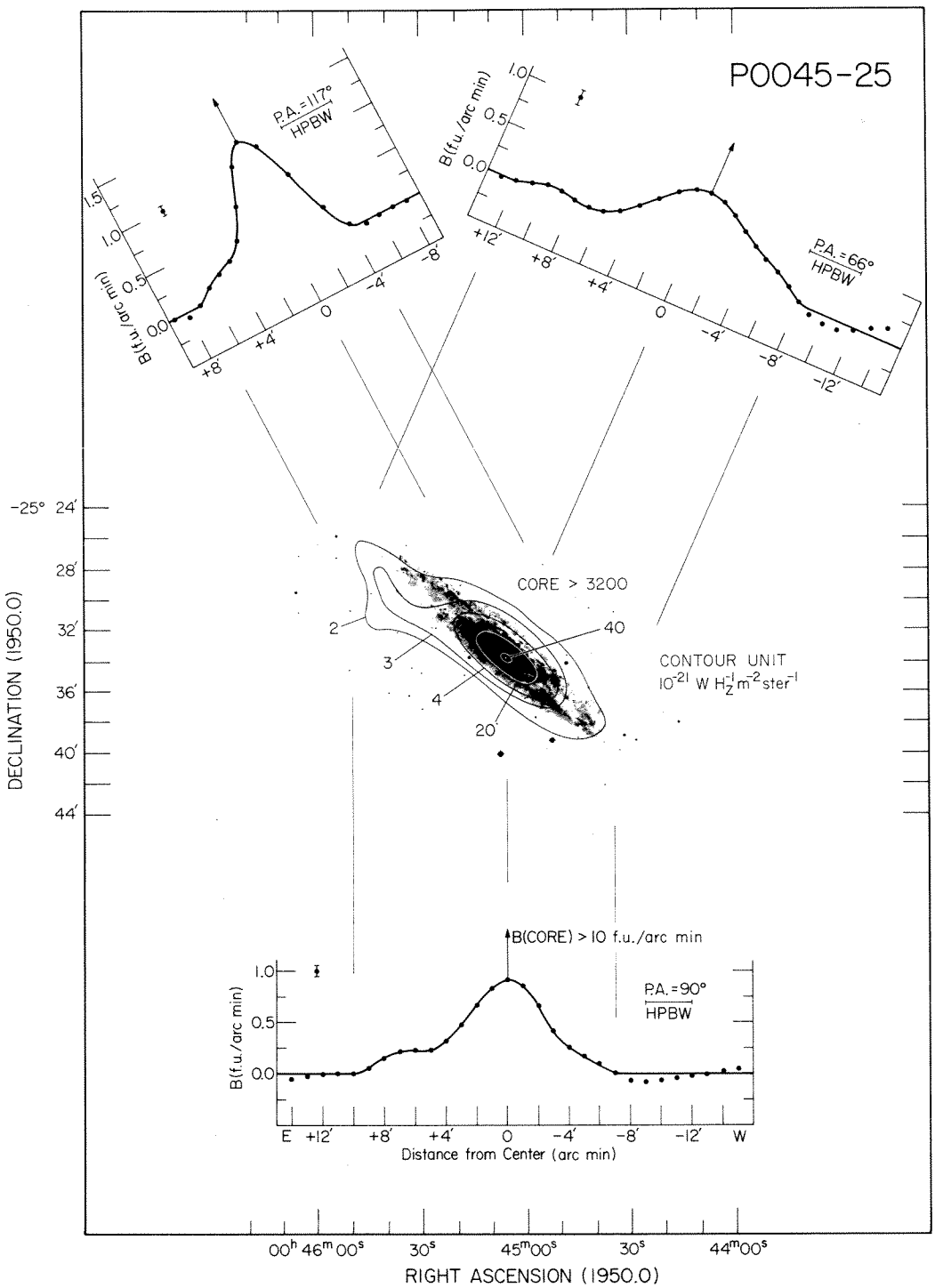
P0045-25
P.A.=117°
HPBW
B(f.u./arc min)
1.5
1.0
0.5
0.0
+8′
+4′
0
-4′
-8′
1.0
0.5
0.0
+12′
+8′
+4′
0
-4′
-8′
-12′
P.A.=66°
HPBW
-25° 24′
28′
32′
36′
40′
44′
DECLINATION (1950.0)
CORE > 3200
2
3
4
20
40
CONTOUR UNIT
10^{-21} W $H_Z^{-1}m^{-2}ster^{-1}$
B(CORE) > 10 f.u./arc min
P.A.=90°
HPBW
B(f.u./arc min)
1.0
0.5
0.0
E +12′ +8′ +4′ 0 -4′ -8′ -12′ W
Distance from Center (arc min)
$00^h 46^m 00^s$
30^s
$45^m 00^s$
30^s
$44^m 00^s$
RIGHT ASCENSION (1950.0)

the nucleus is obscured by dust and shows no corresponding bright spot.

The radio envelope surrounding the core is asymmetric and consists of two components. The inner component, in the east-west scan, is roughly Gaussian with a half power width of 4.'5 (measured from the inversion) and a total flux of 4.2 f.u. At P.A. = 117° the diameter is 3.'3, while the P.A. = 66° scan, which is roughly parallel to the major axis, shows it very broad with a correspondingly low one-dimensional brightness. Assuming that this component is a two-dimensional Gaussian ellipsoid with its major axis parallel to that of the optical object (P.A. = 53°), the lengths of the major and minor axes can be obtained using the relation

$$D^2 = W_{\parallel}{}^2 \cos^2\Phi + W_{\perp}{}^2 \sin^2\Phi$$

where: D = half power width on a one-dimensional strip scan

$W_{\parallel}, W_{\perp}$ = the half power widths of the two-dimensional Gaussian ellipsoid parallel and perpendicular to the major axis

Φ = (P.A. of ellipsoid major axis) − (P.A. of the one-dimensional scan)

Using D = 4.'5 at P.A. = 90° and D = 3.'3 at P.A. = 117°

$$W_{\parallel} = 5' \text{ and } W_{\perp} = 2'.$$

Using all three cuts, one could also solve for the P.A. of the major axis; however, the uncertainty in the width of the broad, low brightness cut at P.A. = 66° would introduce a large uncertainty in this solution. As a later check, all three cuts were used with a two-dimensional model fit program being developed by Fomalont, and essentially the same results were obtained. The peak brightness of the Gaussian ellipsoid was calculated by setting the integrated brightness equal to the measured flux density of this component. The peak is found to be about 35×10^{-21} W $Hz^{-1}m^{-2}ster^{-1}$.

This inner component is superimposed on a more extensive background component. The larger component is seen on all three scans and is roughly $5' \times 20'$, about the size of the optical galaxy. The integrated flux density of this component is 2.2 f.u. The brightness of the outermost contour is set by the noise level of the strip scans and the approximate dimensions of the source and is about 2×10^{-21} W $Hz^{-1}m^{-2}ster^{-1}$. The mean brightness of the extended component is about twice this value. The extended component is asymmetric with much of the radiation coming from the northeast end of the galaxy. Although this

feature has not been resolved as a separate source, it may well be unrelated to the galaxy.

A distance of 2.5 Mpc is obtained for NGC 253 from the distance modulus m - M = 27.0 given by Bottinelli et al. (1968). It is a member of an association of spiral galaxies at the south galactic pole (de Vaucouleurs 1959). The spiral structure of the galaxy is broken by dust lanes and patches to the extent that the arms are difficult to trace. Large random motions, suggested by the mottled appearance, were observed spectroscopically by Burbidge, Burbidge, and Prendargast (1962) who found departures from a smooth rotation curve of ± 30 km sec^{-1} or more, extending over regions of 500 pc.

P1302-49 (NGC 4945)

A single east-west strip scan was synthesized for this galaxy. The extremely large zenith angle of the source at the latitude of the Owens Valley (Z.A. = 86°26' at transit) required a visibility amplitude correction due to atmospheric extinction and a pointing correction for refraction.

The extinction correction, C, is of the form:

$$\log C = F(Z.A.) \log P$$

where P is a function of frequency and F(Z.A.) is proportional to the atmospheric mass in the line of sight. At 605 MHz log P = 0.0026 (Howell and Shakeshaft 1967) at sea

level. When scaled to the height of the Owens Valley (1216 m) by the ratio of the mean atmospheric pressures, 652/760, log P = 0.0022. Schoenberg (1929) gives a table of F(Z.A.); using the zenith angle corrected for refraction, $F(86^\circ 15')$ = 13.07. This yields an extinction correction of 1.07 which was applied to all observations.

Using the same procedure at 21 cm, where log P = 0.0028, a correction of 1.09 should be applied to the flux density listed in EF II.

A position offset due to refraction of $\Delta\delta = +11'$ (Baker 1959) was made. This offset was inadvertently omitted at the 100, 200, 400, 800, and 1600 foot spacings and an additional correction of 1.05 was needed to allow for beam attenuation. The visibility amplitudes listed in Table 3 include both corrections.

The one-dimensional radio brightness distribution is given in Figure 2. A two-dimensional outline of the optical galaxy is shown above the plot. The single optical contour, with a brightness of 27.3 mag sec^{-2} (de Vaucouleurs 1964) is $24' \times 6'$ with the major axis at P.A. = 42°. The radio source consists of a small core plus an extended envelope with a half power width of $7'.8$. The core brightness is based on an upper limit to the diameter of $0'.3$ given by EF II. The noise level on the inversion is

Figure 2 - The brightness distribution of P1302-49 at 605 MHz. The two brightness peaks to the west are probably due to noise. The two-dimensional contour shown is at a brightness of 27.3 mag sec^{-2}.

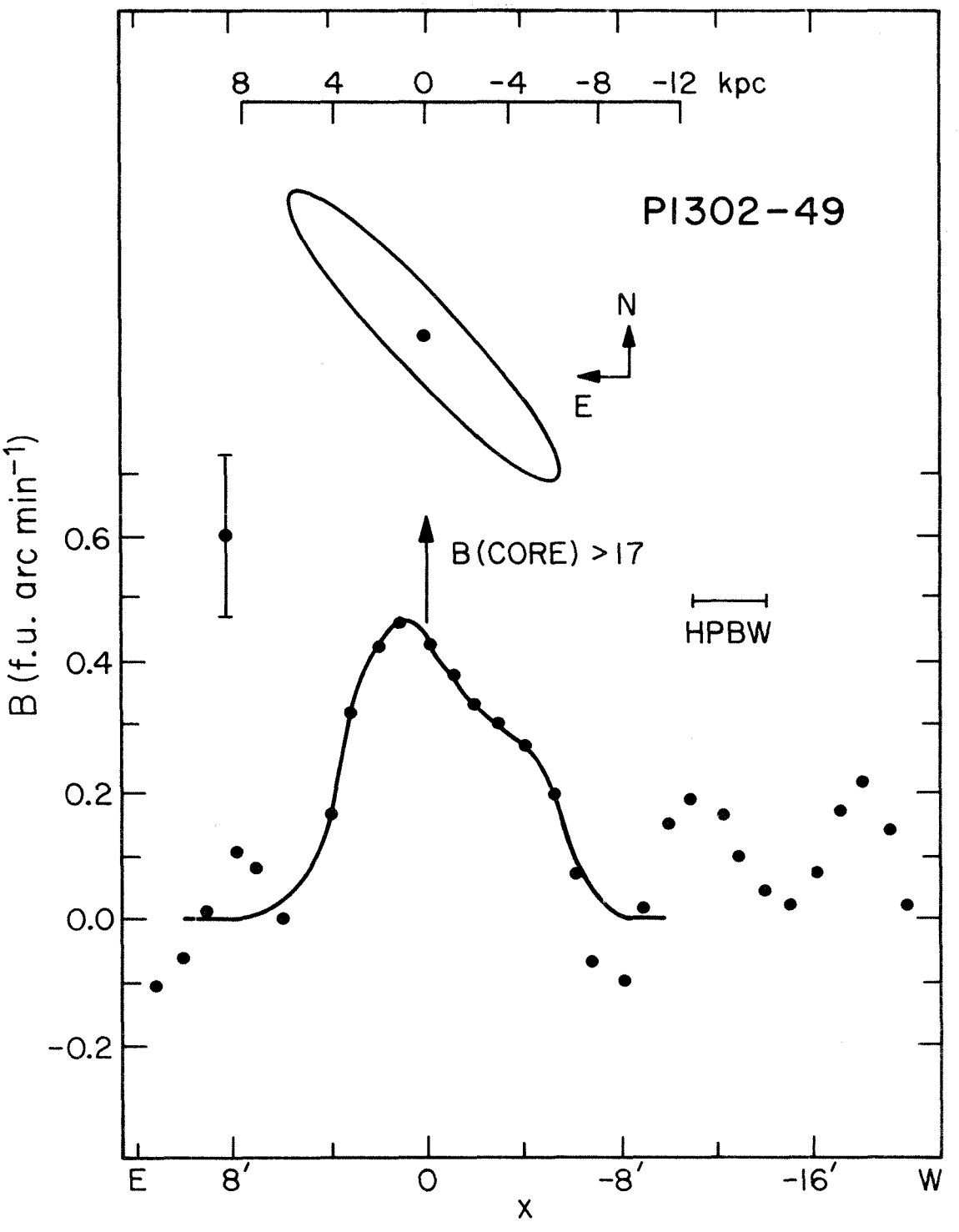
8 4 0 -4 -8 -12 kpc
P1302-49
N
E
B (f.u. arc min^{-1})
0.6
0.4
0.2
0.0
-0.2
B(CORE) >17
HPBW
E 8′ 0 -8′ -16′ W
X

higher than average due to the large ground noise and the corrections needed when observing close to the horizon. The two emission peaks to the west of the halo are questionable. The radio halo appears limited to the optical disk in the east-west direction; however, the high noise level makes it difficult to determine accurately the radio extent.

Ekers (1969) obtained the visibility of P1302-49 at four different position angles and fitted a core-halo model having a halo with half power diameters of $9.'0 \times 4.'5$ with the major axis at P.A. = 34°. This would project onto the east-west axis with a diameter of $6.'3$. The model by Ekers suggest that the radio emission is confined to the optical disk without an extended spherical halo. However, the radio axial ratio of 1:2 is somewhat larger than the optical, which is 1:4. Also, a halo larger than $15'$ would be difficult to detect without spacings less than 150 λ. Therefore a spherical halo extending above the galactic plane cannot be excluded.

A distance of 3.8 Mpc is obtained from the distance modulus m - M = 27.9 given by de Vaucouleurs (1964). Like NGC 253, this galaxy is heavily obscured by dust. Shobbrook and Shaver (1967) have published two photographs of the galaxy taken with the 74-inch reflector at Mt. Stromlo. On the blue plate the nucleus is com-

pletely hidden by the gas and dust in the arms, but in the infrared it is well defined with only moderate obscuration near the center. It has a full angular diameter of about 45" which corresponds to a linear diameter of 800 pc. The core of the radio source coincides with the center of the nucleus to within ± 5".

It is not clear whether the radio core is associated with the entire optical nucleus or if it corresponds to a compact source similar to Sagittarius A at the center of the Galaxy. At the distance of NGC 4945 the limit to the radio half power diameter given by Fomalont (0.'3) corresponds to 330 pc, which is compatible with the 800 pc full extent of the optical nucleus. However, this is only an upper limit and the radio emission could come from an extremely small source.

P1334-29 (NGC 5236, M83)

The central radio core of P1334-29 is much weaker than in the previous two spiral galaxies, contributing only 10% of the total flux at 605 MHz. EF II gives an upper limit of 0.'4 for its diameter. As with the other spirals, the core coincides with the optical nucleus.

The strip scan synthesized from the 605 MHz observations is shown in Figure 3. The size of the optical object is represented by the partial contours above the plot. The galaxy is nearly circular with an axial ratio

Figure 3 - The brightness distribution of P1334-29 at 605 MHz. The partial two-dimensional contours shown are at a brightness of (a) 24.2 mag sec^{-2} and (b) 26.5 mag sec^{-2}.

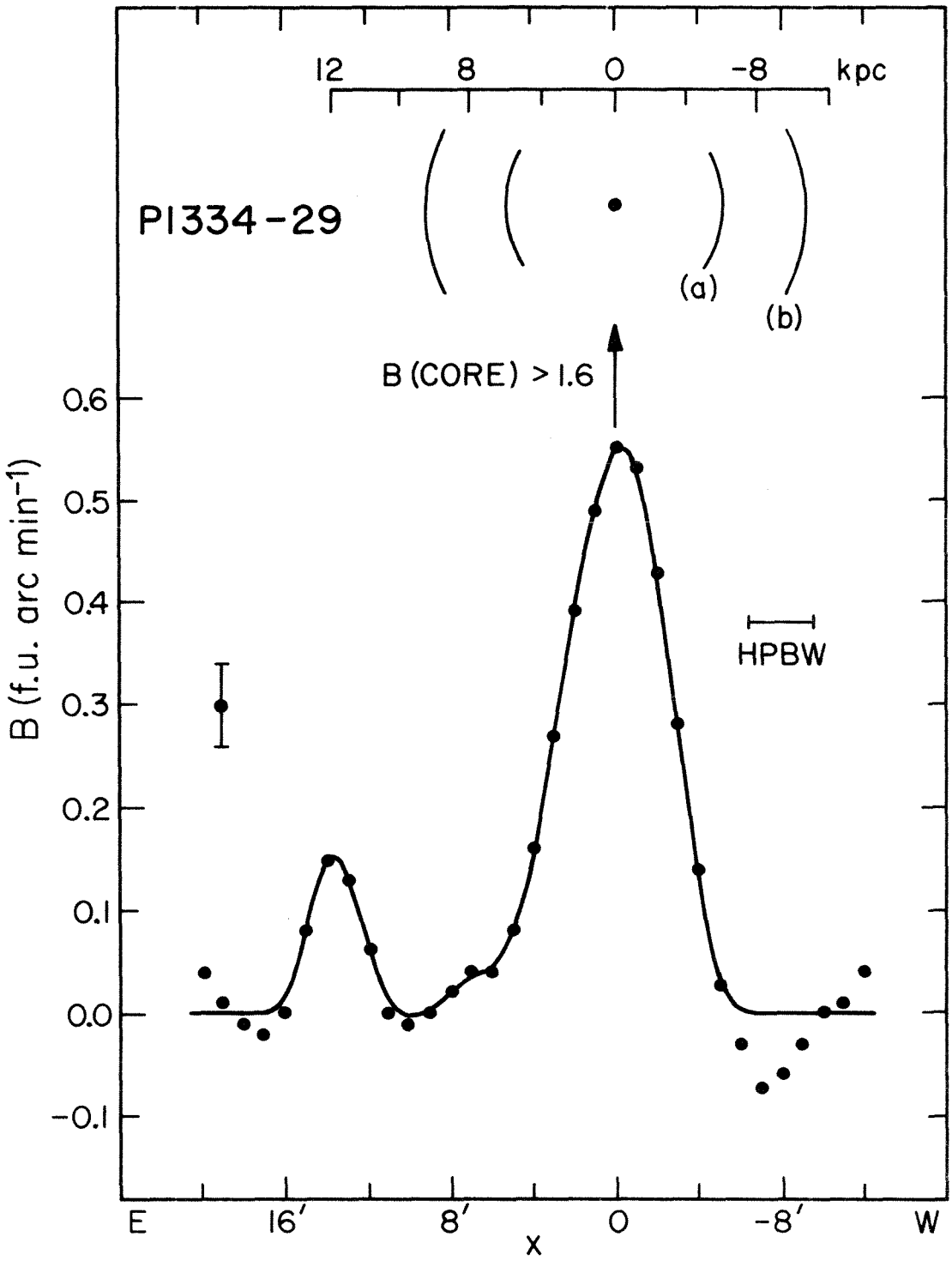
12
8
0
-8
kpc
P1334-29
(a)
(b)
B (CORE) > 1.6
HPBW
B (f.u. arc min^{-1})
0.6
0.5
0.4
0.3
0.2
0.1
0.0
-0.1
E
16′
8′
0
-8′
W
x

of 1:1.1. The brightness of the contour labeled a) is about 24.2 mag sec^{-2} (de Vaucouleurs and de Vaucouleurs 1964) and that labeled b) is 26.5 mag sec^{-2} (Brown and Hazard 1961).

The results presented here and in EF II show the radio envelope to have a half power diameter of 5.'5 in an east-west direction. Ekers (1969), with six cuts, shows it slightly larger and circular. Since the galaxy is seen almost face on, it is impossible to determine whether the extended radio source is a true radio corona or simply a disk component.

Another source appears 14' east of the radio centroid at $\alpha(1950.0) = 13^h\ 35^m\ 16^s$. Since its flux is about equal to the r.m.s. confusion level 0.6 f.u., it is probably not related to the source.

Velocity contours derived from 21 cm hydrogen line observations (Lewis 1968) show large non-circular motions in NGC 5236. A distance of 4.0 mpc is calculated from the distance modulus m - M = 28.0 (Bottinelli 1968). This distance was used to establish the spatial distance scale shown in Figure 3.

c) Simple Halo-Elliptical Galaxies

Ten of the objects observed have simple halos

and are not identified with spiral galaxies. Six of these P0843-33, 3C264, P1216-10, 3C274, 3C287.1, and P2247+11, are discussed in detail in this section, while the remaining four, 3C31, 3C78, P0625-35, and P0715-36, have halos that were only partially resolved, and little more can be said about them on the basis of the present observations.

P0843-33 (NGC 2663)

The 605 MHz brightness distribution is shown in Figure 4. The halo is displaced 0.'6 to the east of the core and has a diameter of 4.'3. Both components have a rather low brightness compared to the other core-halo sources. The halo model given by Ekers (1969) has a 4.'0 major diameter at P.A. = 170° and a 2.'0 minor diameter.

The core is coincident in right ascension with NGC 2663, an E3 galaxy with m_{pg} = 12.3 (C.S.I.R.O. Radiophysics Division 1969). The radial velocity is not available but an estimate of the distance modulus can be made by assuming the absolute magnitude to be M_{pg} = -20.3 (Maltby et al. 1963). A correction for absorption within our own galaxy of $\Delta m = -0.25$ csc b was assumed. For NGC 2663, with b = +5°, m + Δm - M = 29.9, giving a distance of 10 Mpc, which is probably accurate to within a factor of two. Thus the half power diameter of the core is about 2.5 kpc and that of the halo is about 12 kpc. The full extent of the halo is roughly 25 kpc. The full

Figure 4 - The brightness distribution of P0843-33 at 605 MHz. The spatial distance scale is based on a distance of 10 Mpc for NGC 2663, which is coincident with the radio core.

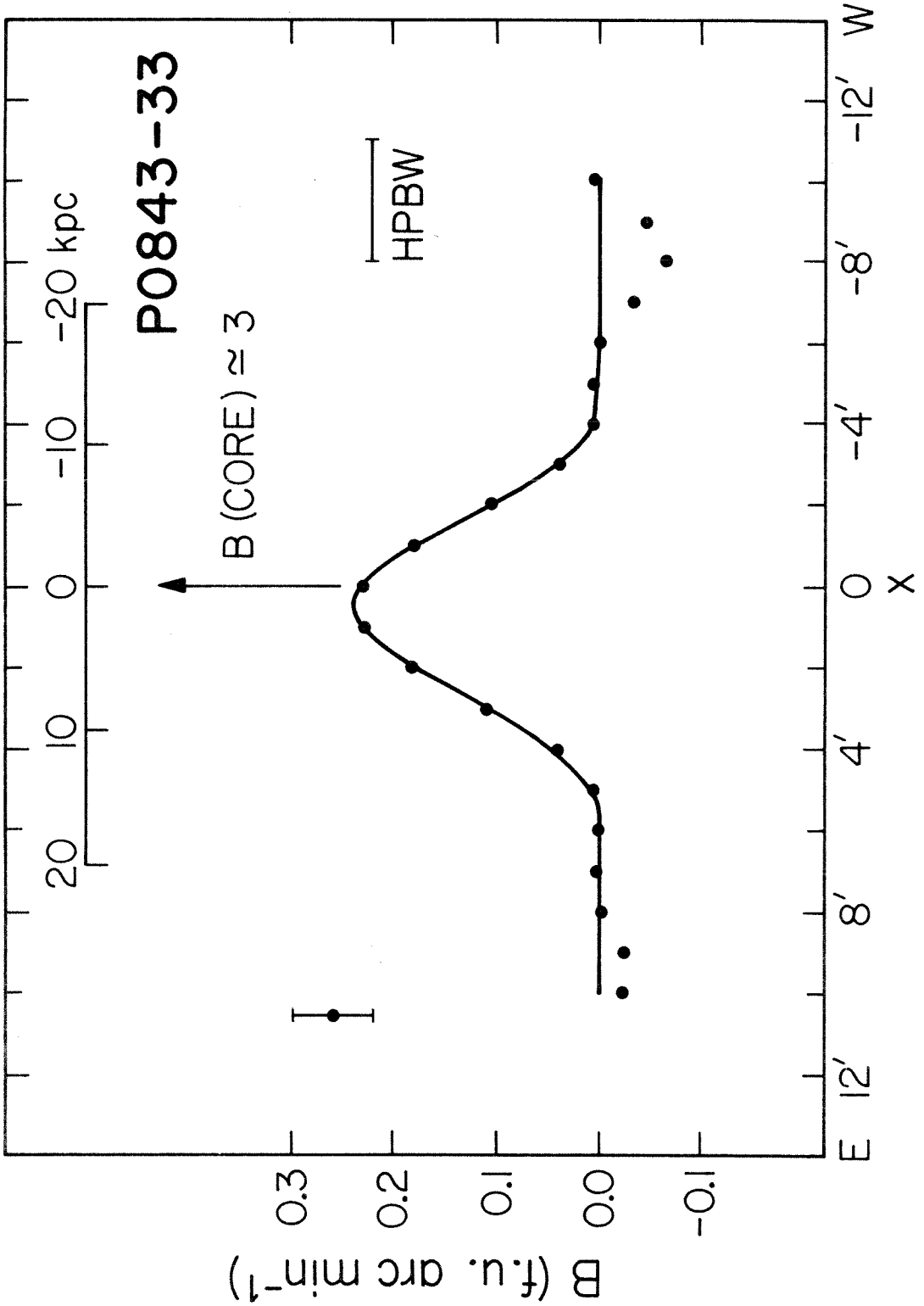
P0843-33
B (CORE) ≃ 3
HPBW
20 kpc
20
10
0
-10
-20
E 12′
8′
4′
0
-4′
-8′
-12′ W
X
0.3
0.2
0.1
0.0
-0.1
B (f.u. arc min⁻¹)

extent of NGC 2663 as seen on a print of the Whiteoak extension of the National Geographic Society - Palomar Observatory Sky Survey is slightly greater than 1', which corresponds to about 3 kpc. This is probably a low estimate of the diameter since the brightness of the object, and thus the isophotal diameter, are reduced by galactic absorption.

3C264 (NGC 3862)

The core of 3C264 is coincident with the galaxy NGC 3862. The radio diameter of the core is 0'.6, which is roughly the size of the optical object as seen on the Sky Survey print.

Surrounding the core is an extensive radio emission region. The radio halo at 605 MHz and 1425 MHz is shown in Figure 5. The higher resolution brightness distribution at 1425 MHz shows that the halo has a 2' diameter component to the east of the core with an extension running out to + 6'. The large component has a steeper spectrum than the core, which causes an increase in the apparent diameter of the source at low frequencies, as was noted by Macdonald et al. (1968). Unpublished north-south interferometric observations by Fomalont and Moffet (private communication) at 1425 MHz show a 2'.3 diameter halo displaced 2'.0 to the north of the core. Thus in two dimensions, the halo is roughly circular and is displaced

Figure 5 - The brightness distribution of 3C264 at 605 MHz and 1425 MHz.

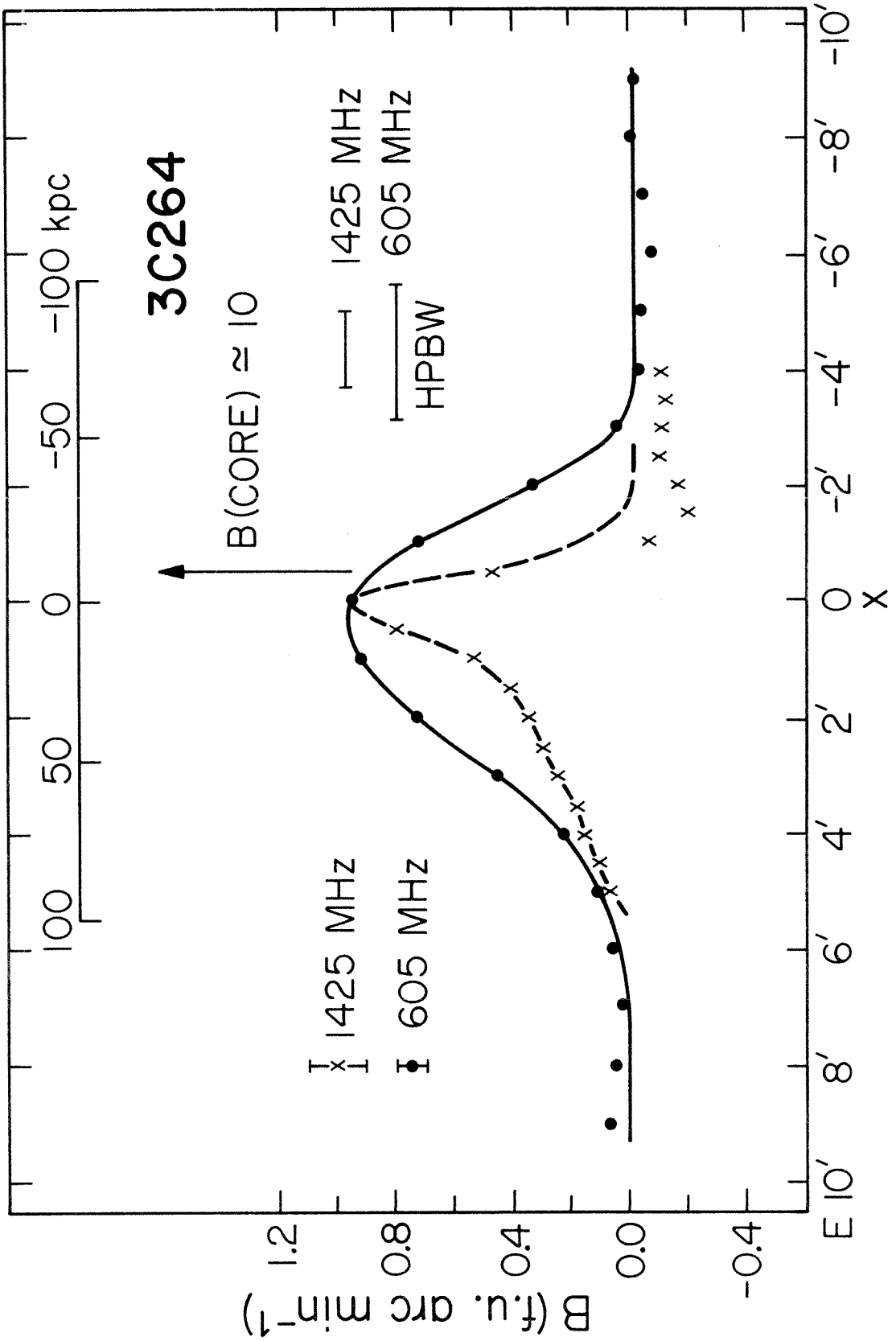
3C264
B(CORE) ≅ 10
1425 MHz
605 MHz
HPBW
1425 MHz
605 MHz
100
50
0
-50
-100 kpc
E 10′
8′
6′
4′
2′
0
X
-2′
-4′
-6′
-8′
-10′ W
1.2
0.8
0.4
0.0
-0.4
B (f.u. arc min⁻¹)

to the northeast.

The spatial distance scale shown in Figure 5 was established using a distance of 62 Mpc for NGC 3862 (Schmidt 1965). The radio halo extends about 110 kpc to the east of the galaxy.

The spectra of the core and halo components of 3C264 are shown in Figure 6. The flux densities of the individual components were obtained by Fomalont (EF II) at 1425 MHz, Maltby and Moffet (1962) at 960 MHz and from the present work at 605 MHz. The total flux measurements are taken from Bridle and Purton (1968) at 10.03 MHz, Roger et al. (1969) at 22.25 MHz and Kellermann et al. (1969) at 38, 178, 750, 1400, 2695, and 5000 MHz. The dashed line represents the sum of the two component spectra. The core spectrum obtained between 605 MHz and 1425 MHz will not fit the total flux measurements above 2000 MHz, and it is necessary to postulate that it turns over somewhere near this frequency. Bash (1968b) shows that 12% of the total radiation at 2695 MHz comes from a component with diameter $<1\overset{''}{.}5$; however, it cannot be established that this extremely small diameter object lies within the core. From Figure 6, at 2695 MHz, 80% of the total radiation comes from the core.

Figure 6 - The component spectra (solid and short-dashed lines) and the combined spectrum (long-dashed line) of 3C264.

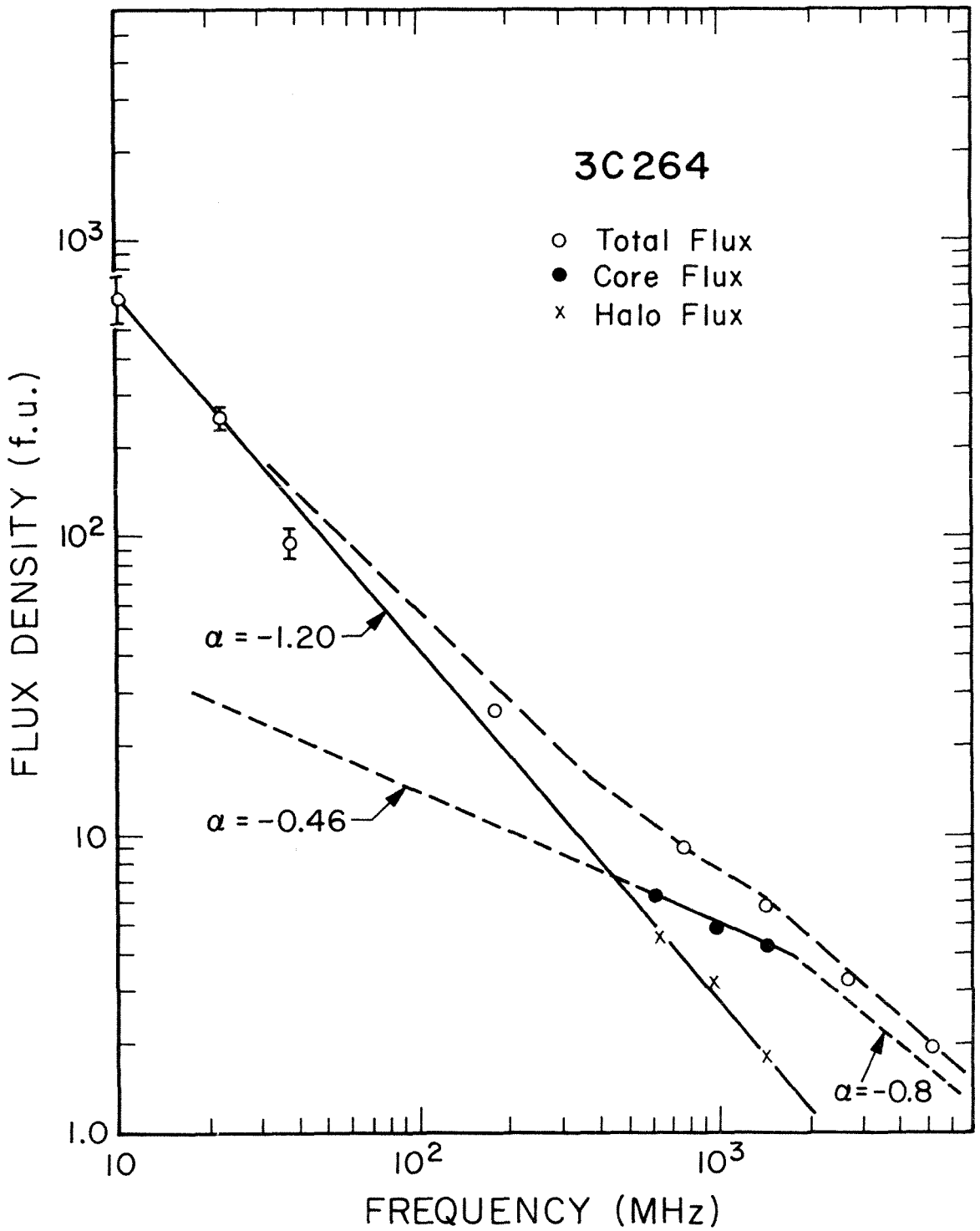
3C264
Total Flux
Core Flux
Halo Flux
FLUX DENSITY (f.u.)
FREQUENCY (MHz)
10
10^2
10^3
1.0
α = -1.20
α = -0.46
α = -0.8

P1216-10

At 1425 MHz P1216-10 has a simple halo and a displaced core (EF II). The 605 MHz brightness distribution plotted in Figure 7 shows two additional components to the west of the core with a combined flux density of 0.7 f.u. Since the noise level is about equal to the brightness of these components, this feature may simply be a single large component or an extension of the halo broken by noise. The absence of this emission region at 1425 MHz could be explained by the greater beam attenuation at that frequency, or by a steep spectrum for this region; alternatively this feature might be due to a confusing source in the first grating response of the 605 MHz synthesized beam.

There is no optical object identified with this source, although the field is unobscured. The coordinates of the core are:

$$\alpha = 12^h\ 16^m\ 00\overset{s}{.}2 \pm 0\overset{s}{.}4$$

$$\delta = -10^\circ\ 01'\ 07'' \pm 3''$$

Figure 7 - The brightness distribution of P1216-10 at 605 MHz.

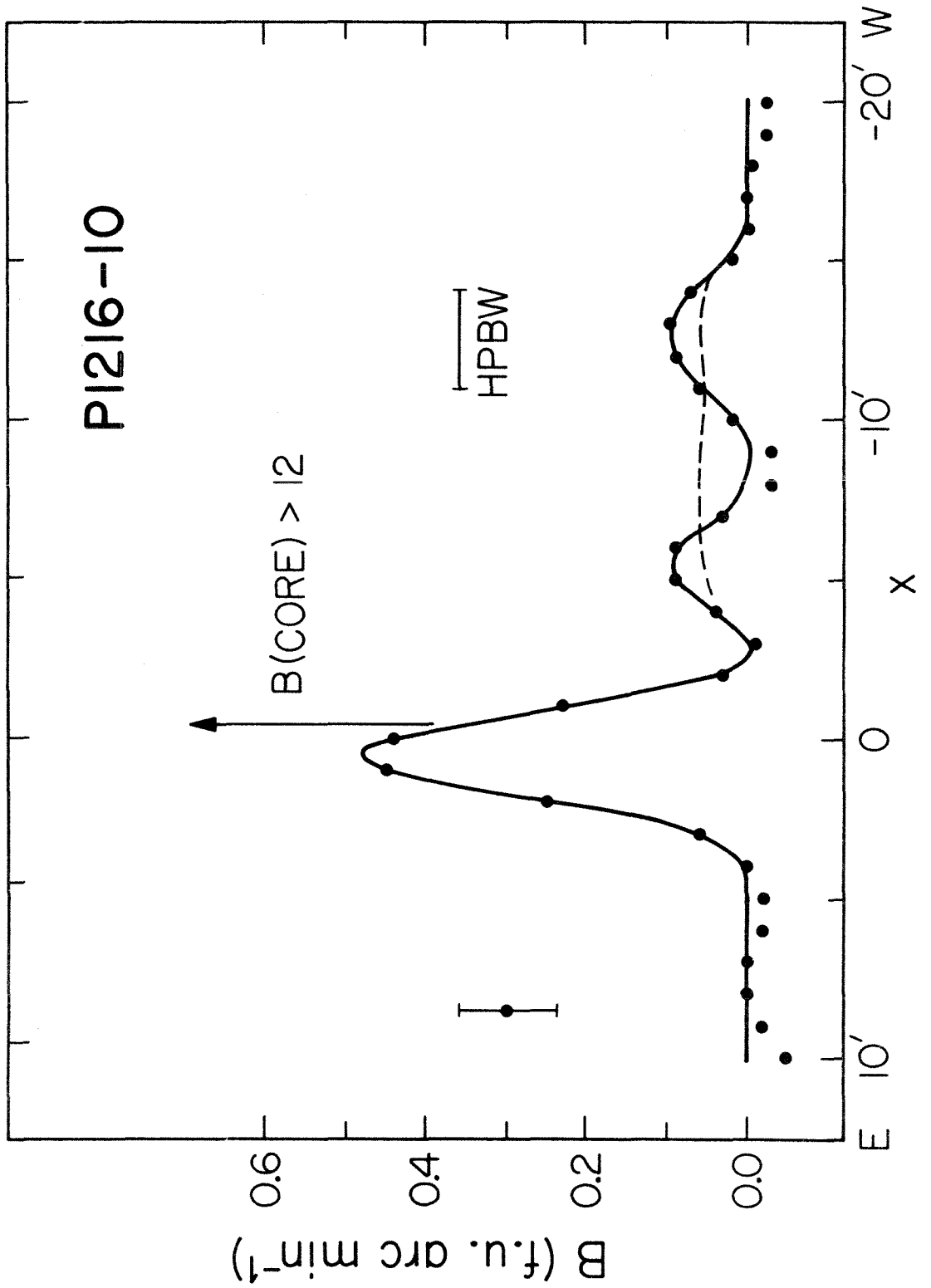
P1216-10
B(CORE) > 12
HPBW
B (f.u. arc min⁻¹)
0.0
0.2
0.4
0.6
E 10′
0
-10′
-20′ W
X

using the 1425 MHz right ascension of Fomalont (EF II) and the declination of Fomalont and Moffet (private communication). A slightly red stellar object lies within 0.'2 of this position and the only other object in the field is another stellar object 1.'2 away.

The north-south 1425 MHz brightness distribution of Fomalont and Moffet (private communication) shows the halo 3.'4 south of the core; both components are larger north-south with a core diameter of 0.'6 and a halo diameter of 5' compared to <0.'3 and 2.'2 for the east-west distributions.

3C274, Virgo A (NGC 4486, M87)

The elliptical galaxy NGC 4486 is one of the brightest numbers of the Virgo cluster. It is a strong radio source and is well known for the luminous jet which extends from the nucleus at P.A. = 290°. Photographs and a discussion of the galaxy are given in the Hubble Atlas of Galaxies (Sandage 1961) and by Baade and Minkowski (1954). Sandage (1968) obtains a distance modulus m - M = 30.85 and thus a distance of 14.8 Mpc for the galaxy.

The radio structure of 3C274 consists of a small diameter core at the center of an extensive envelope. Two dimensional brightness distributions of the core are given by Macdonald et al. (1968) and by Hogg et al. (1969). The latter work shows that 93% of the core flux at 2695 MHz

comes from a 30" x 70" region with the major axis at P.A. = 296°. The rest of the flux comes from two small components, one located at the nucleus of the galaxy and the other situated between the two brightest knots of the jet. Cohen et al. (1969) show that the nucleus component has an angular diameter smaller than 0".002.

The one-dimensional brightness distribution at 605 MHz is shown in Figure 8. The halo has a half power width of 6'.5 and is largely confined to within ± 7' of the core. However, there is some indication that the halo extends at a very low brightness level 15' on either side of the core. Baldwin and Smith (1956) report that 20% of the flux at 80 MHz comes from a region 50' in diameter. The present observations set a limit of 1 f.u./arc-min on the 605 MHz brightness of any component of such size. A two-dimensional map at 408 MHz (Cameron 1969) shows the halo having an overall extent of 16' x 12' with its major axis at P.A. = 34°.

The extent of the optical galaxy is indicated by the partial brightness contours above the radio brightness distribution in Figure 8. The optical brightness (de Vaucouleurs 1969) is written below each contour. The optical isophotes are nearly circular for a radius <2', becoming progressively elliptical further out, reaching

Figure 8 - The brightness distribution of 3C274 at 605 MHz. Two-dimensional optical contours are shown above the plot.

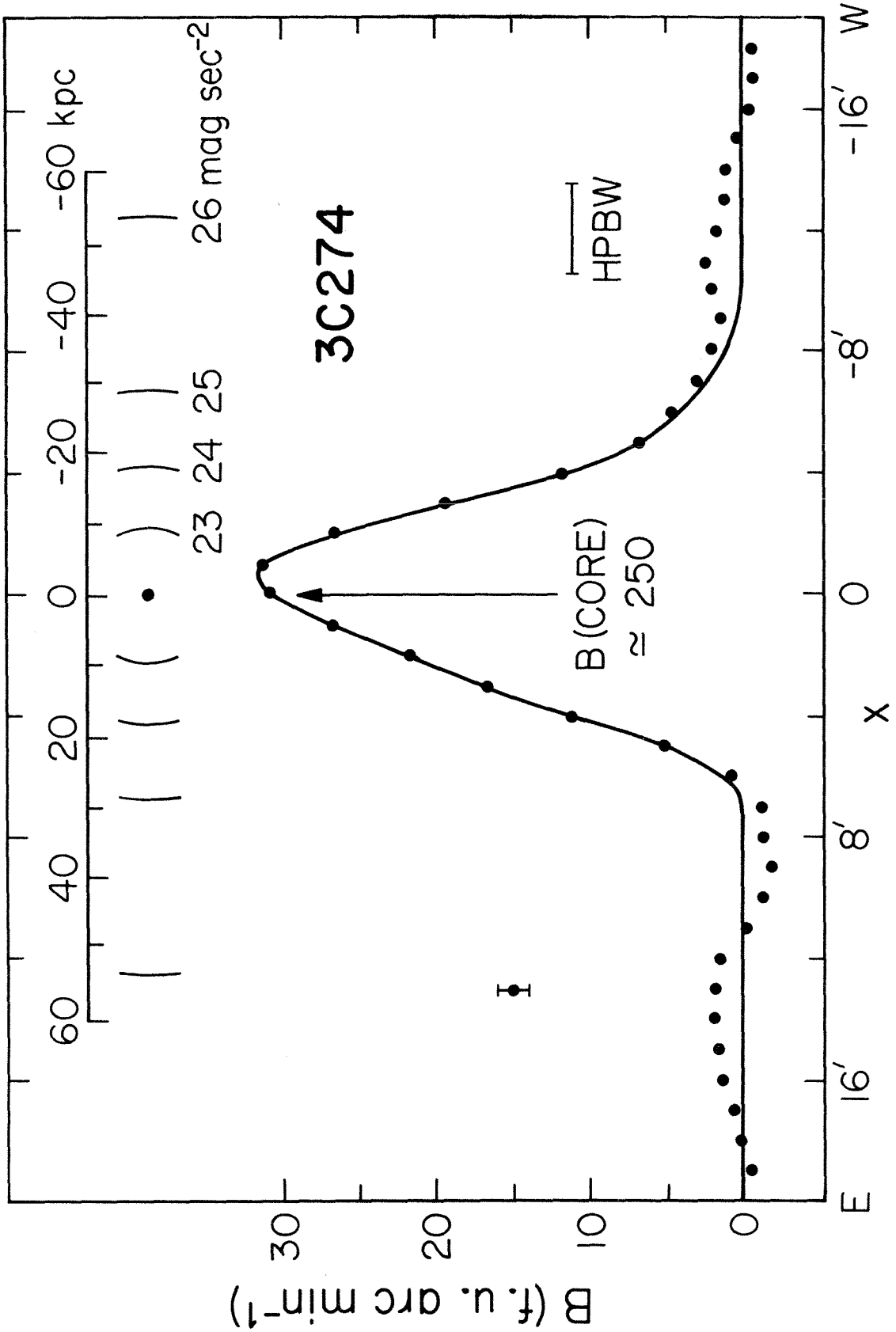
3C274
B (f. u. arc min⁻¹)
30
20
10
0
E
16′
8′
0
-8′
-16′
W
x
B(CORE)
≃ 250
HPBW
60
40
20
0
-20
-40
-60 kpc
23 24 25
26 mag sec⁻²

an eccentricity of 0.37 at radius 7.'4 (Liller 1960). The position angle of the major axis is about 150° (Arp and Bertola 1969). Arp and Bertola (1969) and de Vaucouleurs (1969) show that M87 is surrounded by an optical corona with a diameter in excess of one degree at a brightness $u_B \simeq 27.3$ mag sec^{-2}.

The flux and east-west half power diameter of the radio core and halo are given for several frequencies in Table 5. Error estimates are given next to the measured flux values. The calibrations of the individual measurements have been adjusted to conform to the flux scale of Kellermann et al. (1969). The spectra of the two components and the combined spectrum (dashed line) are shown in Figure 9. The total flux densities are taken from Bridle and Purton (1968) at 10.03 MHz, Roger et al. (1969) at 22.22 MHz, and the rest from Kellermann et al. (1969). At least two spectra of the form $S = S_o \nu^{\alpha}$ are needed to fit the core, with $\alpha = -0.35$ below 3000 MHz and $\alpha = -0.75$ above it. The halo has a steeper spectrum with $\alpha = -1.00$. There is a possible bend in the halo spectrum above 1400 MHz. However, the brightness of the large component is very low at high frequencies, and the flux densities have a large error. The 408 MHz flux densities and spectral indices (-0.80 for both components) given by Macdonald et al. (1968) are probably incorrect.

TABLE 5

PHYSICAL PARAMETERS OF 3C274

freq. (MHz)	Core flux (f.u.)	Core diam. (")	Halo flux (f.u.)	Halo diam. (')	notes	reference
101	340±120		1360±120	6	(1)	Mills 1953
408	350±35		200±20	12		Macdonald et al. 1968
	230±60		320±50	6.5	(1,2)	Cameron 1969
605	178±8		231±9	6.0		
960	143±8	36	131±8	6.5	(1)	Maltby and Moffet 1962
1420	130±13	50				Macdonald et al. 1968
	133±10	42	80±20	6.6		EF II
	129±11	50	86±8	10	(1)	Lequeux 1962
2800	94±4	42	20±10		(3)	Bartlett (private communication)
	82±10		32±11		(1)	Legg et al. 1968
8250	43±2	60				Allen et al. 1968
15500	29±2	32				Ibid.

NOTES TO TABLE 5

(1) The component fluxes were obtained from the flux ratio or the visibilities given and the total flux in Kellermann *et al*. (1969).

(2) The flux ratio and diameter were measured by the author from the two-dimensional map of Cameron (1969).

(3) The halo flux is the difference between the measured core flux and the total flux in Kellermann *et al*. (1969).

Figure 9 - The component spectra (solid or short-dashed lines) and combined spectrum (long-dashed line) of 3C274.

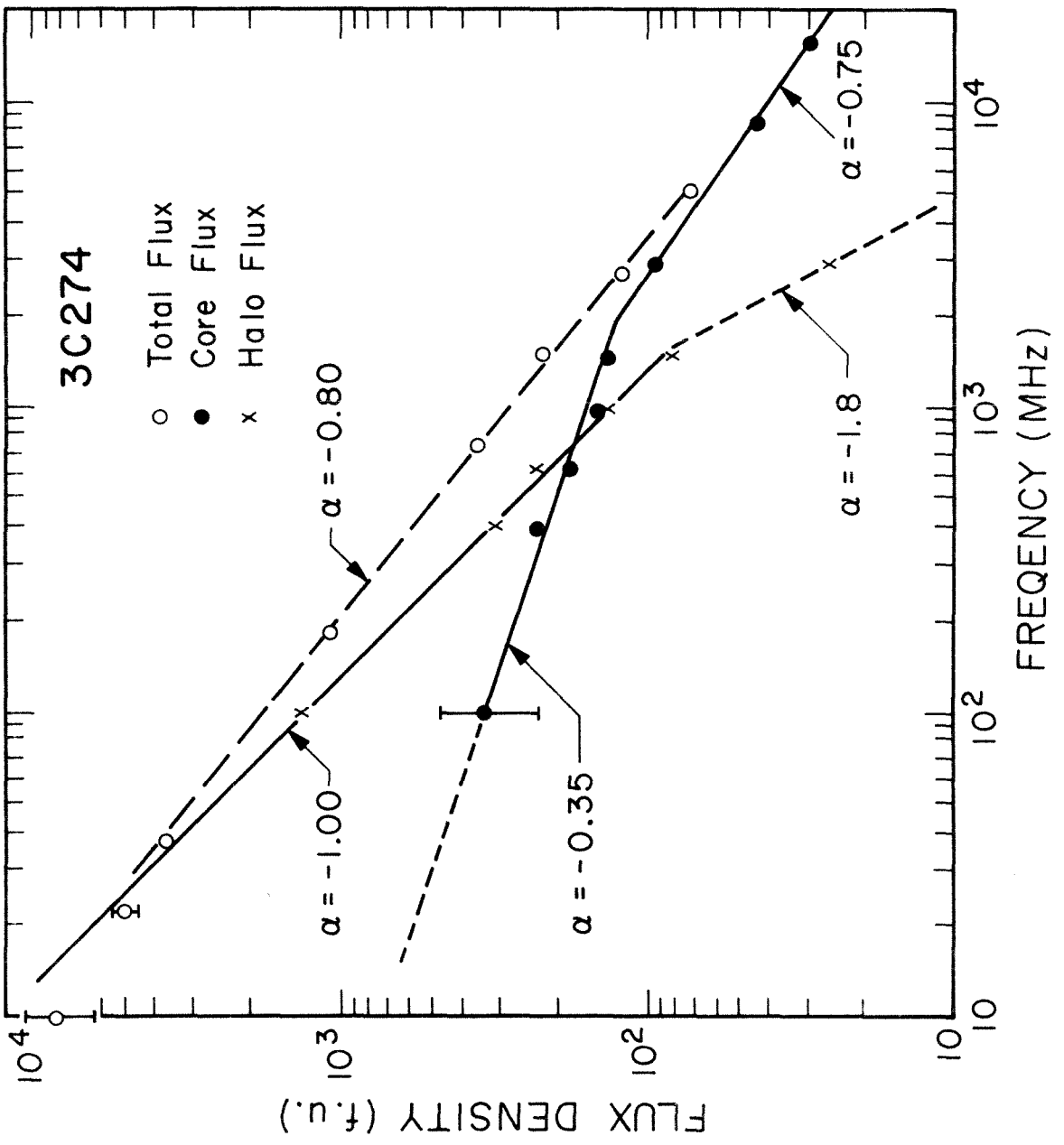
3C274
Total Flux
Core Flux
Halo Flux
α = -0.80
α = -1.00
α = -0.35
α = -1.8
α = -0.75
FLUX DENSITY (f.u.)
FREQENCY (MHz)
10
10²
10³
10⁴

Allen et al. (1968) report that the size of the core decreases between 8.25 GHz and 15.5 GHz. This suggests that the spectral index is not constant across the core.

3C287.1

The brightness distribution of 3C287.1 at 605 MHz is shown in Figure 10. Wyndham (1966) associates the source with an 18.5 magnitude N galaxy. Using the redshift of Sandage (1966), the galaxy is at a distance of 650 Mpc. If the radio source is truly associated with this galaxy, the halo extends more than 1.1 Mpc on either side of the galaxy. The north-south diameter of this object at 1425 MHz (Fomalont and Moffet, private communication) is less than $0.'45$ indicating that the halo has an axial ratio greater than 4:1.

The core is not coincident with the galaxy but lies $0.'6$ to the east. This displacement is based on radio (EF II) and optical positions (Wyndham 1966) with errors less than $\pm\ 0.'1$.

Three confusing sources are seen on the map with positions $+12.'4$ ($\alpha = 13^h\ 31^m\ 11^s$), $-9.'8$ ($\alpha = 13^h\ 29^m\ 42^s$), and $-14.'8$ ($\alpha = 13^h\ 29^m\ 22^s$). The source at $+12.'4$ has a flux density of $\sim$ 0.2 f.u. while the others are just at the noise level with a flux of $\sim$ 0.1 flux units. The source at $-9.'8$ corresponds to 4C01.38 which is $66'$ to the

Figure 10 - The brightness distribution of 3C287.1 at 605 MHz.

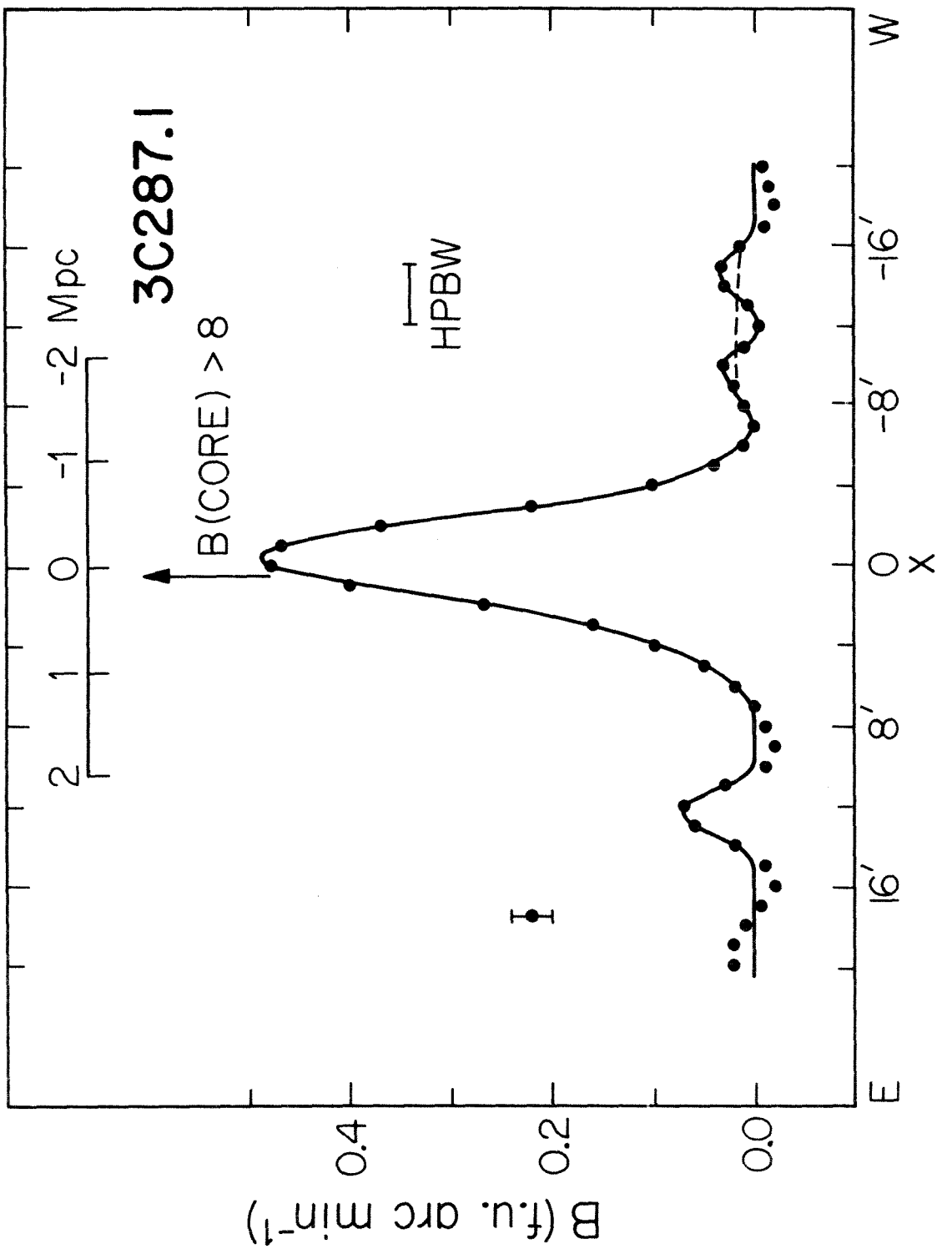
3C287.1
B(CORE) > 8
2 1 0 -1 -2 Mpc
HPBW
B (f.u. arc min⁻¹)
0.0
0.2
0.4
E
16′
8′
0
X
-8′
-16′
W

south of 3C287.1.

P2247+11 (NGC 7385)

This radio source is very similar to 3C264. It has a core of moderate diameter plus a broad halo displaced to one side. The core is coincident with the galaxy NGC 7385 (Clarke 1965) and has a half-power diameter of 1.'0 which is comparable with the size of the optical object, 0.'9, given by de Vaucouleurs and de Vaucouleurs (1964).

Both the 605 and 1425 MHz radio brightness distributions are shown in Figure 11. The core has not been removed from these plots but a strong contribution from P2251+11, 64' to the east in the first grating response, was removed from the 605 MHz visibility before inverting. The 1425 MHz inversion was convolved with a 2.'6 Gaussian to give the same effective beamwidth as the 605 MHz inversion. The brightness of the halo relative to the core is much greater at 605 MHz than at 1425 MHz, indicating a steeper spectrum for the large component.

A distance of 81 Mpc is obtained from the redshift of Humason et al. (1956). The linear scale corresponding to this distance is shown at the top of Figure 11.

Figure 11 - The brightness distribution of P2247+11 at 605 MHz and 1425 MHz. The resolution of the 1425 MHz plot has been reduced to equal that of the 605 MHz plot to show the relative increase in the brightness of the halo at the low frequency.

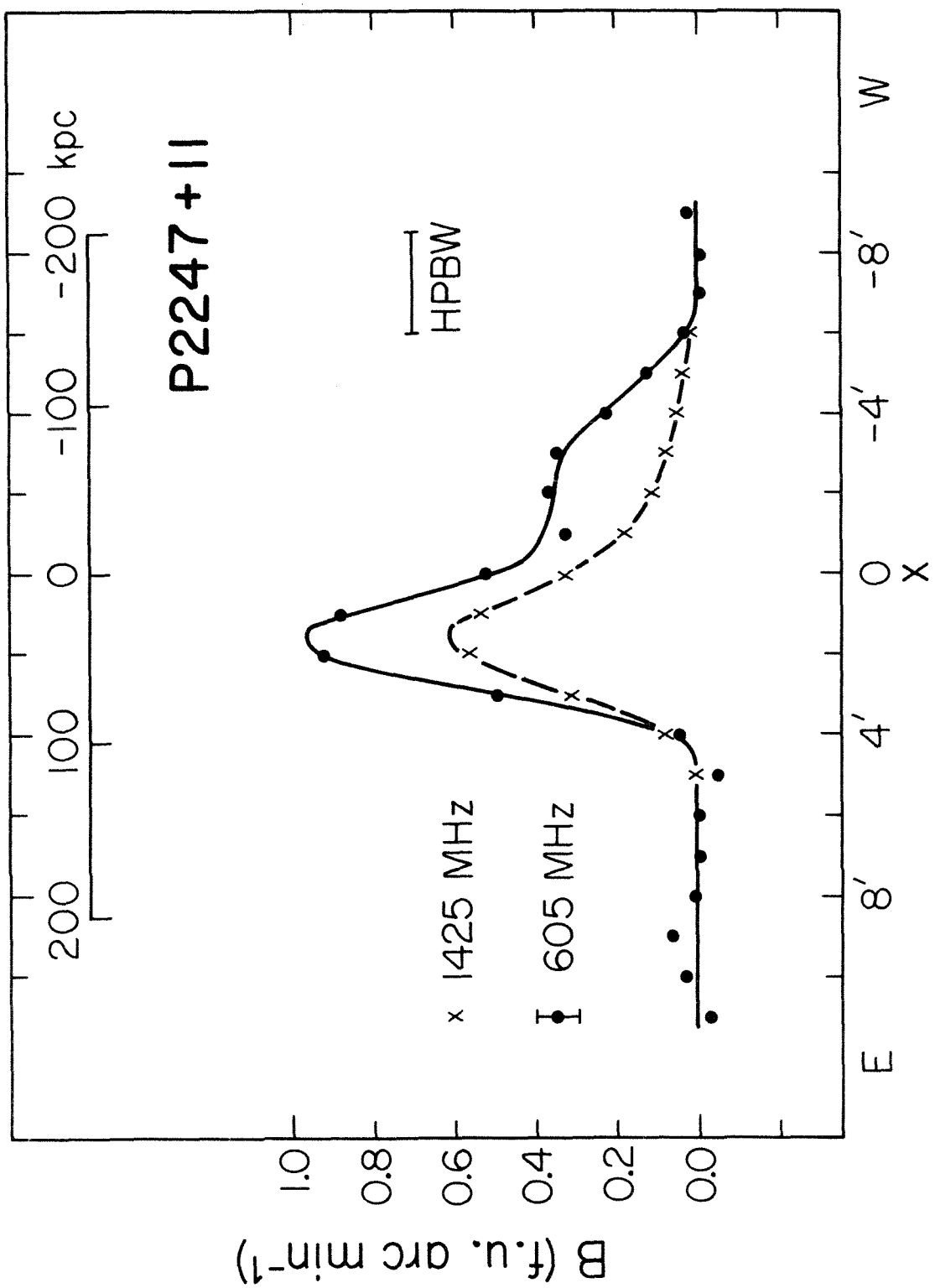
P2247+11
HPBW
× 1425 MHz
I 605 MHz
B (f.u. arc min⁻¹)
1.0
0.8
0.6
0.4
0.2
0.0
200
100
0
-100
-200 kpc
E
8′
4′
0
X
-4′
-8′
W

3C31, 3C78, P0625-35, and P0715-36

These four sources are similar to the other objects discussed in this section. They each consist of a small-diameter core coincident with a galaxy plus an extended radio emission region.

The halos are about 2' in diameter and are centered on the cores, except in 3C31 where the halo is displaced to the east. There is no indication of any large scale structure in the halos. Since the maximum spacing of 977λ was not sufficient to resolve the halos, little more can be learned from the 605 MHz observations.

Table 6 contains the identifications, distances, halo diameters, and additional references with structural information for these sources. The brightness distribution for 3C31 by Macdonald et al. (1968) does not show the large component seen by Fomalont (EF II) but indicates a point source in its place. The confusing source to the east of P0715-36 mentioned in EF II is seen at 605 MHz and is included in Table 4.

TABLE 6

UNRESOLVED HALOS

Source	Identification	Distance (Mpc)	Halo Radio Half Power Width (kpc)	Reference
	(1)	(2)	(3)	
3C31	NGC 383 DE3	51	31	Macdonald et al. (1968)
3C78	NGC 1218 DE3	87	38	Bash (1968a,b)
P0625-35	dumb bell galaxy			Ekers (1969)
P0715-36	elliptical			Ekers (1969)

NOTES TO TABLE 6

(1) Identification of 3C31 and 3C78 are from Wyndham (1966); P0625-35 and P0715-36 are from the Parkes Catalogue (C.S.I.R.O. Radiophysics Division 1969).

(2) Distances for 3C31 and 3C78 are from radial velocities by Humason *et al*. (1956) and Schmidt (1965) respectively.

(3) Widths are based on radio diameters given in Table 4.

d) Double Halo

Two of the twenty-eight objects observed had halos with double structure; these were 3C105 and 3C236. As was noted above, in several other sources separate low-level emission regions may be present, but in the double halo category are included only sources having halos with separate components which are of comparable intensity and are well above the confusion level.

3C105

The 605 and 1425 MHz brightness distributions are given in Figure 12. The split in the halo is clearly seen in the higher resolution plot from EF II. On both plots the halo is well displaced to the west of the core.

The core and halo components have nearly the same spectral indices. Observations at 605 MHz, 960 MHz (Maltby and Moffet 1962), 1425 MHz (EF II) and 2695 MHz (Bash 1968b) all show about 50% of the total radiation coming from the core. Bash (1968b) sets an upper limit of 2".3 on the diameter of the core. This diameter is used to establish the lower limit to the core brightness shown in Figure 12.

There is no optical identification for this source. At the position of the core,

Figure 12 - The brightness distribution of 3C105 at 605 and 1425 MHz.

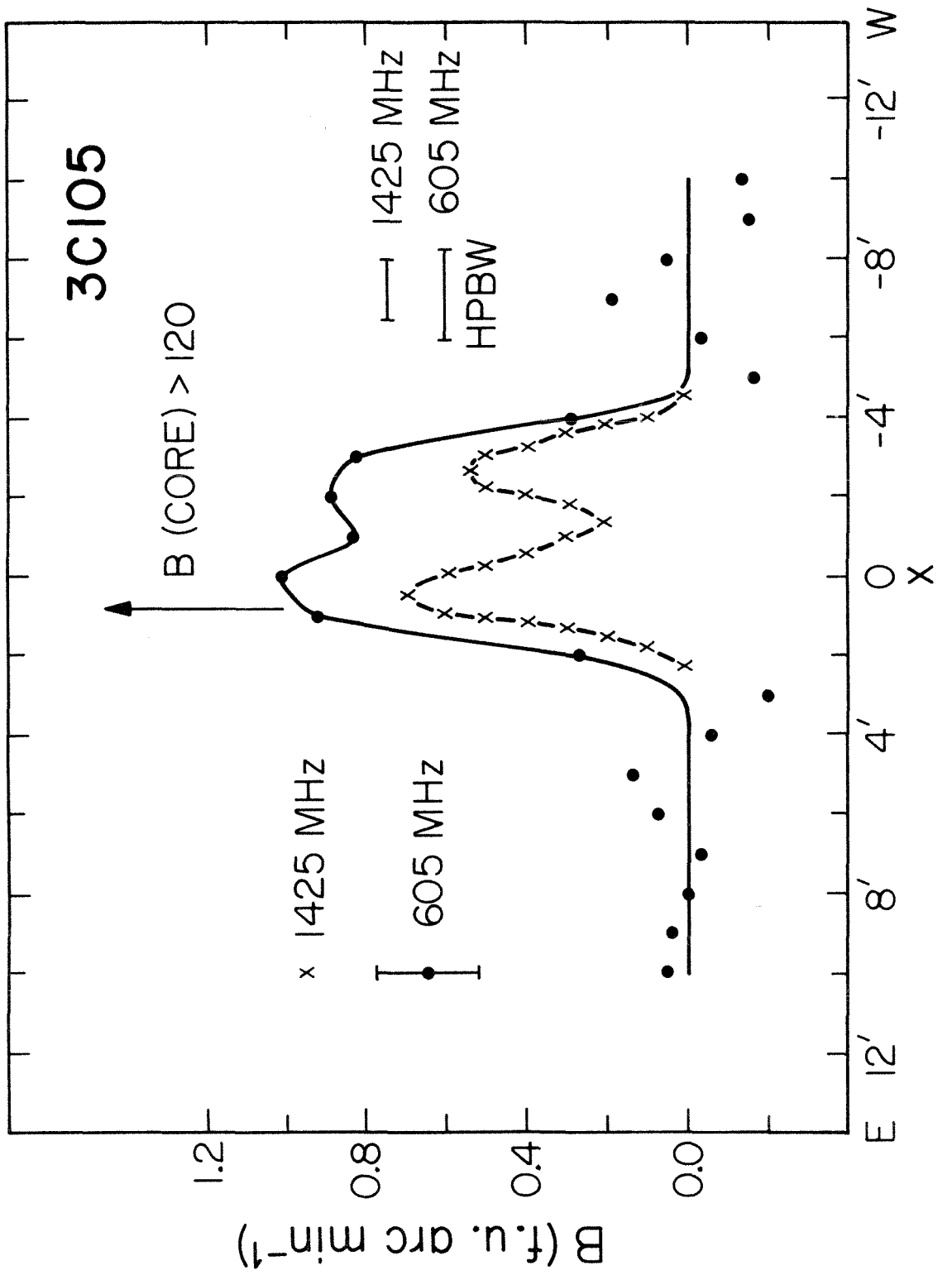
3C105
B (CORE) > 120
1425 MHz
605 MHz
HPBW
× 1425 MHz
605 MHz
B (f.u. arc min⁻¹)
1.2
0.8
0.4
0.0
E 12′ 8′ 4′ 0 -4′ -8′ -12′ W
X

$\alpha(1950.0) = 04^h\ 04^m\ 48^s.0 \pm 0^s.4$ (EF II)

$\delta(1950.0) = 03^\circ\ 32'\ 48''\ \pm\ 15''$ (Fomalont and Moffet private communication),

the Sky Survey print shows an unobscured blank field.

3C236

The brightness distribution of 3C236 is shown in Figure 13. The core has a diameter $<0'.25$ (EF II) and is coincident with a 15.0 magnitude DE4 galaxy (Wyndham 1966). Using the redshift given by Sandage (1967), a distance of 300 Mpc is obtained for the galaxy.

The point source is situated in a very extensive emission region consisting of two components connected by a bridge. Although the brightness of this large region is very low, the double structure is probably real. The depression between the two components is more than twice the r.m.s. noise level. Another broad source is seen $17'$ to the east of the core and corresponds to NRAO 346 (Pauliny-Toth et al. 1966). The position of NRAO 346 lies $22'$ to the southeast of the core of 3C236; at the distance of the DE4 galaxy this separation corresponds to 1.9 Mpc.

In the NRAO catalog, 3C236 (NRAO 344) has a 1400 MHz diameter of $6'.2$ and a flux density which is 0.9 f.u. greater than that of the point source given in EF II. This indicates that at least part of the large double shown in Figure 13 was in the $10'$ beam used for the NRAO

Figure 13 - The brightness distribution of 3C236 at 605 MHz. The broad source at +17' is NRAO 346.

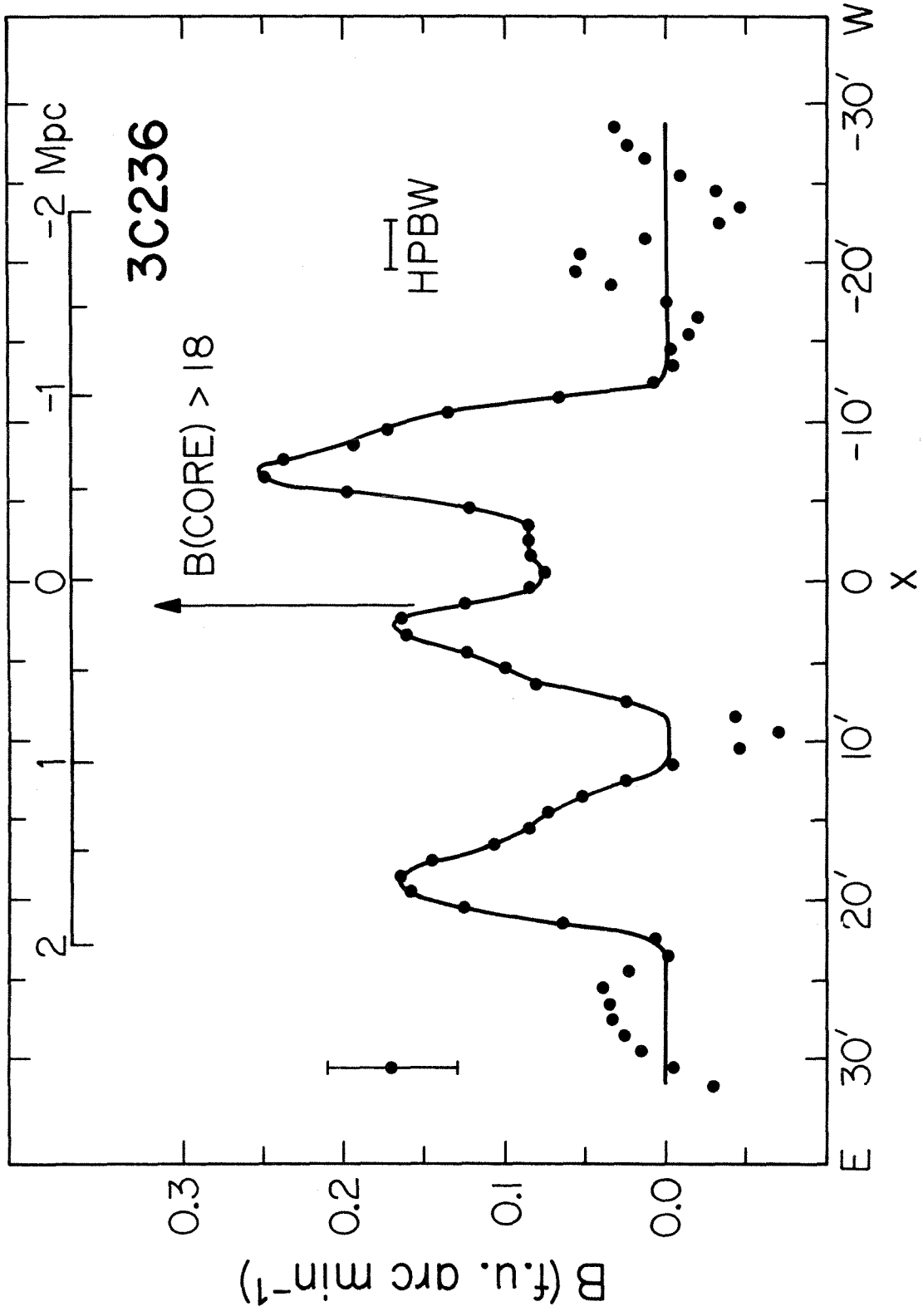
3C236
B(CORE) > 18
HPBW
-2 Mpc
-1
0
1
2
E
30′
20′
10′
0
X
-10′
-20′
-30′
W
0.0
0.1
0.2
0.3
B (f.u. arc min⁻¹)

survey and thus lies close to the point source in the north-south direction.

e) Undetermined Halo Structure

Four sources, 3C120, 3C130, 3C218, and 3C293 definitely have both large and small scale components but the signal to noise ratio of the inversions is so low that the structure cannot be determined.

3C120

This object is a variable radio source (Kellermann and Pauliny-Toth 1968) associated with a fifteenth magnitude Seyfert galaxy (Arp 1968, Sargent 1967). Using the redshift given by Wills (1967), it is at a distance of 98 Mpc.

The positions of the radio core (EF II) and the optical galaxy (Clarke et al. 1966) agree to within the errors given. Very long baseline interferometry at 18 and 6 cm by Kellermann et al. (1968) indicates that there are at least three components in the core with diameters ranging from 3×10^{-3} arc-sec to 8×10^{-4} arc-sec.

The radio variations of 3C120 are discussed by Pauliny-Toth and Kellermann (1969). They describe two outbursts which were observed between 1966 and 1968. Each

event was first seen at a high frequency and then later at progressively lower frequencies with smaller changes in flux. These variations are explained by an expanding cloud of relativistic electrons and magnetic field which becomes transparent to its own synchrotron radiation at lower frequencies as it expands. The following expressions relating flux change, frequency, and time are given by Kellermann and Pauliny-Toth (1968). If Δt is the time since the creation of the expanding cloud, at a given frequency the flux of the new component increases as Δt^3. This goes on until the cloud is optically thin, and then the flux starts to fall due to electron energy loss and decreasing magnetic field strength. Let S_m be the maximum flux of the variable component and Δt_m be the time of the maximum. Both of these quantities are frequency dependent. If the original outburst had an electron energy distribution given by $N\,dE = K\,E^{-\gamma}\,dE$, the time of maximum flux is given by $\Delta t_m \propto \nu^{-(\gamma+4)/(4\gamma+6)}$ and the total flux change is $S_m \propto \nu^{(7\gamma+3)/(4\gamma+6)}$. Using the observed flux change at 2 cm and the $S \propto \Delta t^3$ law, Pauliny-Toth and Kellermann (1969) found the initial epochs of the two bursts in 3C120 to be $t_o = 1965.97 \pm 0.07$ for event 1 and $t_o = 1967.38 \pm 0.05$ for event 2. From these epochs and observations of S_m and Δt_m, they found $\gamma \approx 1$ for both bursts. At 2 cm,

Δt_m = 0.37 yr and S_m = 13.5 f.u. for the second event (Pauliny-Toth and Kellermann 1969). Combining this data with the expressions given above, the expected variation at 605 MHz is

$$S_m = 0.5 \text{ f.u. at } \Delta t_m = 1.8 \pm 0.3 \text{ yr.}$$

Approximately the same values apply for the first event. Therefore, the first event peaked at 605 MHz late in 1967 and the second early in 1969.

Observations were made of 3C120 with a 62λ spacing in 1968 January and November. The November flux was 0.4 ± 0.2 f.u. greater than in January. To correct for the appearance of this new component, a 0.4 f.u. point source with zero phase was added to the 1967 December and 1968 January observations and 0.3 f.u. to the 1968 July observations. In this way all values obtained for the visibility function refer to the same source structure. The visibility given in Table III includes this correction.

A 0.4 f.u. contribution is made to the visibility by P0432+04 (4C04.16) which is 58' northeast of 3C120. The true 605 MHz flux density of this source, obtained by applying a primary beam correction factor of four, is 1.6 f.u. This agrees well with the value of 1.5 f.u. calculated from the flux densities at 408 MHz and 1410 MHz given in the Parkes Catalogue (C.S.I.R.O. Radiophysics

Division 1969).

The 605 MHz observations confirm that 3C120 has a core-halo structure. The halo is 2.'7 in diameter and contains 1.1 f.u. (20% of the total flux) at this frequency. The core and halo are concentric to within ± 0.'2. The displacement of the halo in the model in EF II is very much dependent on the Fomalont's 289λ data point, which has an unusually high error.

Nothing can be said about the structure of the halo from these observations. Errors introduced by the corrections for variations, the subtraction of the confusion source, and the relatively small flux of the halo make any features in the brightness distribution unreliable.

The core has a spectral index of $\alpha = -0.34$ between 605 and 1425 MHz. Since the two outbursts discussed by Pauliny-Toth and Kellermann (1969) have $\gamma \sim 1$ and thus $\alpha \sim 0$, the majority of the electrons in the core either originated with a steeper spectrum or have had their spectrum steepened by energy losses.

3C130

Most of the flux of 3C130 comes from an unequal-diameter double which was only partially resolved at 605 MHz. Fomalont (EF II) shows that the east-west component diameters are 1.'7 and <0.'4 with a separation of 1.'6. Three

one-dimensional strip scans were obtained at 605 MHz at position angles of 41°, 90°, and 128°. Although the resolution was not sufficient to determine the sizes or flux densities of the components, the centers are separated by 2.'7 at a position angle of about 40°. There is an additional large emission region about 20' to the east of the core. This source is roughly 6' in diameter with a flux density of about 1.0 f.u. Another large component with about half this flux may be coincident with the unequal double.

3C218 (Hydra A)

Maltby and Moffet (1962) and Fomalont (EF II) report a core-halo structure for 3C218. The halo is indicated by a rise in the visibility amplitude of about 5% for spacings less than 500λ. Though this rise is close to the error level of individual visibility measurements, it is probably significant since it is seen in both studies, which together include 10 observations at spacings less than 400λ.

At 1425 MHz the core consists of a small component with an east-west diameter of 10" containing 20% of the source flux plus a 42" diameter component with most of the remaining flux (Lequeux 1962). The core is elongated to 1.'2 at P.A. = 30° (Maltby and Moffet 1962).

The observations obtained at 605 MHz do not cover a sufficient range of baselines to independently define the core. However, from the visibility given in EF I, the halo is resolved out by 700λ. With this information the relative amplitudes of the core and halo components at 605 MHz are obtained; 15% of the source flux lies outside the core. With the core removed, the main brightness peak lies 1' to the east of the core position and has a diameter of roughly 6'. Two other peaks, at 8' east and 16' west are just at the noise level and may not be real. The redshift by Minkowski (quoted by Maltby et al. 1963) for the galaxy identified with 3C218 gives a distance of 160 Mpc; the 6' halo would have a diameter of 280 kpc.

The spectra of the core and halo components and the combined spectrum are shown in Figure 14. The component flux densities are from the present work at 605 MHz. Maltby and Moffet (1962) at 960 MHz, and EF I at 1425 MHz. The total flux densities are from Bridle and Purton (1968) at 10.03 MHz, Roger et al. (1969) at 22.25 MHz, Conway et al. (1963) at 38, 240, 408, and 412 MHz, Pauliny-Toth et al. (1966) at 750 and 1400 MHz (the flux densities have been adjusted to conform to the scale of Kellermann et al. 1969), Kellermann, Pauliny-Toth, and Tyler (1968) at 2695 MHz, and Pauliny-Toth and Kellermann (1968) at

Figure 14 - The component spectra (solid and short-dashed lines) and the combined spectrum (long-dashed line) of 3C218.

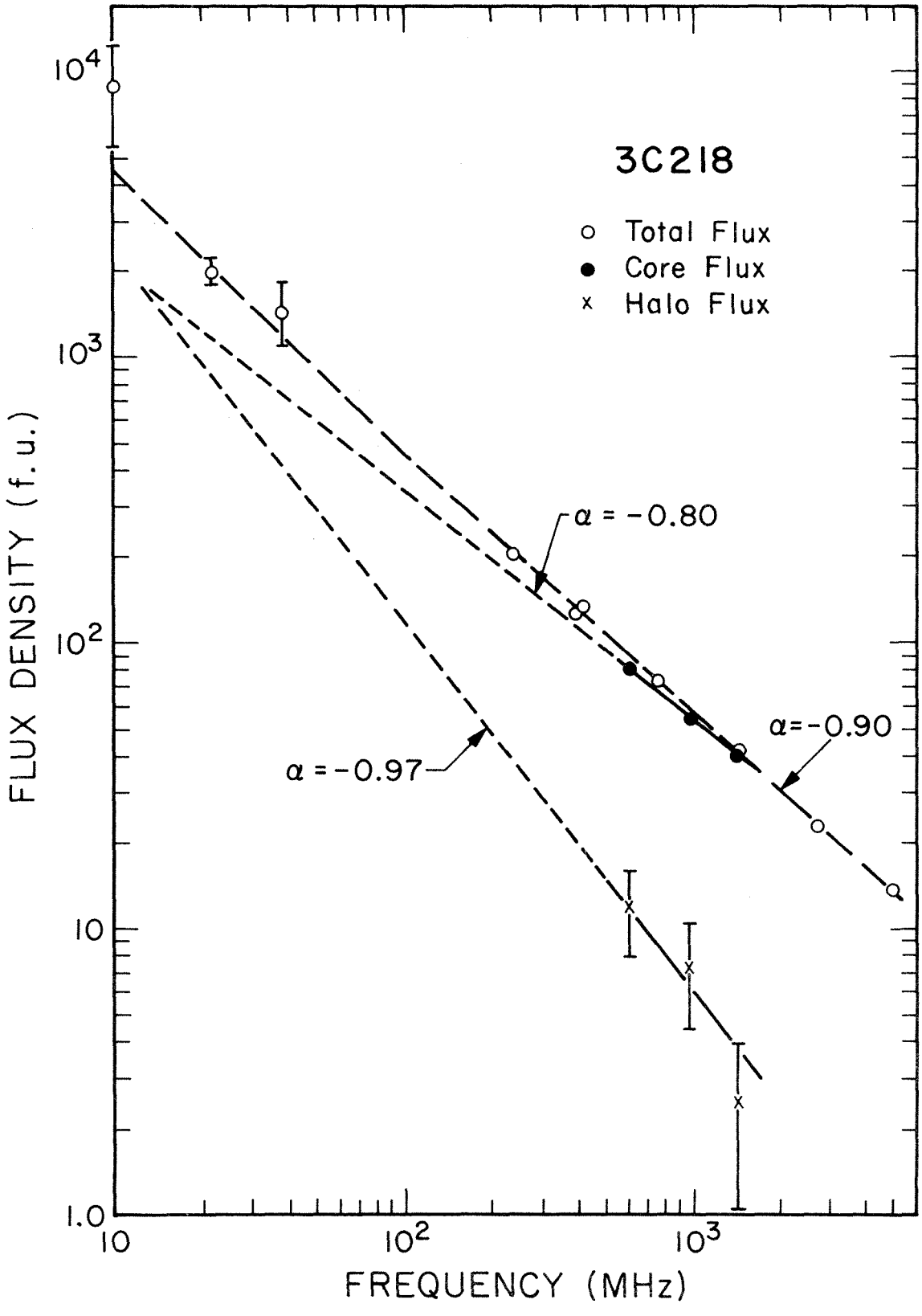
3C218
Total Flux
Core Flux
Halo Flux
α = -0.80
α = -0.90
α = -0.97
FLUX DENSITY (f.u.)
FREQUENCY (MHz)
10⁴
10³
10²
10
1.0
10
10²
10³

5000 MHz. Two power law spectra are used to fit the core flux densities and a single power law spectrum for the halo. Although the spectrum of the halo is very poorly determined due to the large flux density errors, the combined spectrum shown in Figure 14 agrees rather well with the observed total flux densities. Since there are no low frequency measurements of the component fluxes, their spectra could be more complicated than shown at frequencies below 600 MHz.

3C293

A diagram of the two-dimensional brightness distribution of 3C293 is given in Figure 15. Observations were made at three position angles, P.A. = 64°, 90°, and 119°. The core has a flux density of 6.6 f.u. and there is an additional 1.6 f.u. from a large emission region extending to the southwest. This large component has a one-dimensional brightness of about 0.2 f.u. arc-min^{-1}, which is only twice the noise level. The halo may consist of two broad components with brightness peaks to the northeast and southwest of the core.

The core is coincident in right ascension with a D galaxy (Wyndham 1966). From the redshift measured by Sandage (1966), its distance is 135 Mpc. Therefore one arc-minute equals 39 kpc, and the extent of the large component is roughly 0.4 Mpc.

Figure 15 - The two-dimensional brightness distribution of 3C293.

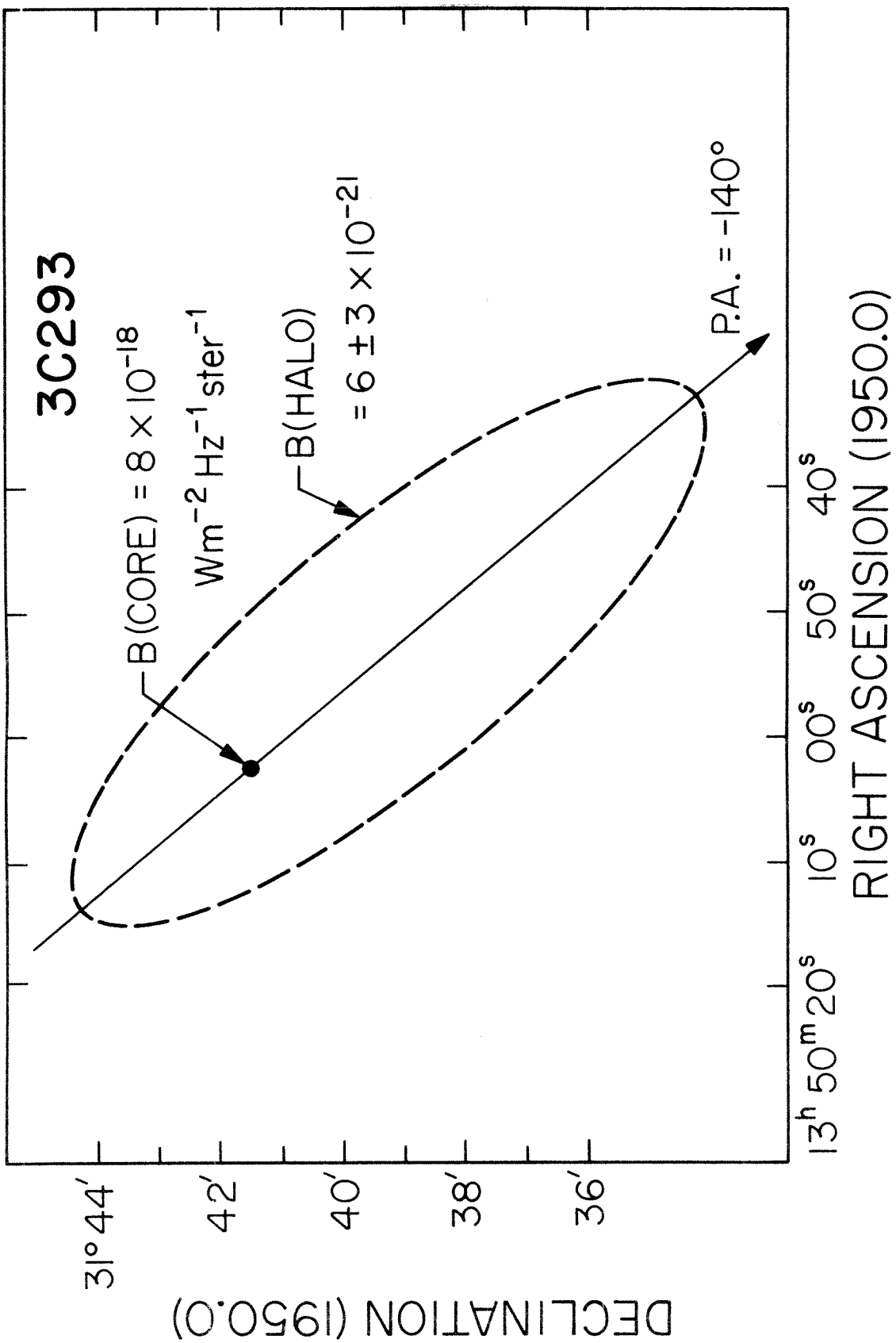
3C293
B(CORE) = 8 × 10⁻¹⁸
Wm⁻² Hz⁻¹ ster⁻¹
B(HALO)
= 6 ± 3 × 10⁻²¹
P.A. = -140°
31° 44′
42′
40′
38′
36′
13h 50m 20s
10s
00s
50s
40s
DECLINATION (1950.0)
RIGHT ASCENSION (1950.0)

f) No Halo Detected

The remainder of the sources on the observing list are those which contain a point source but do not show a large diameter component close by. These are 3C20, 3C40, 3C66, P0935-28, 3C231, 3C247, P2058-28, 3C435, P2331-41. Additional information on four of these sources, 3C40, 3C66, 3C231, and 3C247, is presented in this section. For the rest, there is nothing more to be said from the present observations.

3C40 (NGC 541, 545, and 547)

The two-dimensional radio brightness distribution of 3C40 derived by Moffet (private communication) is shown in Figure 16. The model is based on observations made with the Owens Valley interferometer at 10 cm (Bartlett private communication), 21 cm (EF II, Fomalont and Moffet private communication), 31 cm (Moffet 1962, Maltby 1962), and the present 50 cm observations, and with the 210 foot antenna of the N.A.S.A. Deep Space Network at Goldstone at 3.75 cm (Moffet private communication). The source contains three large components, A, B, and C, and a possible point source marked A_p.

The spectra of component C and of the sum of the fluxes of components A, A_p, and B are shown in Figure 17.

Figure 16 - The two-dimensional half power radio contours of three components of 3C40 are shown. A possible small diameter source is labeled A_p. The positions of three elliptical galaxies are indicated.

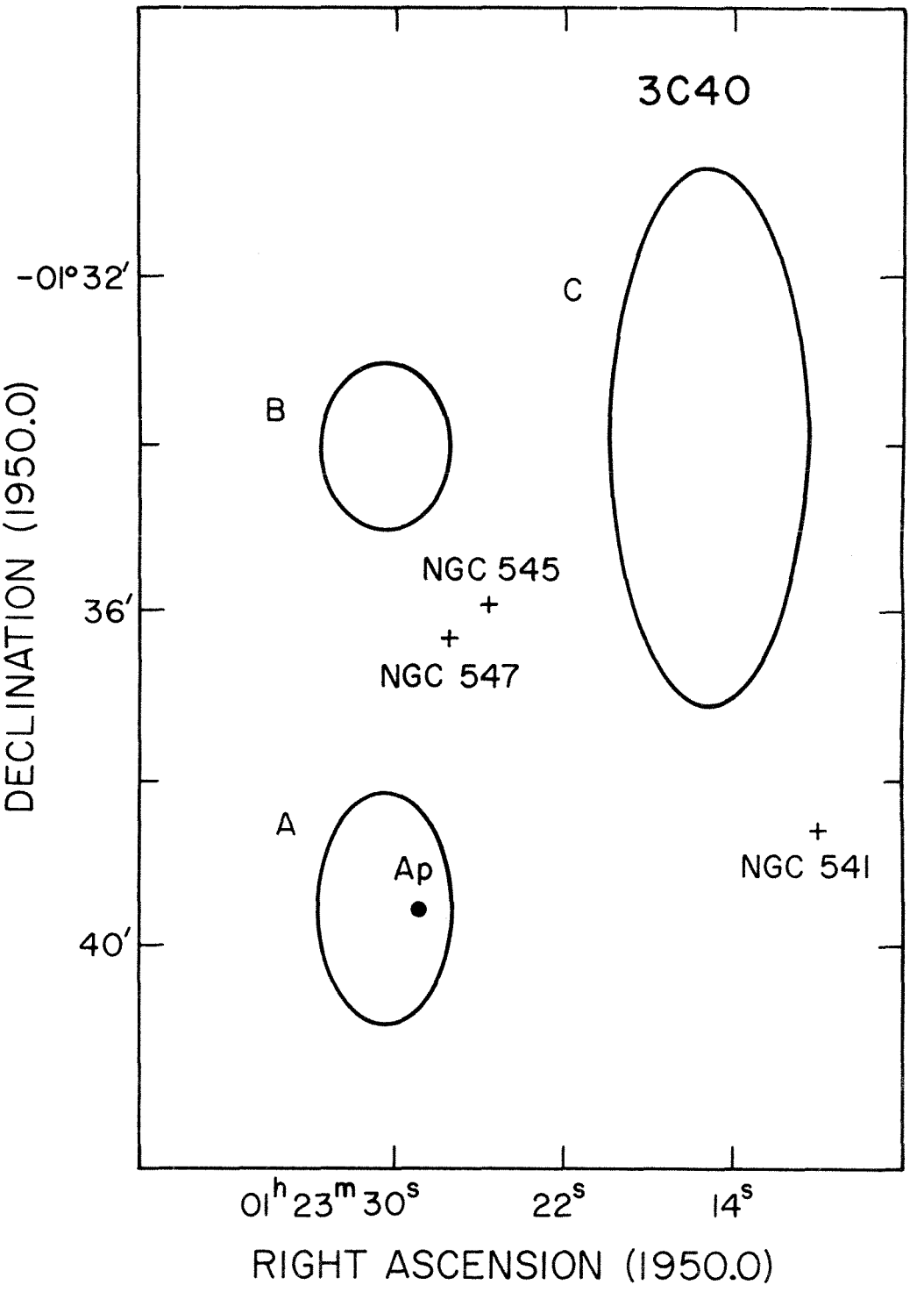
3C40
-01°32′
36′
40′
DECLINATION (1950.0)
B
C
A
Ap
NGC 545
+
+
NGC 547
+
NGC 541
01h23m30s
22s
14s
RIGHT ASCENSION (1950.0)

Figure 17 - The component spectra (solid and short-dashed lines) and combined spectrum (long-dashed line) of 3C40.

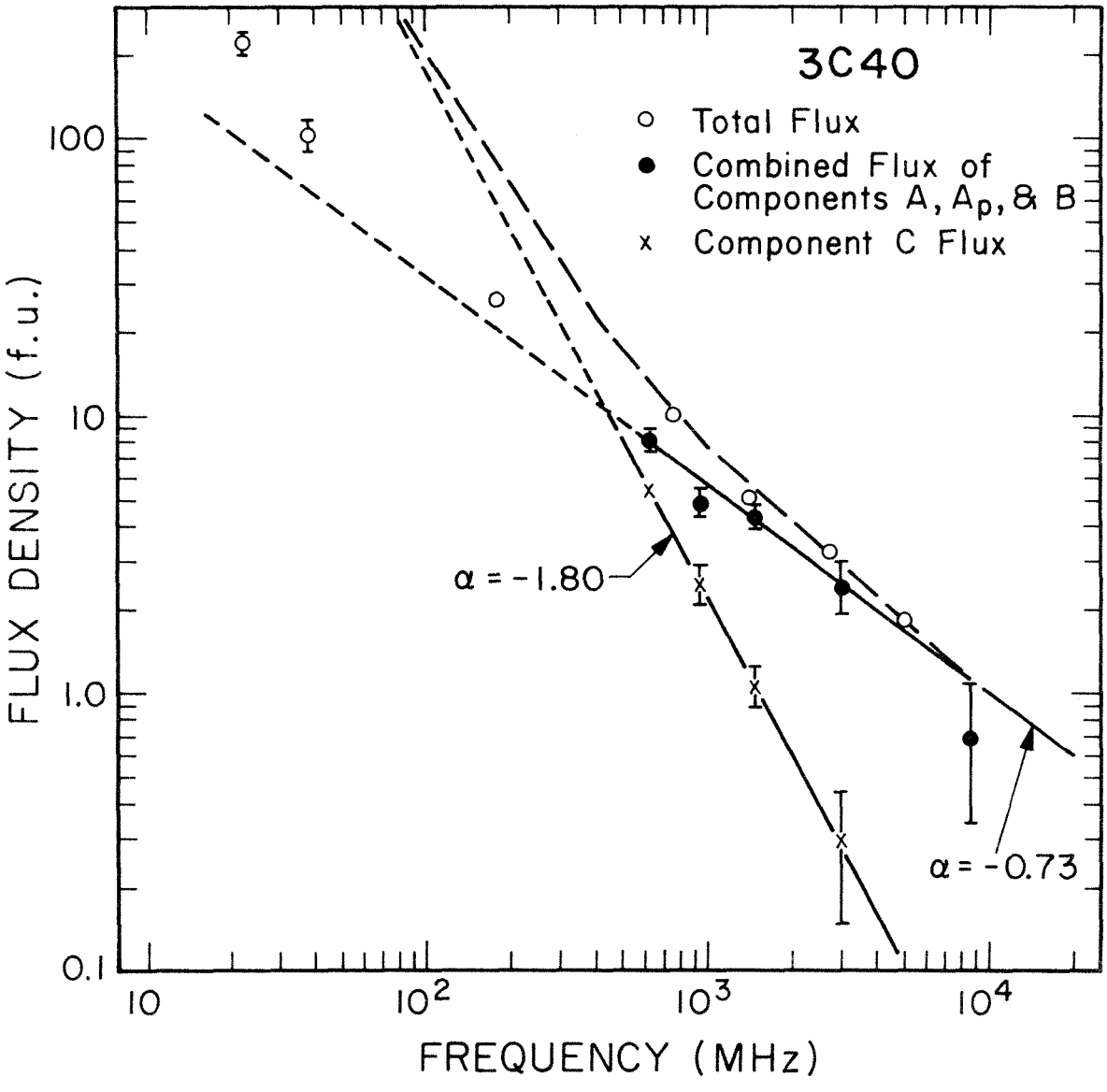
3C40
Total Flux
Combined Flux of Components A, Ap, & B
Component C Flux
α = -1.80
α = -0.73
FLUX DENSITY (f.u.)
FREQUENCY (MHz)
100
10
1.0
0.1
10
10²
10³
10⁴

References for the component flux densities are given above. The total flux densities are from Roger et al. (1969) at 22.25 MHz and the rest from Kellermann et al. (1969). Since the sum of the power law spectra extrapolated to low frequencies does not fit the observed total flux densities one or both of the component spectra must flatten below 600 MHz.

The 605 MHz brightness distribution is shown in Figure 18. The slightly resolved small component corresponding to the sum of components A, A_p, and B has been removed. The remaining feature is component C.

The source lies in the Abell cluster (Abell 1958) A194. A photograph of the region is given by Maltby et al. (1963). The three brightest members of the cluster are the elliptical galaxies NGC 541, 545, and 547, and their positions are indicated in Figure 16. The latter two galaxies share a common envelope. The radio components do not coincide with any galaxy in the cluster. Redshifts by Minkowski and Zwicky (quoted by Maltby et al. 1963) give a distance 53 Mpc for these galaxies. This distance was used to establish the linear scale in Figure 18.

3C66

The brightness distribution of 3C66 obtained at 605 MHz agrees with that of Fomalont (EF II) and Macdonald et al. (1968). The double component is unresolved at

Figure 18 - The brightness distribution of 3C40 at 605 MHz. The dashed line indicates an alternative interpretation.

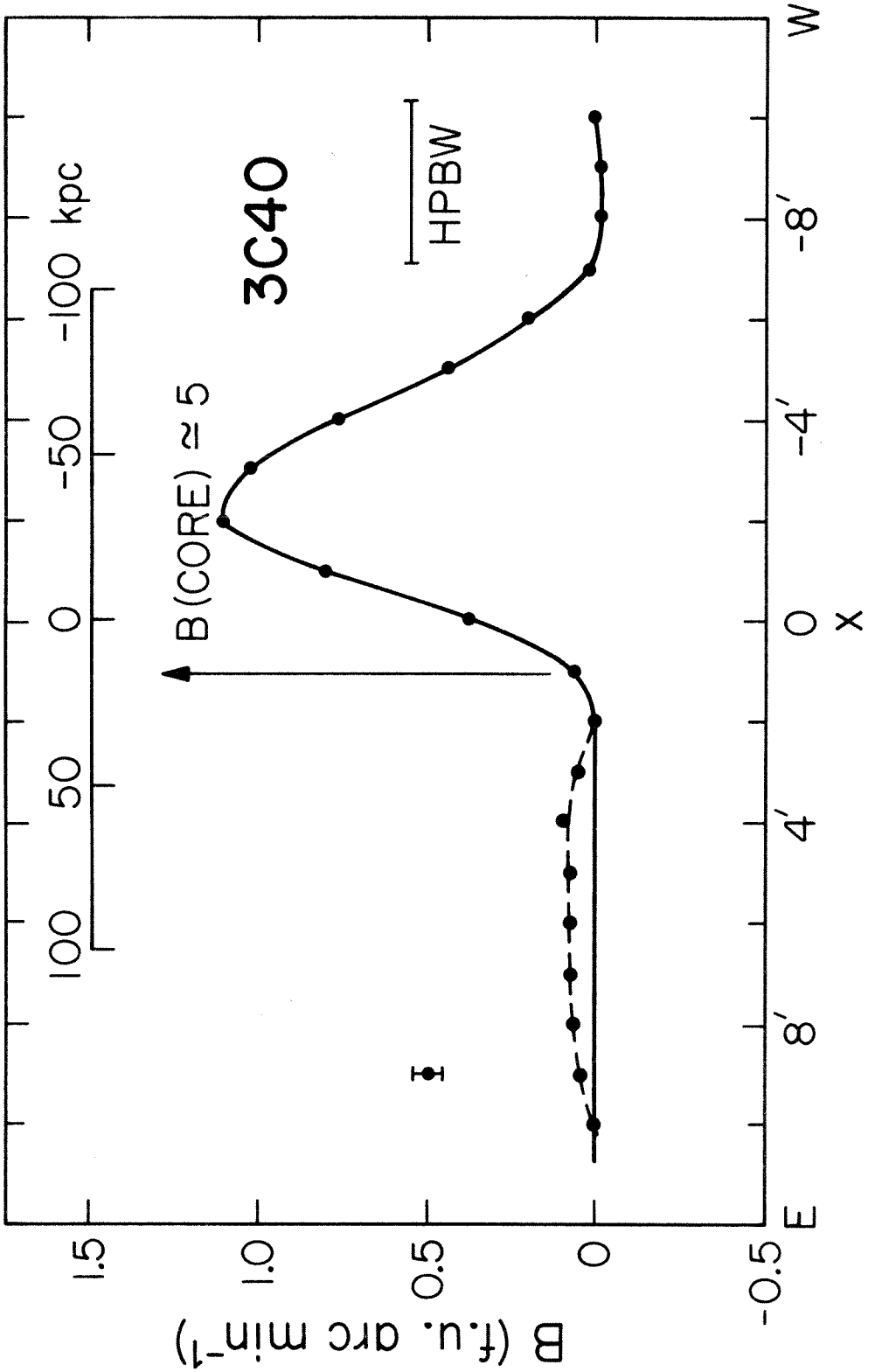
3C40
HPBW
B(CORE) ≃ 5
-100 kpc
-50
0
50
100
E
W
8′
4′
0
-4′
-8′
X
B (f.u. arc min⁻¹)
1.5
1.0
0.5
0
-0.5

605 MHz, but the extension to the west and the point source stand out clearly. The spectra of the point source and the double plus extension are shown in Figure 19. The 1425 MHz fluxes are from Fomalont (EF II), and the 2850 MHz fluxes are from Bartlett (private communication). The total flux densities are from the same sources referred to for 3C264. Since the combined spectrum shown in Figure 19 does not fit the observed total flux densities at 38 and 178 MHz, it is likely that one or both of the simple power law spectra for the components is curved at low frequencies. Except for the 408 MHz flux density of the double component, the flux densities given in Macdonald et al. (1968) are not compatible with Figure 19. This may be due to a different interpretation of the boundaries of the components in this region.

3C247

Fomalont (EF II) reports a core-halo structure for this source. Observations at 605 MHz reveal only a point source at the position of the core and two faint emission regions 10' to the west. Observations were made at three position angles, P.A. = 45°, 90°, and 124°. A diagram of the two-dimensional structure is given in Figure 20. The two displaced emission regions lie at roughly the same right ascension, with the southern one elongated in a north-south direction. The very low surface brightness

Figure 19 - The component spectra (solid and short-dashed lines) and combined spectrum (long-dashed line) of 3C66.

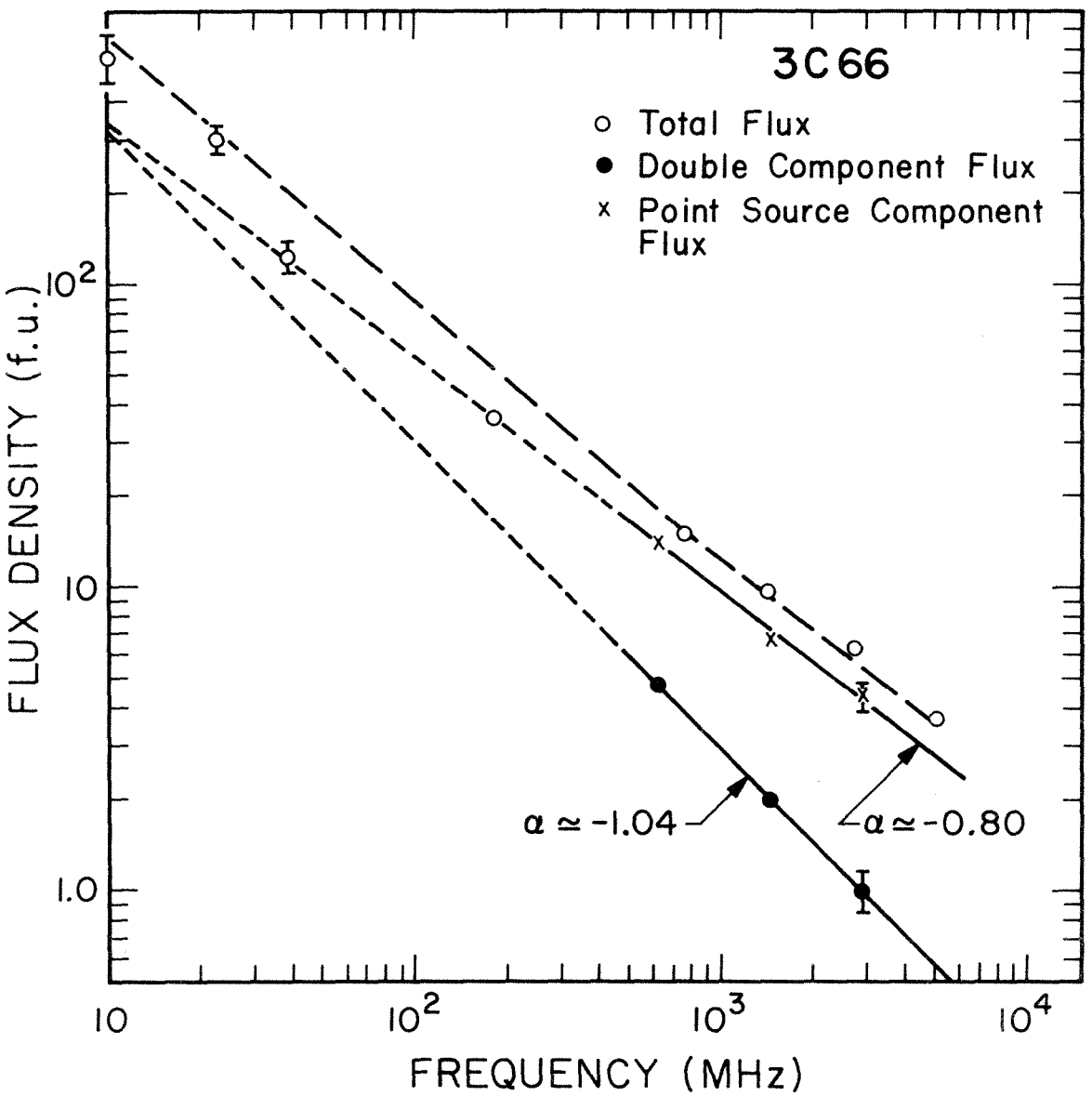
3C66
Total Flux
Double Component Flux
Point Source Component Flux
FLUX DENSITY (f.u.)
FREQUENCY (MHz)
10
10^2
10^3
10^4
1.0
10
10^2
$\alpha \simeq -1.04$
$\alpha \simeq -0.80$

Figure 20 - The two-dimensional brightness distribution of the region near 3C247.

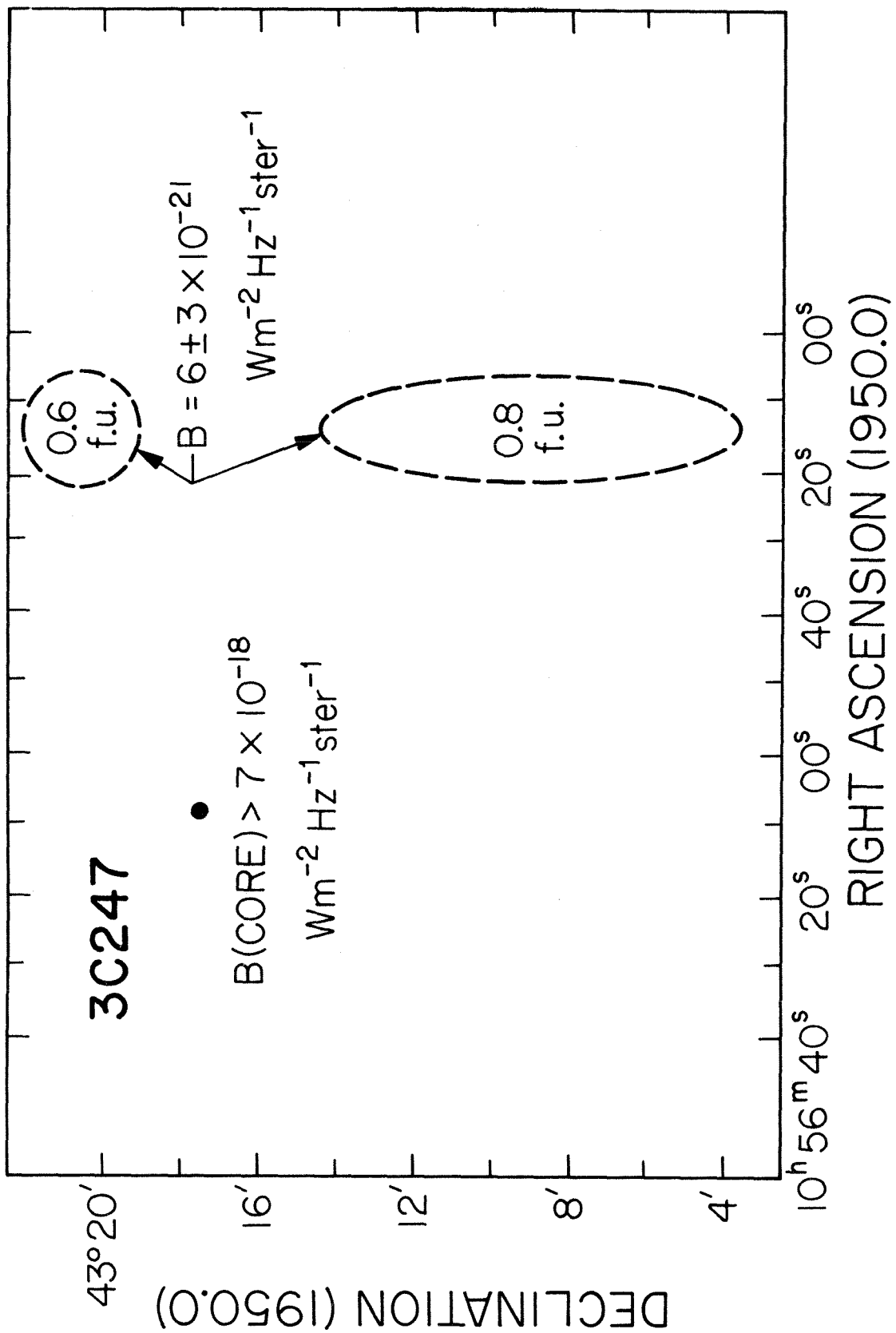
3C247
B(CORE) > 7 × 10⁻¹⁸
Wm⁻² Hz⁻¹ ster⁻¹
B = 6 ± 3 × 10⁻²¹
Wm⁻² Hz⁻¹ ster⁻¹
0.6 f.u.
0.8 f.u.
43°20′
16′
12′
8′
4′
DECLINATION (1950.0)
10h56m40s
20s
00s
40s
20s
00s
RIGHT ASCENSION (1950.0)

of these objects makes it impossible to determine their shapes with any accuracy.

There is no satisfactory optical identification for the point source. The object given by Wyndham (1966) is an ordinary star (Schmidt private communication). A minimum distance of 10^3 Mpc is obtained for the point source by assuming that the apparent magnitude of the optical object is less than the Sky Survey plate limit (19.5 magnitude) and that the absolute magnitude is that of a strong radio galaxy (-20.5 magnitude). If the point source and the faint emission regions are at the same distance, the 10' separation would correspond to about 3 Mpc. Although this is rather large, it is only a factor of four greater than the extreme dimensions of other objects with well-established redshifts such as 3C236.

3C231 (M82)

M82 is an odd-looking galaxy long noted for the extensive dust patches which obscure its surface. Numerous filaments are seen in Hα extending about 1'.5 beyond the galaxy in directions perpendicular to the major axis (Lynds and Sandage 1963). At a distance of 3.1 Mpc (Solinger 1969a) 1' corresponds to 0.9 kpc. In addition to these emission line filaments, long exposure plates reveal continuum filaments extending out twice as far (Sandage and Miller 1964). There is strong evidence that matter is

being ejected by an explosion in the center of the galaxy. In addition to the radial appearance of the filaments, their spectra show the gas to be receding from the center of the galaxy with the more distant gas moving the fastest. Estimates of the peak recession velocity range from 450 km sec^{-1} for a model with the gas optically thick (Burbidge et al. 1964) to 1500 km sec^{-1} if it is optically thin, (Lynds and Sandage 1963).

The nature of the continuum radiation is unknown. It is highly polarized and has colors which differ strongly from those of the main body of the galaxy (Elvius 1962, 1969, Sandage and Visvanathan 1969). Lynds and Sandage (1963) propose that it is synchrotron radiation (Lynds 1961, Sandage and Visvanathan 1969). Ultrarelativistic electrons generated by the initial explosion radiate in a magnetic field being carried out by the ejected matter. The continuum filaments correspond to the lines of strong field.

An alternative explanation is offered by Solinger (1969a,c) who suggests that the continuum radiation arises from Thomson scattering of light from an intense point source in the galaxy, presumably a Seyfert nucleus. The compact source of scattered light would explain both the polarization and the circular arcs which the polarization vectors make about the center of the galaxy. The absence

of a visible Seyfert nucleus is explained by the large amount of absorbing dust in the galactic plane. A hot plasma behind the expanding shock wave caused by the original explosion provides the excitation for the observed Hα emission lines and the free electrons needed for Thomson scattering.

Most of the radio emission of 3C231 comes from a component within M82 which has a half power diameter of 0.'7 (Lequeux 1961, EF II, Macdonald et al. 1968). The position of this component coincides with the center of the explosion given by Solinger (1969b).

At 605 MHz, the source was observed at three position angles, P.A. = 47°, 90°, and 134°. In each case the brightness distribution is dominated by a small bright core. Macdonald et al. (1968) conclude that the size and shape of the source are frequency dependent, with the major axis diameter going from 0.'58 at 1420 MHz to 0.'85 at 408 MHz and the axial ratio decreasing from 1.8:1 to 1.3:1. At 605 MHz, the half power diameter is about 0.'7 on all three cuts compared to the 0.'6 at 1425 MHz seen by Fomalont (EF II).

The central source was subtracted from the visibility at each position angle, and the inversions were examined for a faint halo. The noise level on the maps had an r.m.s. value of about 0.08 f.u. per arc minute.

Some peaks with twice this brightness are seen on the three maps but it is impossible to build up a two-dimensional model without more data. The total flux of these peaks is about 0.7 f.u. None of these is centered on the galaxy and they are therefore unrelated to the optical continuum radiation. An upper limit of 1.0 f.u. can be set, on the basis of the present observations, for the flux coming from a halo about the galaxy. This limit is 10% of the core flux density. Sandage and Visvanathan (1969) and Solinger (1969a) have noted that a limit of this magnitude plus the observed radio spectrum of the source seriously weakens the synchrotron explanation for the optical continuum emission. From photometric measurements the optical continuum emission is between 10^{-27} (Solinger 1969a) and 10^{-28} Wm^{-2} Hz^{-1} (Sandage and Visvanathan 1969) at 6.7×10^{14} Hz (the middle of the B filter band). Assume that the core and halo have the same spectrum with $\alpha = -0.24$ between 38 MHz and 750 MHz and $\alpha = -0.54$ above 750 MHz (Kellermann et al. 1969). Then the expected halo flux density at 605 MHz is between 30 and 300 f.u. An even higher flux density would be needed if there is any high energy cutoff in the electron energy distribution. Unless the relativistic electrons in the halo have a flatter energy distribution than those in the core, the synchrotron explanation is precluded.

V. DISCUSSION

Fourteen core-halo or asymmetric double sources were sufficiently resolved at 605 MHz to obtain the flux densities of the individual components and the positions and diameters of the large emission regions. This sample will be used in discussing the general properties of objects of this type. The remainder of the twenty-eight observed sources either did not have a core-halo or asymmetric double structure or the halos were unresolved. Detailed structural information is also available on Centaurus A and 3C84, each of which has extended components and a bright central core. These sources will be included in the discussion.

The extended component of Centaurus A has a double structure with emission regions on either side of NGC 5128; its overall extent is $\approx 8^\circ \times 2^\circ$. The core is also double with an extent of about $10'$ and is coincident with the galaxy (Cooper et al. 1965). Ryle and Windram (1968) give a detailed discussion of 3C84. The halo is circular and has an angular extent of about $5'$. The core is rather complex. There is a small component with a diameter of $0''.0012$ and a larger component with a diameter of $0''.03$ (Kellermann et al. 1968). In the model proposed by Ryle and Windram (1968), the spectrum of the small

component is cut off by synchrotron self-absorption below 6000 MHz, and the large component is cut off below 400 MHz. VLB interferometry at 408 and 448 MHz by Clarke et al. (1969) show the core to have a double structure with $0''.0008$ diameter components separated by $0''.037$. They associate this double with the $0''.03$ component of Kellermann et al. (1968).

a) Physical Properties

The fourteen sources in the sample are listed in Table 7. For the galaxies for which a distance has been established several physical properties of the core and halo components are given. These include the half power diameter (generally in one dimension), d, the absolute integrated luminosity, L, the absolute spectral power at 605 MHz, P_{605}, the minimum total source energy, E, and the equipartition magnetic field, H.

References for the distances are given in Chapter IV. The total luminosity for most of the components was calculated by integrating a simple power law spectrum from 10 to 10^5 MHz using the spectral indices given in Table 4. For 3C264, 3C274, and 3C218 the spectra shown in Figures 6, 9, and 14 were integrated. The minimum total source energy was calculated by assuming an equipartition of particle and magnetic field energies. Such

TABLE 7

PHYSICAL PROPERTIES OF WELL RESOLVED

CORE-HALO AND ASYMMETRIC DOUBLE SOURCES

Source	r (Mpc)	d (kpc)	log L (erg s^{-1})	log P_{605} (W Hz^{-1} $ster^{-1}$)	log H (oersted)	log E (erg)
Spiral Galaxies						
P0045-25	2.5		39.04	20.76		
core		< 0.2	38.88	20.28	> -3.7	< 53.6
halo		10.0	38.53	20.59	-5.1	56.0
P1302-49	3.8		39.75	21.08		
core		< 0.3	39.64	20.86	> -3.7	< 54.2
halo		8.6	39.08	20.69	-5.0	55.9
P1334-29	4.0		39.04	20.81		
core		< 0.5	38.30	19.79	> -4.2	< 53.8
halo		5.5	38.96	20.77	-4.8	55.7
Elliptical Galaxies - Simple Halos						
P0843-33	10		40.28	21.49		
core		2.3	40.11	21.32	-4.3	55.7
halo		12.5	39.77	21.00	-5.0	56.4
3C264	62		41.55	23.59		
core		11	41.38	23.36	-4.4	57.4
halo		72	41.08	23.20	-5.0	58.7

TABLE 7 CONT.

Source	r (Mpc)	d (kpc)	log L (erg s^{-1})	log P_{605} (W Hz^{-1} $ster^{-1}$)	log H (oersted)	log E (erg)
Elliptical Galaxies - Simple Halos Cont.						
P1216-10	------					
3C274	15		41.89	23.93		
core		3	41.74	23.57	-3.9	56.8
halo		26	41.34	23.68	-4.5	58.4
3C287.1	650		43.35	25.32		
core		< 57	43.04	25.00	> -4.5	< 59.4
halo		720	43.08	25.04	-5.4	60.8
P2247+11	81		41.63	23.43		
core		28	41.50	23.15	-4.7	58.0
halo		118	41.04	23.11	-5.1	59.1
Elliptical Galaxies - Double Halos						
3C105	-----					
3C236	300		43.08	24.80		
core		< 20	43.04	24.60	> -4.2	< 58.6
halo		1200	42.20	24.36	-5.7	61.0

TABLE 7 CONT.

Source	r (Mpc)	d (kpc)	log L (erg s^{-1})	log P_{605} (W Hz^{-1} $ster^{-1}$)	log H (oersted)	log E (erg)
Elliptical Galaxies - Undetermined Halo Structure						
3C120	98		42.18	23.69		
core		~.001	42.15	23.59	-0.8	52.6
halo		77	40.86	23.00	-5.1	58.5
3C218	160		43.23	25.34		
core		23	43.18	25.28	-4.0	59.1
halo		280	42.32	24.46	-5.2	60.1
3C293	135		42.34	24.18		
core		< 12	42.18	24.08	> -4.2	< 58.0
halo		400	41.84	23.48	-5.6	59.6

calculations have been described by Burbidge (1956), Burbidge and Burbidge (1957) and Maltby et al. (1963). The energy of heavy particles in the source is assumed to be 100 times that of electrons. The radio component volumes used for the equipartition calculations were obtained by assuming the components are spherical with diameters given in Table 7.

No correction was made for the redshift or other cosmological effects. For all but two of the objects $Z = \Delta\lambda/\lambda < 0.05$. The maximum redshift encountered was for 3C287.1 where $Z \simeq 0.21$. For a cosmological model with a deceleration parameter $q_o = 0$, the corrections for L, P, H, and E are generally less than 10%. The main sources of error are uncertainties in the Hubble constant, the spectral indices, and the upper and lower cut off frequencies.

The results shown in Table 7 agree with similar calculations done by Maltby et al. (1963) and Macdonald et al. (1968). The luminosities, magnetic field strengths, and total energies will be used in the next section during the discussions of source ages. The core energies could be much higher than those shown if the equipartition assumption is not valid.

A correlation diagram of the absolute radio luminosity versus diameter of the large components is given in Figure 21. The twelve objects in Table 7 with

known distances plus 3C84 and Centaurus A are plotted. Typical objects with a simple large component (P0843-33, 3C264, and 3C274) and a double large component (Centaurus A and 3C236) are indicated.

The absence of low luminosity sources with large diameters is due to two selection effects. First, components with brightness less than 0.1 f.u./arc-min would probably not be recognized on the inversions. This excludes a region of the luminosity diameter diagram with $\log L < 36.3 + \log r_{Mpc} + \log d_{kpc}$ if the halos are assumed to have a spectral index of -0.9. This region, evaluated for R = 10 and 100 Mpc, lies below the slanted dashed lines in Figure 21. Also a halo with a flux density less than 10% of the core flux density would probably not be recognized in the original survey. This corresponds to a limit of about 1 f.u. at 605 MHz and excludes a region of the diagram where $\log L < 36.8 + 2 \log r_{Mpc}$. This region lies below the horizontal dashed lines in Figure 21.

The absence of sources with small diameter and high luminosity is probably due to the requirement that the halos be well resolved with a 1000λ antenna spacing; this requires that the halos have a diameter greater than 3'. Therefore objects with halos less than 10 kpc in diameter must be closer than 10 Mpc to be included in this study. However, the space density of radio galaxies with

Figure 21 - A correlation diagram of the radio luminosity versus the diameter for the large components of core-halo and asymmetric double sources. The dashed lines represent the limit below which a large component at a given distance would not be recognized due to low brightness or low flux relative to the core.

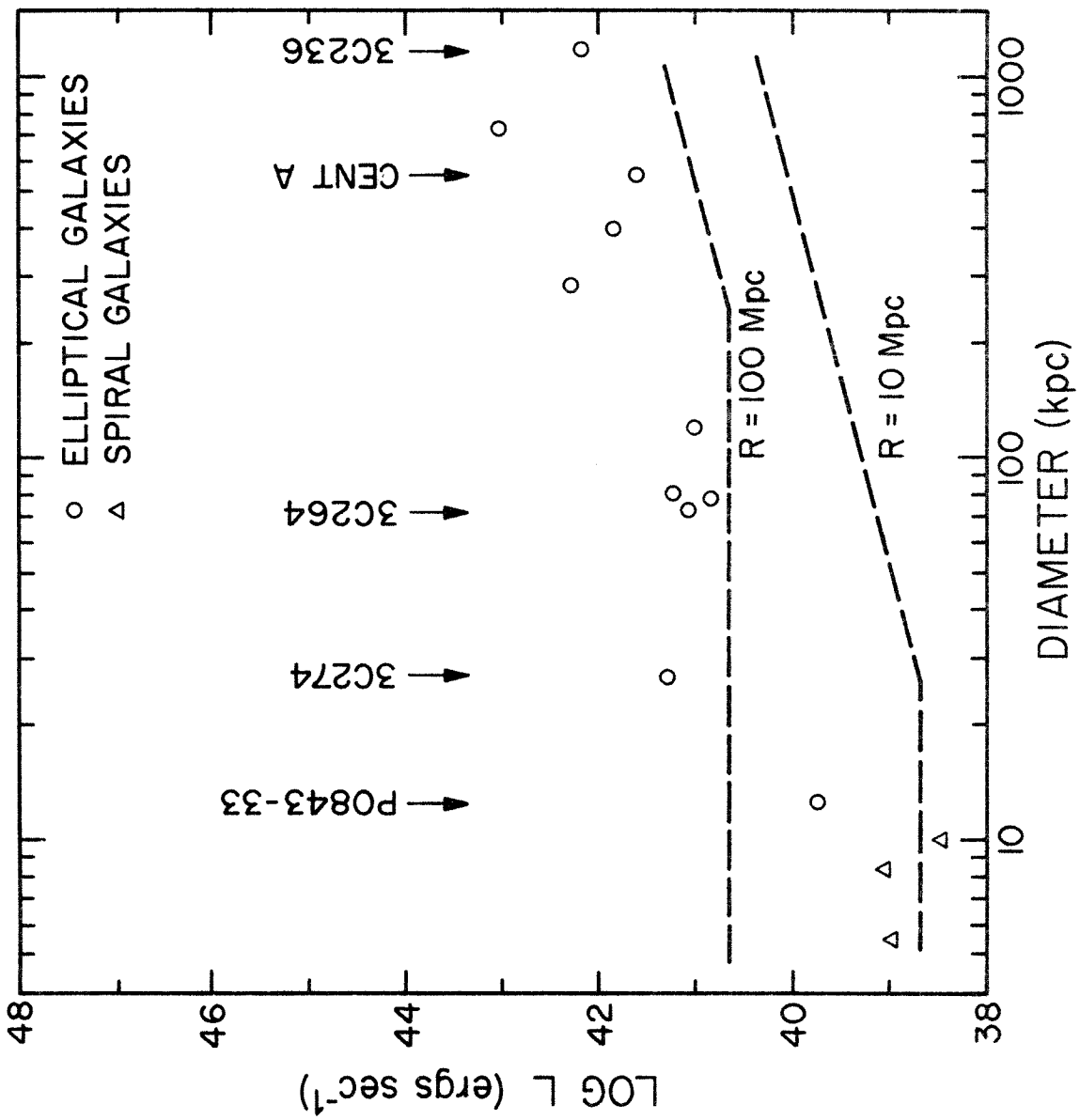
ELLIPTICAL GALAXIES
SPIRAL GALAXIES
3C236
CENT A
3C264
3C274
P0843-33
R = 100 Mpc
R = 10 Mpc
LOG L (ergs sec⁻¹)
DIAMETER (kpc)
48
46
44
42
40
38
10
100
1000

luminosity greater than 3×10^{41} erg s^{-1} is only 0.7×10^{-5} Mpc^{-3} (Schmidt 1966). Since about one third of the sky is unobservable at the latitude of the Owens Valley and only about one quarter of all radio galaxies have a core-halo structure, the probability for a high luminosity core-halo source with diameter < 10 kpc to be seen is < 0.01. Considering these selection effects, there is no apparent correlation between luminosity and halo size.

b) Spectral Indices

The spectral index, α, is related to the flux density at frequency ν by $S = S_o \nu^{\alpha}$. For extragalactic radio sources α is usually negative with the steeper spectra having more negative indices.

The spectra of the large components given in Table 4 are generally steeper than those of the cores. The spectral index of the small component minus the spectral index of the large component is shown in Figure 22 for the fourteen objects in Table 7 plus 3C84 and Centaurus A. Both the small and large components of Centaurus A have $\alpha \approx -0.58$ (Cooper et al. 1965) and thus $\Delta\alpha \approx 0$. The 5' halo of 3C84 has a spectral index of -1.36. Both components of the core are cut off by synchrotron self- absorption at frequencies below 1000 MHz. The 0".03 component has

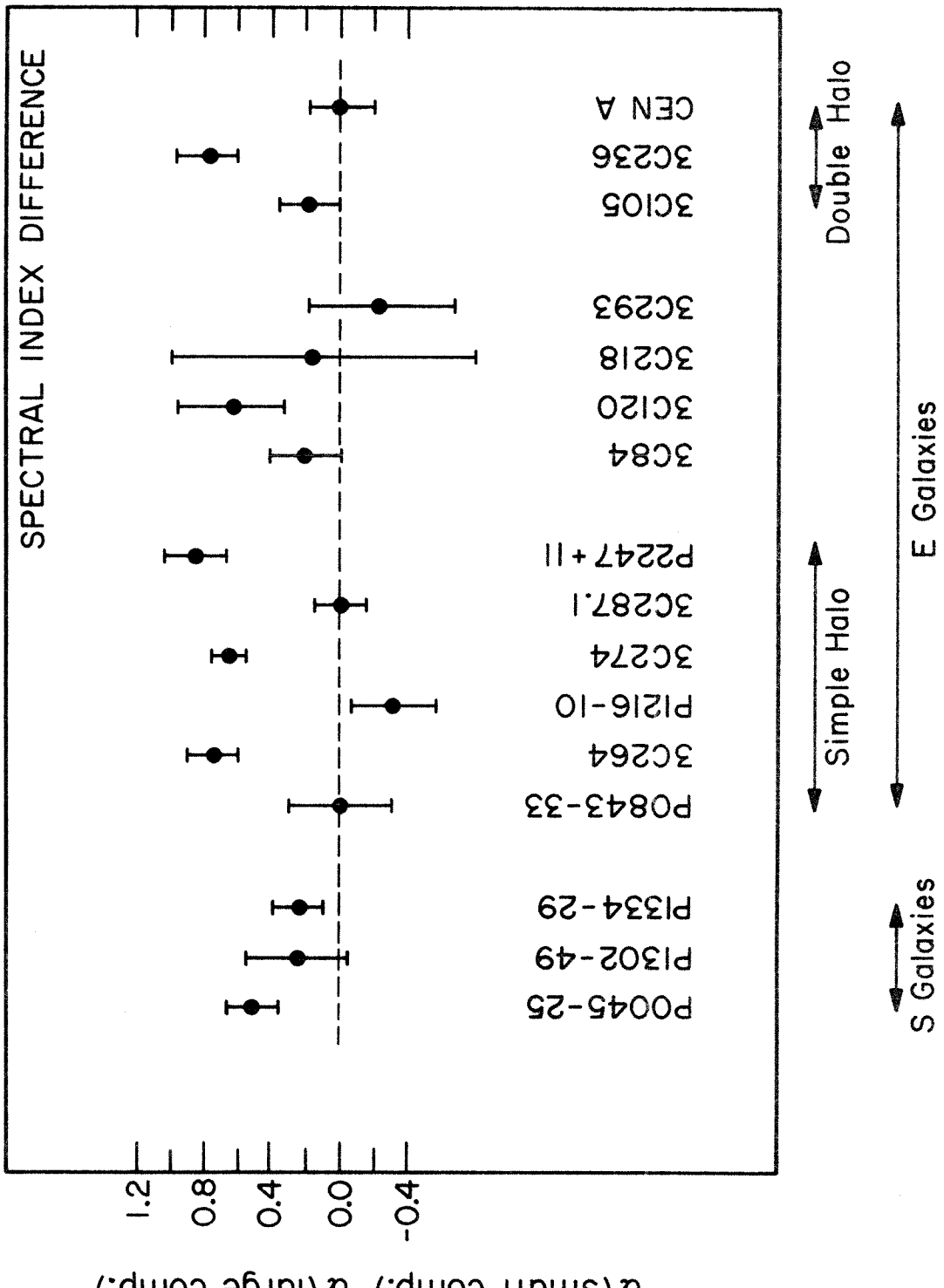
SPECTRAL INDEX DIFFERENCE
P0045-25
P1302-49
P1334-29
P0843-33
3C264
P1216-10
3C274
3C287.1
P2247+11
3C84
3C120
3C218
3C293
3C105
3C236
CEN A
1.2
0.8
0.4
0.0
-0.4
α(small comp.)-α(large comp.)
Double Halo
Simple Halo
E Galaxies
S Galaxies

a high frequency spectral index of -1.2 ± 0.2. Using this, $\Delta\alpha \approx 0.2 \pm 0.2$. The differences plotted in Figure 22 have an average value of +0.30 and are not dependent on the halo structure or the optical type.

It is unlikely that the difference in spectral indices for the sample used here is due to a selection effect. Sources with extended components that are i) larger than 15' or ii) smaller than 2' are less likely to be included among the sources selected for this investigation. Figure 23 shows the large and small component spectral indices plotted against the half power extent of the large components. There is little indication that the spectral index differences are dependent on the size of the halos. Since the extended components larger than 200 kpc have very low brightness, their flux densities and thus their spectral indices are poorly determined. There is some tendency for the spectra of the small components to become steeper with increasing size of the large component. However, this is not well established with only 14 data points.

The difference in spectral index could be explained by a difference in the evolution of the core and halo components. The relativistic electrons responsible for the synchrotron radiation from a radio source will lose energy by a variety of mechanisms as the source ages

Figure 23 - Spectral index versus large component diameter for core-halo and asymmetric double sources. Filled symbols refer to the cores and unfilled refer to the halos.

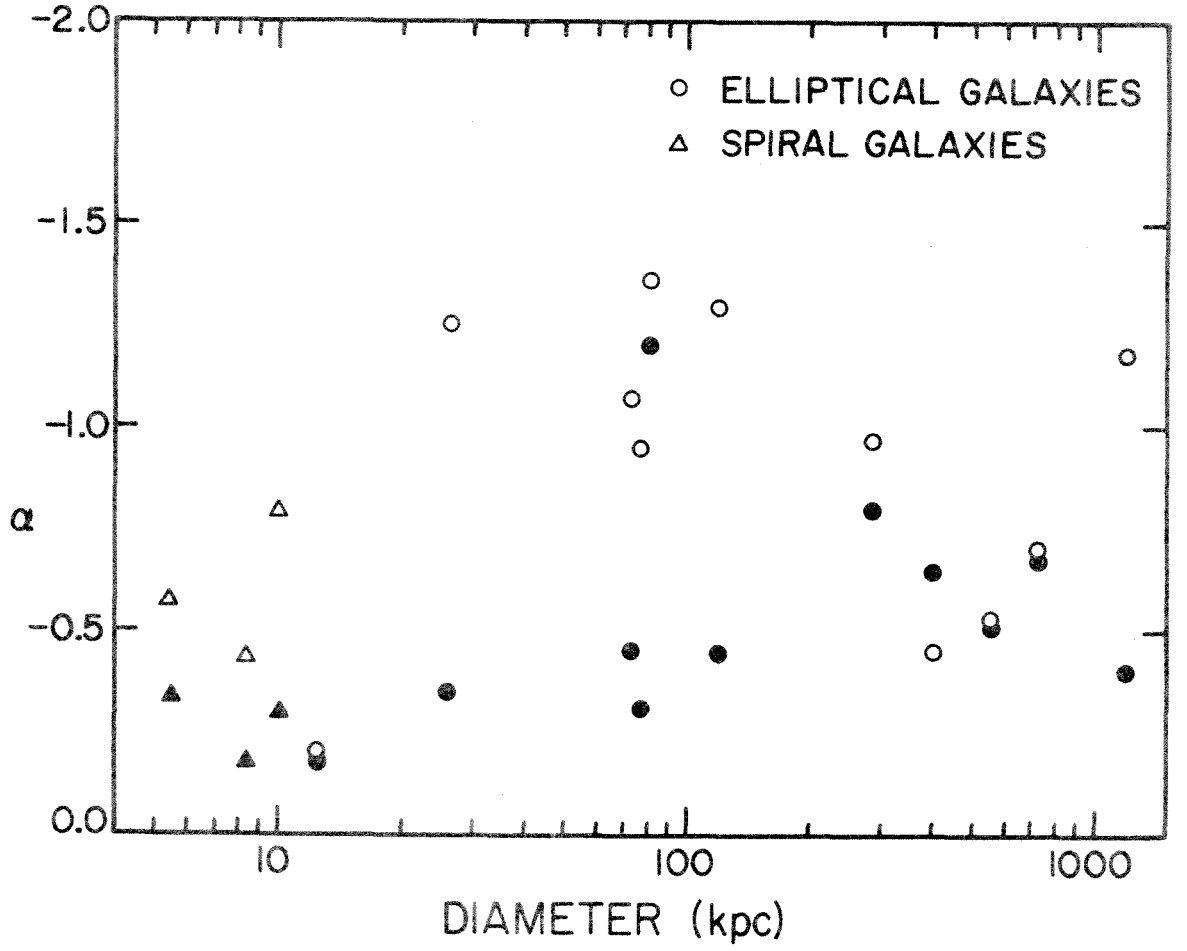
-2.0
-1.5
-1.0
-0.5
0.0
α
10
100
1000
DIAMETER (kpc)
ELLIPTICAL GALAXIES
SPIRAL GALAXIES

(Kardashev 1962). This will cause a simple power law spectrum to become a multi-component spectrum. Kellermann (1966) discusses a model which only considers synchrotron radiation losses. If new high energy electrons are not supplied, after t years any power law spectrum will show a break at

$$\nu_b = 1000\ H^{-3}_{(\text{gauss})}\ t^{-2}_{(\text{years})}\ \text{MHz} \qquad (7)$$

where H is the magnetic field in the radiating region. If the initial spectral index is α_o, then at frequencies $\nu > \nu_b$ the spectrum will have $\alpha = 4/3\ \alpha_o - 1$. If new electrons are supplied every T years, then in the frequency range for which T is short compared to the time for synchrotron losses to be important,

$$1000\ H^{-3}\ t^{-2} \leq \nu \leq 1000\ H^{-3}\ T^{-2}, \qquad (8)$$

the supply will be <u>quasi-continuous</u> and the spectrum will have $\alpha = \alpha_o - \frac{1}{2}$.

Assume that the halos are formed by a single event and their age is such that $\nu_b < 605$ MHz, then $\alpha_{halo} = 4/3\ \alpha_o - 1$. Consider two cases for the cores, i) that they are also formed by a single event but that ν_b for the cores is above 1425 MHz or alternatively ii) the cores have been renewed since their birth and have spectra in the range 605 to 1425 MHz produced by the quasi-continuous mechanism. For the first case $\alpha_{core} = \alpha_o$ and

$$\Delta\alpha = \alpha_{core} - \alpha_{halo} = -1/3\alpha_o + 1,$$

and for the second case $\alpha_{core} = \alpha_o - \frac{1}{2}$ and

$$\Delta\alpha = -1/3\ \alpha_o + 1/2$$

In either case the core need not originate simultaneously with the halo, but it is assumed that the initial spectrum α_o is the same for core and halo.

It is not clear what value to use for α_o. The average of the spectral indices of the small components is -0.47 which gives $\alpha_o \approx -0.5$ for the first case and $\alpha_o \approx 0$ for the second. Recent outbursts in 3C120 have $\alpha_o \approx 0$ (Pauliny-Toth and Kellermann 1968) while outbursts in 3C273 have $\alpha_o \approx -0.4$ (Dent 1968). However, with either case i) or ii) $\Delta\alpha$ is not very sensitive to the choice of α_o. The observed values of $\Delta\alpha$ vary from +0.86 to -0.32 which is too large a range to be explained by any reasonable range of α_o. More detailed component spectra may show that for some sources the present measurements correspond to curved parts of the spectra, and the required range of α_o will be reduced. However, this model is certainly not applicable to sources where $\Delta\alpha \leq 0$. Sources with $\Delta\alpha > 1.0$ are not observed, which precludes case i) unless α_o is positive.

It is not necessary that the spectral index differences be due to energy loss and aging. An alternative

explanation is that the large and small components originated with different electron energy distributions. This is particularly attractive for the spiral galaxies where the large radio component is roughly the size of the optical galaxy. In these cases the high energy electrons might originate from supernova explosions in the disk with the core being a completely independent event. Even if the halo electrons were ejected from the nucleus, it is possible that the halo and the presently observed core started with a different α_o. A third explanation is that the spectra of some of the compact cores are flattened by synchrotron self-absorption.

c) Ages and Lifetimes

The sizes of the large components set a strict lower limit to their ages. Most of the halos are between 40 and 400 kpc in diameter. Since the expansion velocity must be less than the speed of light, these components are at least 10^5 to 10^6 years old.

If the spectral index differences discussed in the last section are explained by synchrotron energy loss, Equation 7 can be used to place some limits on the component ages. Most of the component spectra are determined between 605 and 1425 MHz. If the halo is the result of only one ejection, in order for its spectrum to be steeper than

the core spectrum ν_b must be below 605 MHz. Using typical magnetic field strengths given in Table 7, $t_{halo} > 10^6$ years if $H = 10^{-4}$ oersted and $t_{halo} > 4 \times 10^7$ years if $H = 10^{-5}$ oersted. Since $t \propto H^{-3/2}$, the age limit determined in this way is sensitive to the choice of H, which is not well known for radio galaxies.

The time t in Equation 7 corresponds to the time it would take an electron with infinite energy to radiate enough energy in magnetic field H by synchrotron emission for its critical frequency to fall to ν_b. This time may be reduced considerably for the halo by using a model in which the halo expands adiabatically from a volume the size of the core, carrying its magnetic field with it. However, with such adiabatic expansion, the source flux density will decrease $S \propto (x/x_o)^{-2(1-2\alpha_o)}$ where x_o and x are the initial and final source diameters (Shklovskii 1960). Using $\alpha_o = -0.5$ and $x_o = 1$ kpc, for x between 40 and 400 kpc the halo flux density will be reduced by a factor between 10^6 and 10^{10} by the expansion. With any reasonable initial flux density, an adiabatic expansion would quickly render the halo invisible.

Equation 7 can also be used to set an upper limit to the age of the core. If the core is the result of a single injection of electrons, ν_b must be above 1425 MHz in order for a reasonably flat spectrum to be observed. This requires that the time since the burst be less than

10^6 years for a magnetic field H = 10^{-4} oersted. If the core is quasi-continuously renewed, then the period between injections must be less than 10^6 years.

The total radio source energy in the form of energetic particles and magnetic field along with the radio luminosity is given in Table 7 for the large and small components. The total energy divided by the luminosity gives an estimate of the source lifetimes. The halos typically contain enough energy ($\sim 10^{59}$ - 10^{60} ergs) to maintain the source for $\sim 10^9$ to 10^{10} years. These lifetimes assume that the luminosity remains constant and that all of the energy will be converted to radio radiation. If other energy loss mechanisms are included (such as inverse Compton scattering of the 3°K background radiation, adiabatic expansion, ionization losses, etc.) these estimates may be reduced considerably (Rees and Setti, 1968).

A total energy of 10^{60} ergs represents the mass to energy conversion of 10^{10} solar masses if the conversion efficiency is 10^{-4}. This is comparable to the mass of a fairly large galaxy. It is unlikely that the source started out with much higher energy and therefore the 10^{10} years represents the maximum possible lifetime of the source.

The luminosities of the cores are generally equal to or greater than the luminosities of the halos. Since the small cores contain only about 10^{-1} to 10^{-2} of the energy of the halos their lifetimes are much shorter. This assumes that the core energy equals the equipartition value, which may be incorrect.

d) The Core-Halo Structure

Past surveys of radio source structures show conclusively that many radio sources have both extended and very small components. These are called core-halo sources when the small component is centrally located in the large component. The core-halo objects may have halos with either a simple or a close double structure. (The question of halo shape will be discussed later.) Not all objects that appear to have a core-halo structure actually have physically centered components. There are two types of objects which might be mistaken for core-halo sources. First, a bright point source with confusing objects nearby may be mistaken for a core-halo object if low resolution is used or if, in the case of aperture synthesis, the sampling in the u-v plane is sparse. Sources of this type will be recognized as higher resolution surveys of source structure are made. Second, a small component with large displaced

components nearby may often appear as a core-halo source when projected to two or one dimension. Measurements of the two-dimensional brightness distributions will eliminate some of these sources, but ultimately the core-halo sources can be separated from the asymmetric doubles only in a statistical sense. The true space structure of any individual source will never be known. Fomalont (EF III) argues that there are too many core-halo objects in his sample for them to be explained as a projection of the asymmetric doubles, and therefore the core-halo objects form a physically distinct class.

The fourteen sources listed in Table 7 have small diameter cores with large, nearby emission regions. Four of these (P1216-10, 3C264, 3C287.1, and P2247+11) are listed in EF II as asymmetric doubles. The distinction between core-halo and asymmetric double is somewhat arbitrary and a moderate amount of asymmetry should be allowed in the former class. Two of these objects (3C287.1 and 3C264) each have their halo displaced from their core by less than one quarter of their halo half-power diameter and will be retained in the class of core-halo objects (this ratio is frequency dependent for 3C264). This displacement is greater than one half of the halo diameter for the other two objects (P1216-10 and P2247+11), and these should probably not be called core-halo sources.

They resemble 3C83.1 which has a halo displaced from a small component coincident with NGC 1265. Ryle and Windram (1968) suggest that the displaced halo is due to intergalactic streaming of electrons which originated in an explosion in the neighboring galaxy NGC 1275 (3C84).

Having excluded P1216-10 and P2247+11, the remaining twelve objects in Table 7 still do not form a homogeneous sample of core-halo sources. The spiral galaxies should probably be kept separate from the ellipticals. Matthews et al. (1964) show that spiral galaxies are weak radio sources with radio luminosities $L \leq 10^{40}$ erg/s, while the strong radio galaxies have $L \geq 10^{40}$ erg/s. This same division is seen in Table 7 among the core-halo objects, with the ellipticals being about 10^3 times more luminous than the three spiral galaxies. Although these spirals are at the high end of the spiral radio luminosity distribution with $L \sim 10^{39}$ erg/s this is not unexpected since most spirals were excluded from this study by the flux density limit of 2 f.u. at 1425 MHz used by Fomalont.

Very little is known about the brightness distribution of spiral galaxies. Among the detected sources, some show the emission concentrated in the nuclear region while others show it distributed in the galactic disk; in no case is a double structure seen. It is uncertain how common the core-halo structure is among the spirals. Three out of the four Sc galaxies observed by Fomalont had core-

halo structures. The fourth galaxy NGC 4696 (P1245-41) was only slightly resolved with a diameter of 0.'36 which is about one quarter of the optical diameter. Surveys of spiral galaxies (Mathewson and Rome 1963b, de la Beaujardière et al. 1968) have revealed no new core-halo objects, although this could be due to a lack of resolution. In general, the radio emitting regions of spiral galaxies are less than or equal to the size of the optical disk (de la Beaujardière et al. 1968). Among the elliptical galaxies with core-halo structure, the halos often extend far beyond the optical galaxy. It is possible that the same process that leads to the formation of the core-halo structure in spirals is working in the strong radio galaxies but with higher energies and resulting in larger halos; however until there is more evidence to show the connection, it is best to treat them separately.

Most of the 28 core-halo objects listed in EF III's Table 5 were too small to be studied here. Two of these objects, 3C247 and probably 3C231, should be excluded from the list since it is unlikely they have halos; also the spiral galaxies might be removed since their relation to the other core-halo sources is questionable.

Twenty-eight of Fomalont's original 532 sources were large enough to be well resolved at a spacing of 1000λ or resolved with only the core remaining, and were extragalactic but not associated with a spiral galaxy. These

can be used to estimate the relative frequency of the core-halo structure among strong radio sources. Nine of these sources (32%) have a core-halo structure. This includes objects with simple, double, and undetermined halo structures. If 3C264 and 3C287.1 are considered asymmetric doubles rather than core-halo objects, then 25% of the sources have a core-halo structure. This agrees fairly well with Fomalont's conclusion that 20% of the radio sources have a core-halo structure.

With the asymmetric double and spiral galaxies removed there are nine objects in Table 7 which are likely to have a physically real, three-dimensional, core-halo structure. An interesting question which is quite difficult to answer is whether the halos have a double or simple structure. Because the appearance of any particular source may be affected by projection, this question can only be answered in a statistical sense.

In order to discuss this problem, it is necessary to calculate the percentage of randomly-oriented double sources that would be recognized as doubles from their brightness distributions projected to two or one dimension. To calculate the effects of projection, consider a double radio source consisting of two identical prolate spheroidal emission regions with their major axes parallel to the line separating their centers. Let a and b be the half intensity diameters of the spheroids parallel to the major and

minor axes; let the separation of the centers be D and the angle between the line of centers and the line of sight be θ. The two-dimensional brightness distribution obtained by integrating the emissivity along the line of sight will have major and minor axes given by

$$a'^2 = a^2 \sin^2 \theta + b^2 \cos^2 \theta$$

$$b'^2 = b^2$$

and a component separation given by $D' = D \sin \theta$. If this brightness distribution is projected to one dimension, the component half power diameter a'' will be given by

$$a''^2 = a^2 \sin^2 \theta \cos^2 \phi + b^2 \cos^2 \theta \cos^2 \phi + b^2 \sin^2 \phi$$

and the component separation will be

$$D'' = D \sin \theta \cos \phi$$

where ϕ is the angle between the line of separation and the one-dimensional brightness distribution axis. Let R be the ratio of the component separation to the major axis half power diameter for the three-dimensional emission region, $R = D/a$. If $b = \alpha a$, this ratio for the projected two-dimensional brightness distribution will be

$$R' = D'/a' = R\,(1 + \alpha^2 \cot^2 \theta)^{-\frac{1}{2}}$$

and for the one-dimensional brightness distribution will be

$$R'' = D''/a'' = R(1 + \alpha^2 \cot^2 \theta + \alpha^2 \operatorname{cosec}^2 \theta \tan^2 \phi)^{-\frac{1}{2}}.$$

When R' or R'' = 1, the brightness minimum between the two components is only 7% below the brightness peaks, and the double source is virtually indistinguishable from a single broad component. With the low signal to noise ratio of the halo inversions presently obtained, a dip less than 30% of the peak brightness would probably not be recognized as a double source; this requires that R'' or R' be greater than 1.2 to recognize a double. Assuming that the axes of the doubles are distributed randomly, for a given value of R and α, the fraction of sources with $R' > 1.2$ and $R'' > 1.2$ can be calculated. These fractions are given in Table 8.

Of the nine objects likely to be physically real core-halo sources, two have a double halo (3C105 and 3C236) and four (P0843-33, 3C264, 3C274, and 3C287.1) appear to have a simple halo (we may define a simple halo as one having $R < 1.0$). The rest have an undetermined halo structure. The classification of 3C287.1 is questionable. The core is not coincident with the optical galaxy, and the halo is elongated rather than circular with an axial ratio greater than four. Its half power diameter is about 700 kpc which is between 10 and 60 times as large as the other simple halos. Finally the spectral indices of the components are nearly the same. This source bears little resemblance to the prototype core-halo source

TABLE 8

PREDICTED FRACTION OF DOUBLES OBSERVED

WITH R' OR R'' > 1.2

Two-Dimensional - R' > 1.2

R	α				
	0.2	0.4	0.6	0.8	1.0
1.30	.902	.721	.570	.462	.385
1.50	.966	.882	.781	.684	.600
1.70	.981	.929	.853	.782	.708
2.00	.989	.958	.912	.857	.800
2.50	.994	.977	.950	.916	.877
3.00	.996	.985	.967	.944	.917
3.50	.997	.990	.977	.960	.939
4.00	.998	.992	.983	.970	.954

One-Dimensional - R'' > 1.2

R	α				
	0.2	0.4	0.6	0.8	1.0
1.30	.567	.307	.179	.113	.077
1.50	.742	.529	.375	.270	.200
1.70	.805	.630	.487	.377	.294
2.00	.852	.713	.590	.486	.400
2.50	.891	.786	.688	.599	.520
3.00	.913	.828	.747	.670	.600
3.50	.927	.856	.786	.720	.657
4.00	.937	.875	.815	.756	.700

3C274. The classification of 3C105 is also uncertain since there is no optical identification and the core is displaced with respect to the halo.

Since Centaurus A (double halo) and 3C84 (simple halo) meet the selection criteria given in Chapter II, they should be added to the list of core-halo objects. This gives 2 or 3 double halos and 4 or 5 simple halos, and thus the fraction of observed double halos is between 0.29 and 0.43. This could be interpreted in several ways. If all of these halos are really doubles, then from Table 8, R is between 1.7 and 2.2 for $\alpha = 1.0$ and between 1.4 and 1.6 for $\alpha = 0.6$. Alternatively we might assume that the observed halos have a wide distribution of R with some simple ($R < 1$) and some double ($R > 1$) structures. If two of the halos have a true simple structure and the remaining five or six are doubles, then the fraction of observed doubles (2 or 3 sources) is between 0.40 and 0.60. From Table 8 R for the doubles is between 2.0 and 3.0 if $\alpha = 1.0$ and between 1.6 and 2.0 if $\alpha = 0.6$.

Other distributions of the parameter R will lie between these two extreme cases; thus it may be concluded from these observations that at least 30% and probably 60 to 100% of the core-halo objects have $R < 2$. Fomalont (EF III) finds that $2 \leq R \leq 4$* for ordinary doubles not

---

* In EF III the ratio R is denoted by A

associated with a small core. Therefore, the core-halo objects have a significantly smaller value of R. It is possible that they are an extension of the ordinary double distribution to small R. From the present investigation it is impossible to conclude whether there exists a class of core-halo radio galaxies with simple halos ($R \leq 1$).

A remaining question concerning core-halo objects is whether the cores and halos have the same age. This is a separate question from whether the halos have a simple or double structure. With either structure the cores could have been formed at the same time as the halos or they could be more recent.

Fomalont (EF III) points out that if the cores were much younger than the halos one would expect to see a number of simple sources corresponding to the halos before the formation of the cores. However, since the observed fraction of simple sources (15%) is about that expected from the number of doubles which would be seen end on, the halos must exist with a core most of the time. This could be accomplished with either a single long-lived core or a succession of short-lived cores.

The component separation to diameter ratio, R, is a useful parameter to associate with radio galaxies. Fomalont (EF III) has shown that objects with small R tend to have lower radio luminosities. In addition the observed

properties of the core-halo sources indicate that when $R < 2$ the galaxies are likely to retain a small bright core or a succession of such cores. This is in contrast with normal double sources ($R > 2$) which seldom have a core associated with the parent galaxy.

e) Conclusion

Fourteen of the twenty-eight sources observed have a large radio emission region lying close to a small bright core. The spectra of the large regions are in general steeper than those of the cores. No correlation is seen between the spectral indices or radio luminosities of the large emission regions and the component diameters. There is a weak indication that the core spectra are steeper in sources with larger extended components.

The sizes of the halos require that they be at least 10^5 to 10^6 years old. Ages greater than 10^6 to 10^7 years are required if the differences of the core and halo spectral indices are to be explained by synchrotron losses. Using the equipartition energies ($\sim 10^{60}$ erg) and observed luminosities ($\sim 10^{42}$ erg/s) of the halos, the total lifetimes of the large components may be as great as $\sim 10^9$ to 10^{10} years. If the equipartition assumption holds for the cores, their lifetime is about 10^7 years.

Three of the fourteen sources are associated with spiral galaxies and may not be physically related to the others which are associated with elliptical galaxies or are unidentified. Two others are best considered asymmetric doubles. However, eight or nine objects remain which are likely to be physically real core-halo sources.

It is uncertain whether the halos of these objects have a simple or a double structure in three dimensions. Thirty to forty percent of the halos are observed to have a double structure. This would be expected from an ensemble of randomly oriented double sources having a ratio of component separation to diameter, R, less than two. If the sample used is a mixture of simple and double halos, at least 30% and probably 60 to 100% of the sources still have R less than two.

It is possible that the process that leads to the formation of radio sources produces double structures with a wide range of R and that the low end of the distribution is populated by the core-halo objects. This implies that when $R < 2$ the galaxy is likely to produce or retain a core, a fact which should be considered in any theoretical model for radio galaxy formation and evolution.

APPENDIX A

The expectation value of the confusion flux density at 605 MHz was determined by observing 51 random regions of the sky with the interferometer and taking the average measured flux density. Most of the observations were made at the 244λ spacing. The 51 regions were at random declinations between + 65° and - 35° with right ascensions corresponding to the Local Sidereal Time during free time in the core-halo observing schedule. Positions within 10° of the galactic plane were excluded. The distribution of the observed flux densities is shown in Figure 24. The expectation value of the confusing flux density is 0.60 f.u.

Figure 24 - The distribution of measured flux density at 605 MHz from 51 random regions of sky.

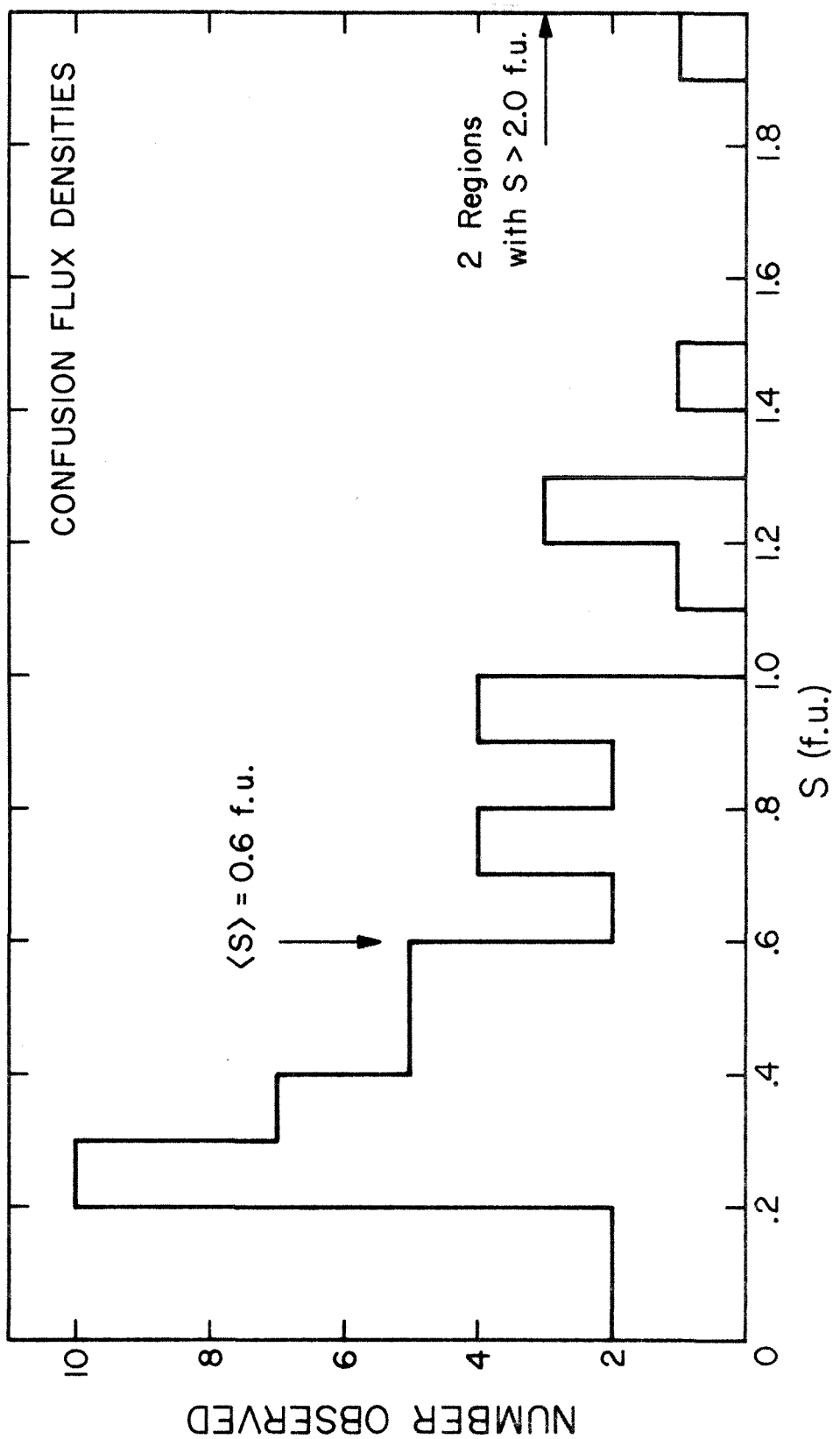
CONFUSION FLUX DENSITIES
2 Regions
with S > 2.0 f.u.
⟨S⟩ = 0.6 f.u.
NUMBER OBSERVED
S (f.u.)
0
2
4
6
8
10
.2
.4
.6
.8
1.0
1.2
1.4
1.6
1.8

APPENDIX B

Sagittarius A

The radio emission from the galactic center is due to a mixture of thermal and non-thermal radiation. A review is given by Lequeux (1966) who gives extensive references to earlier work. At high frequencies eight discrete sources are seen superimposed on an extended thermal source. The brightest discrete source, which is called Sagittarius A, has a half power diameter of about $2' \times 3'$ arc-min and a non-thermal spectrum with $\alpha = -0.25 \pm 0.1$ (Maxwell and Taylor 1968); its galactic coordinates are $l^{II} = -2'.5$ and $b^{II} = 2'.0$. The other seven discrete sources have thermal spectra with diameters of order $5'$ to $10'$ and lie approximately along the galactic equator. The extended thermal component has a half power diameter of about $1^{\circ}.0$ in galactic longitude and $0^{\circ}.4$ in galactic latitude. At low frequencies the thermal component is seen in absorption against a larger $1^{\circ}.0 \times 3^{\circ}.0$ non-thermal emission region.

The brightness distribution at 605 MHz is shown in Figure 25. Since no direct measurements were made to determine the A.G.C. correction, an indirect determination was used (the A.G.C. correction is discussed in Section II-c). The flux density of Sagittarius A at 605 MHz taken from the

Figure 25 - The brightness distribution of Sagittarius A at 605 MHz. The true zero level of the plot is negatively displaced by an unknown amount. The dashed line represents the zero level with 780 f.u. in the beam.

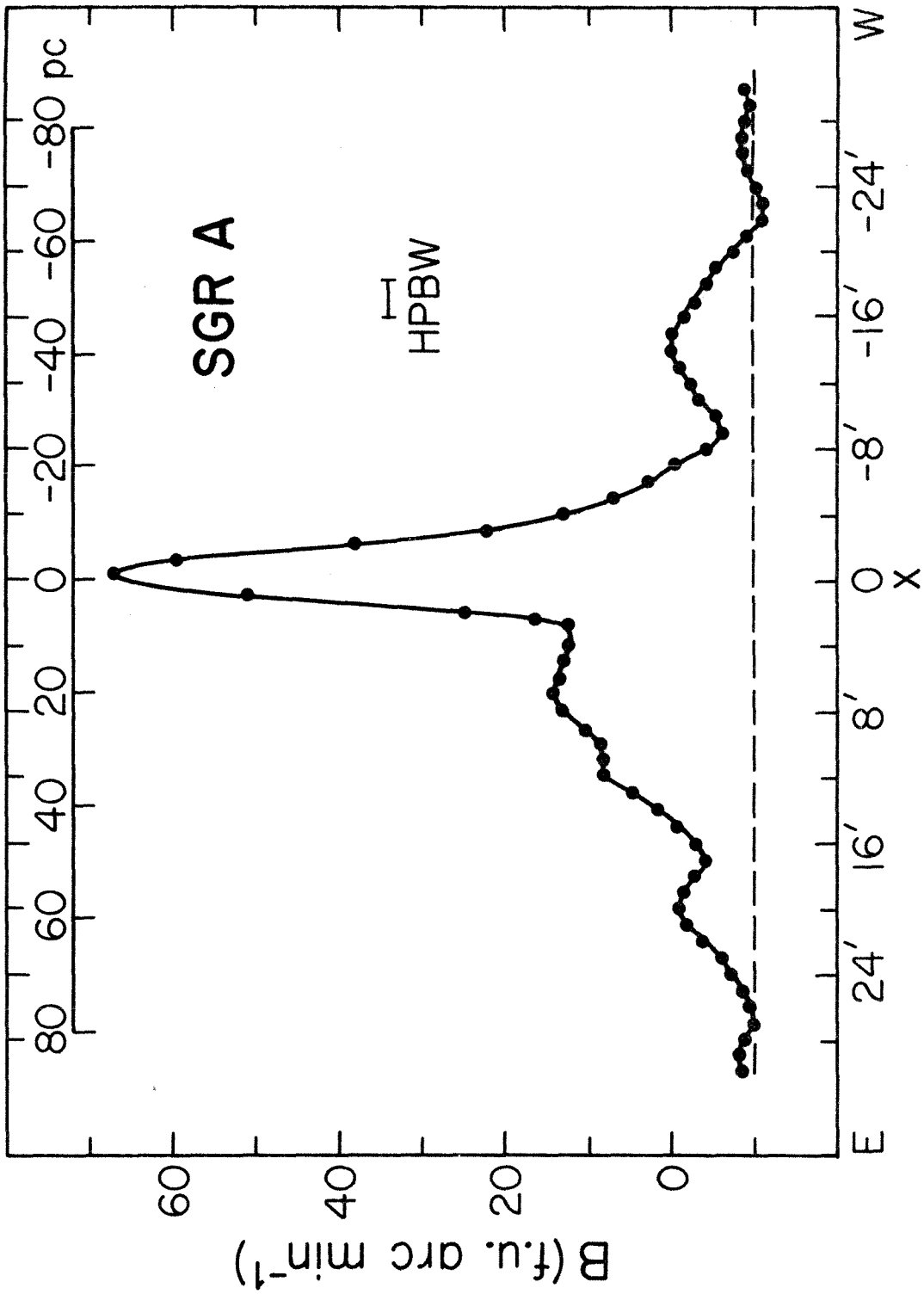
SGR A
HPBW
B (f.u. arc min^{-1})
60
40
20
0
E
W
24′
16′
8′
0
X
-8′
-16′
-24′
80
60
40
20
0
-20
-40
-60
-80 pc

spectrum of Maxwell and Taylor (1968) is 225 f.u. The observed visibilities indicate that the flux density is 170 f.u. im plying that an A.G.C. correction of 1.33 is needed.

Since the galactic center is a very complex region the total flux density in the beam is unknown; a flux of 225 f.u. is assumed. This flux density is low since it neglects the contribution from the discrete thermal sources and the extended thermal and non-thermal sources. The result is the negative displacement of the zero level of the inversion in Figure 25. The shape of the brightness distribution is independent of the choice of total flux as can be seen in Equation 6. The dashed line in Figure 25 represents the zero level for 780 f.u. in the beam. The true zero is probably much lower since the thermal component alone should contribute about 3000 f.u.

A number of the discrete thermal sources are seen in Figure 25. The feature at - 14' corresponds to G-0.6-0.1 and to G1.1-0.1 in the first grating response to the east. G0.2+0.0 is at + 7' and G0.5+0.0, G0.7+0.0, and G0.9+0.1 correspond to the feature at + 20'. The brightness distribution has not been corrected for primary beam attenuation.

REFERENCES

Abell, G. O. 1958, Ap. J. Suppl., 3, 211.

Adgie, R. L., and Gent, H. 1966, Nature, 209, 549.

Allen, L. R., Anderson, B., Conway, R. G., Palmer, H. P., Reddish, V. C., and Rowson, B. 1962, M.N.R.A.S., 124, 477.

Allen, R. J., Barrett, A. H., and Crowther, P. P. 1968, Ap. J., 151, 43.

Allen, W. C. 1955, Astrophysical Quantities, (London: Athlone Press).

Anderson, B., and Donaldson, W. 1967, M.N.R.A.S., 137, 81.

Arp, H. C. 1967, Ap. Lett., 1, 1.

_____. 1968, Ap. J., 152, 1101.

Arp, H., and Bertola, F. 1969, Ap. Lett., 4, 23.

Baade, W., and Minkowski, R. 1954, Ap. J., 119, 215.

Baker, R. H. 1959, Astronomy, (Princeton, N.J.: D. Van Nostrand Co., Inc.) p. 91.

Baldwin, J. E., and Smith, F. G. 1956, Observatory, 76, 141.

Basart, J. P., Clark, B. G., and Kramer, J. S. 1968, Pub. A.S.P., 80, 273.

Bash, F. 1968a, Ap. J., 152, 375.

_____. 1968b, Ap. J. Suppl., 16, 373.

de la Beaujardière, O., Kazès, I., le Squeren, A.M., and Nguyen-Quang-Rien. 1968, Ann. d'ap., 31, 387.

Bottinelli, L., Gouguenheim, L., Heidmann, J., and Heidmann, N. 1968, Ann. d'ap., 31, 205.

Bracewell, R. N. 1958, Proc. I.R.E., 46, 97.

Bracewell, R. N., and Roberts, J. A. 1954, Australian J. Phys., 1, 615.

Bridle, A. H., and Purton, C. R. 1968, A. J., 73, 717.

Brown, R. H., and Hazard, C. 1961, M.N.R.A.S., 122, 479.

Burbidge, E. M., Burbidge, G. R., and Prendergast, K. H. 1962, Ap. J., 136, 339.

Burbidge, E. M., Burbidge, G. R., and Rubin, V. C. 1964 Ap. J., 140, 942.

Burbidge, G. R. 1956, Ap. J., 124, 416.

Burbidge, G. R., and Burbidge, E. M. 1957, Ap. J., 125, 1.

Cameron, M. J. 1969, Proc. A.S.A., 1, 229.

Clarke, M. E., Bolton, J. G., and Shimmins, A. J. 1966, Australian J. Phys., 19, 375.

Clarke, R. W., Broten, N. W., Legg, T. H., Locke, J. L., and Yen, J. L. 1969, M.N.R.A.S., 146, 381.

Cohen, M. H. 1969, Ann. Rev. Astr. and Ap., 7, 619.

Cohen, M. H., Moffet, A. T., Shaffer, D., Clark, B. G., Kellermann, K. I., Jauncey, D. L., and Gulkis, S. 1969, Ap. J. (Letters), 158, L83.

Conway, R. G., Daintree, E. J., and Long, R. J. 1965, M.N.R.A.S., 131, 159.

Conway, R. G., Kellermann, K. I., and Long, R. J. 1963, M.N.R.A.S., 125, 261.

Cooper, B. F. C., Price, R. M., and Cole, D. J. 1965, Australian J. Phys., 18, 589.

C.S.I.R.O. Radiophysics Division. 1969, Australian J. Phys. Ap. Suppl., 7, 1.

Dent, W. A. 1968, Ap. J. (Letters), 153, L29.

Ekers, R. 1969, Australian J. Phys. Ap. Suppl., 6, 1.

Elsmore, B., Kenderdine, S., and Ryle, M. 1966, M.N.R.A.S., 134, 87.

Elvius, A. 1962, Lowell Obs. Bull., 5, 281.

_____. 1969, Lowell Obs. Bull., 7, 117.

Fomalont, E. B. 1967, Pub. Owens Valley Rad. Obs., Vol. 1, #3.

_____. 1968, Ap. J. Suppl, 15, 203.

_____. 1969, Ap. J., 157, 1027.

Fomalont, E. B., Wyndham, J. D., and Bartlett, J. F. 1967, A. J., 72, 445.

Griffin, R. F. 1963, A. J., 68, 421.

Hogg, D. E., Macdonald, G. H., Conway, R. G., and Wade, C. M. 1969, A. J., 74, 1206.

Howell, T. F., and Shakeshaft, J. R. 1967, J. Atmos. and Terr. Phys., 29, 1559.

Humason, M. L., Mayall, N. U., and Sandage, A. R. 1956, A. J., 61, 97.

Kardashev, N. S. 1962, Soviet Astronomy - AJ, 6, 317.

Kellermann, K. I. 1966, Ap. J., 146, 621.

Kellermann, K. I., Clark, B. G., Bare, C. C., Rydbeck, O., Ellder, J., Hansson, B., Kollberg, E., Hoglund, B., Cohen, M. H., Jauncey, D. L. 1968, Ap. J. (Letters), 153, L209.

Kellermann, K. I., and Pauliny-Toth, I. I. K. 1968, Ann. Rev. Astr. and Ap., 6, 417.

Kellermann, K. I., Pauliny-Toth, I. I. K., and Tyler, W. C. 1968, A. J., 73, 298.

Kellermann, K. I., Pauliny-Toth, I. I. K., and Williams, P. J. S. 1969, Ap. J., 157, 1.

Legg, T. H., Bell, M. B., and Bignell, R. C. 1968, A. J., 73, 749.

Lequeux, J. 1962, Ann. d'ap., 25, 221.

_____. 1967, I.A.U. Symp. No. 31, ed. H. van Woerden (New York: Academic Press, Inc.) p. 393.

Lewis, B. M. 1968, Proc. A.S.A., 1, 104.

Liller, M. H. 1960, Ap. J., 132, 306.

Love, A. W. 1962, Microwave J., 5, p. 117.

Lynds, C. R. 1961, Ap. J., 134, 659.

Lynds, C. R., and Sandage, A. R. 1963, Ap. J., 137, 1005.

Macdonald, G., Kenderdine, S., and Neville, A. 1968, M.N.R.A.S., 138, 259.

Maltby, P. 1962, Ap. J. Suppl., 7, 124.

Maltby, P., and Moffet, A. 1962, Ap. J. Suppl, 7, 141.

Maltby, P., Matthews, T. A., and Moffet, A. T. 1963, Ap. J., 137, 153.

Matthews, T. A., Morgan, W. W., and Schmidt, M. 1964, Ap. J., 140, 35.

Mathewson, D. S., and Rome, J. M. 1963a, Observatory, 83, 20.

_____. 1963b, Aust. J. Phys., 16, 360.

Maxwell, A., and Taylor, J. H. 1968, Ap. Lett., 2, 191.

Mills, B. Y. 1953, Australian J. Phys., 6, 452.

_____. 1955, Australian J. Phys., 8, 368.

Mills, B. Y., and Glanfield, J. R. 1965, Nature, 208, 10.

Moffet, A. T. 1962, Ap. J. Suppl., 7, 93.

Moffet, A. T., and Palmer, H. P. 1965, Observatory, 85, 45.

Palmer, H. P., Rowson, B., Anderson, B., Donaldson, W., Miley, G. K., Gent, H., Adgie, R. L., Slee, O. B., and Crowther, J. H. 1967, Nature, 213, 789.

Pauliny-Toth, I. I. K., and Kellermann, K. I. 1968, A. J., 73, 953.

_____. 1969, Ap. J. (Letters), 152, L169.

Pauliny-Toth, I. I. K., Wade, C. M., and Heeschen, D. S. 1966, Ap. J. Suppl., 13, 65.

Read, R. B. 1963, Ap. J., 138, 1.

Rees, M. J., and Setti, G. 1968, Nature, 219, 127.

Roger, R. S., Costain, C. H., and Lacey, J. D. 1969, A. J., 74, 366.

Rowson, B. 1963, M.N.R.A.S., 125, 177.

Ryle, M. 1962, Nature, 194, 517.

Ryle, M., and Hewish, A. 1960, M.N.R.A.S., 120, 220.

Ryle, M., and Windram, M. D. 1968, M.N.R.A.S., 138, 1.

Sandage, A. 1961, Hubble Atlas of Galaxies (Washington, D.C.: Carnegie Institute of Washington).

_____. 1966, Ap. J., 145, 1.

_____. 1967, Ap. J. (Letters), 150, L145.

_____. 1968, Ap. J. (Letters), 152, L149.

Sandage, A. R., and Miller, W. C. 1964, Science, 144, 405.

Sandage, A. R., Véron, P., and Wyndham, J. D. 1965, Ap. J., 142, 1307.

Sandage, A. R., and Visvanathan, N. 1969, Ap. J., 157, 1065.

Sargent, W. L. W. 1967, Publ. A.S.P., 79, 369.

Schmidt, M. 1965, Ap. J., 141, 1.

_____. 1966, Ap. J., 146, 7.

Schoenberg, E. 1929, Handbuch der Astrophysik, Vol. 2 pt.1 (Berlin: Springer Publ.) p. 268.

Shklovskii, I. S. 1960, Soviet Astronomy - AJ, 4, 243.

Shobbrook, R. R., and Shaver, P. 1967, Cornell-Sydney University Astronomy Center Publ. #47.

Solinger, A. B. 1969a, Ap. J., 155, 403.

_____. 1969b, Ap. J. (Letters), 158, L21.

_____. 1969c, Ap. J. (Letters), 158, L25.

Swenson, G. W. 1969, Ann. Rev. Astr. and Ap., 7, 353.

de Vaucouleurs, G. 1959, Ap. J., 130, 718.

_____. 1964, Ap. J., 139, 899.

_____. 1969, Ap. Lett., 4, 17.

de Vaucouleurs, G., and de Vaucouleurs, A. 1964, Reference Catalogue of Bright Galaxies (Austin: Un. of Texas Press).

Véron, P. 1966, Ap. J., 144, 861.

Wills, D. 1967, Ap. J. (Letters), 148, L57.

Wyndham, J. D. 1966, Ap. J., 144, 459.